Computational Models and Emergent Properties of Respiratory Neural Networks

Bruce G. Lindsey[1,*], **Ilya A. Rybak**[2], and **Jeffrey C. Smith**[3]

[1]Department of Molecular Pharmacology and Physiology and Neuroscience Program, University of South Florida College of Medicine, Tampa, Florida [2]Department of Neurobiology and Anatomy, Drexel University College of Medicine, Philadelphia, Pennsylvania [3]Cellular and Systems Neurobiology Section, National Institute of Neurological Disorders and Stroke, National Institutes of Health, Bethesda, Maryland

Abstract

Computational models of the neural control system for breathing in mammals provide a theoretical and computational framework bringing together experimental data obtained from different animal preparations under various experimental conditions. Many of these models were developed in parallel and iteratively with experimental studies and provided predictions guiding new experiments. This data-driven modeling approach has advanced our understanding of respiratory network architecture and neural mechanisms underlying generation of the respiratory rhythm and pattern, including their functional reorganization under different physiological conditions. Models reviewed here vary in neurobiological details and computational complexity and span multiple spatiotemporal scales of respiratory control mechanisms. Recent models describe interacting populations of respiratory neurons spatially distributed within the Bötzinger and pre-Bötzinger complexes and rostral ventrolateral medulla that contain core circuits of the respiratory central pattern generator (CPG). Network interactions within these circuits along with intrinsic rhythmogenic properties of neurons form a hierarchy of multiple rhythm generation mechanisms. The functional expression of these mechanisms is controlled by input drives from other brainstem components, including the retrotrapezoid nucleus and pons, which regulate the dynamic behavior of the core circuitry. The emerging view is that the brainstem respiratory network has rhythmogenic capabilities at multiple levels of circuit organization. This allows flexible, state-dependent expression of different neural pattern-generation mechanisms under various physiological conditions, enabling a wide repertoire of respiratory behaviors. Some models consider control of the respiratory CPG by pulmonary feedback and network reconfiguration during defensive behaviors such as cough. Future directions in modeling of the respiratory CPG are considered.

Introduction

The mammalian respiratory system and neural control of breathing: Brief overview

Breathing is an extraordinarily robust and complex innate motor act that continues, albeit with intermittent disruptions, from before birth to death. Breathing-like behavior occurs in the mammalian embryo and is necessary for normal lung development (116, 141, 147). Following birth, breathing is essential for ventilation, the maintenance of lung volume, and other conditions necessary for gas exchange.

---

*Correspondence to blindsey@health.usf.edu.

The brainstem contains bilateral ponto-medullary circuits necessary for breathing (18, 36, 64, 72, 82, 177, 250, 340). Each side has a "ventral (or ventrolateral) respiratory column" (VRC) of neurons interconnected with several pontine nuclei, which comprise the pontine respiratory group (PRG) (297). A schematic of the brainstem with several different views of regions containing respiratory neural structures, whose functions are described later, is shown in Figure 1. This ponto-medullary network is essential for respiratory rhythm and motor pattern generation (18); its elements are also coordinated and modulated by numerous afferent systems. The nucleus of the solitary tract (NTS) is the "entry point" of lung afferents (157), carotid baroreceptors and peripheral chemoreceptors (172, 269), and other influences important for respiratory control. Rhythmically active neurons in the NTS form a dorsal respiratory group (DRG). Collectively, the VRC, DRG, and PRG constitute the brainstem respiratory central pattern generator (CPG). The VRC contains core CPG elements, which provide neural machinery for generating rhythmic respiratory activity patterns. These core elements drive the activity of motor neurons and receive convergent inputs from the NTS, PRG, and higher central nervous system (CNS) structures such as the cerebral cortex (71), cerebellum (118, 346), hypothalamus (341), midbrain periacqueductal gray (327), and other suprapontine brain regions (119).

Central chemoreceptors that monitor the level of CO_2 and pH in the brainstem, and peripheral chemoreceptors, which are sensors of arterial O_2 and CO_2 and pH, provide essential components of the drive necessary for respiratory rhythm generation and breathing (49, 92, 111). Changes in tidal volume, breathing frequency, and the underlying motor pattern are controlled by numerous other afferent systems, including slowly and rapidly adapting pulmonary receptors (172), baroreceptors (20, 108, 124, 268), and respiratory muscle afferents (301). Changes in sleep and other brain states (117), exercise (195), and network plasticity induced by prior experience (39, 309, 319) can also alter breathing. Intermittent hypoxia can evoke "long-term facilitation" (LTF), a respiratory memory expressed as an increased drive to breathe that outlasts the inducing stimuli (178, 192, 196, 209, 332). Extreme hypoxia can lead to apnea—the cessation of breathing—followed by gasping, an autoresuscitative reconfiguration of the respiratory network involving O_2-sensing neurons (317, 332). The network is also functionally reconfigured during breathing-related behaviors, such as coughing (21, 302), swallowing (135, 288), vocalization (7, 142, 214), and vomiting (e.g., 105, 215).

The output of the brainstem respiratory network is transmitted through premotor neurons that drive spinal phrenic, intercostal, and lumbar motor neuron pools, innervating the diaphragm, intercostal, and abdominal respiratory "pump" muscles, respectively (18, 44, 47, 130). Although the brainstem has a major role in generating the complex patterns expressed by these respiratory motoneurons, spinal circuits also contribute to rhythm generation (130, 146, 171, 291, 295). Both cats and rats have upper cervical propriospinal inspiratory (I) neurons driven by inputs from the VRC and DRG. These spinal interneurons excite ipsilateral phrenic motor neurons (149). Other brainstem premotor and motor neurons control muscles of the upper airways, such as tongue, oropharyngeal, and other accessory muscles that influence airway resistance and protect lung volume (9, 11, 18, 72, 127, 129, 249, 266, 347).

Mathematical and computational modeling as a tool for studying the neural control of breathing

There is a long tradition of modeling the respiratory neural control system. Computational models provide a framework for representing current knowledge, explaining previously known phenomena by reproducing experimental observations, and formulating hypotheses and predictions. While experimental approaches provide increasingly detailed information on structural and functional characteristics of the neural system and its components

controlling breathing, it is difficult to understand many features of the complex cellular and neural circuit behaviors that are integrated for network- and systems-level functions. It is generally recognized that computational models can provide invaluable aid for understanding nervous system function at all levels, from cellular and microcircuit mechanisms to complex large-scale network and neural system dynamics. The fast-growing field of computational neuroscience provides new approaches for studying and understanding the operational principles and mechanisms of the respiratory CPG. The basic organizational principles (e.g., 106, 107, 181, 308, 325) and instructive modeling of other CPGs and related motor circuits [e.g., reference (46)] provides cross-fertilization. Like other neural and physiological control systems, the respiratory system is a very complex dynamical system. Not surprisingly, this system has attracted the attention of mathematicians and modelers interested in applying dynamical systems and other modeling approaches to understand vital neurophysiological functions. Some of these approaches are illustrated herein. The enterprise of understanding neural circuit and system dynamics including rhythmic neural systems [see reference (31)] is at the forefront of computational neuroscience. Comprehensive descriptions of the mathematical foundations of neural modeling and computational neuroscience, including perspectives and approaches from dynamical systems theory, are now available (43, 70, 131, 150). Concise reviews with perspectives on computational neuroscience (1, 182) and how computational approaches contribute to understanding neurobiological mechanisms and processes [e.g., references (45, 180)] can also be consulted.

A major goal of respiratory neural models is to explain how the spatiotemporal patterns of brainstem-spinal respiratory neuron and network activity are generated. This ultimately entails modeling and analysis at multiple spatiotemporal scales. Model development involves choosing the appropriate levels of computational and neurobiological detail and complexity. Respiratory models with different levels of complexity at the neuron, neural population, circuit, and system levels have been developed. These models include: (i) integrated system-level models incorporating respiratory and cardiovascular components with very simplified neural models used [e.g., references (12, 34)]; (ii) network models based on interacting neural populations with each population represented as a single "lumped" nonspiking element (modeled by continuous activity-based neuron descriptions as in references (271, 276)]; (iii) models describing interacting populations of simplified spiking neurons modeled in the "integrate and fire" style with distributed connections (10, 279); and (iv) complex multiscale network models describing interacting populations of neurons modeled in the Hodgkin-Huxley (H-H) style (i.e., ion conductance-based models), which provide a more detailed representation of cellular biophysics such as kinetics of multiple ionic conductances to capture more realistic features of neuronal spiking and electrophysiological behavior. Such models include an explicit simulation of synaptic kinetics and typically intracellular processes, such as the kinetics of intracellular concentrations of Ca^{2+}, including its influx buffering and accumulation for modulation of ion channel gating [e.g., references (28, 29, 67, 200, 278, 280–282, 285–287, 310, 312, 337)]. For descriptions of various mathematical formulations for modeling of single neurons, neural populations, and networks, including advantages and limitations of each model type, the reader is referred to the recent comprehensive books on mathematical foundations of neural modeling noted earlier [e.g., reference (131)].

Increasingly, as illustrated in this review, most contemporary computational models are developed in connection with particular neurobiological experiments employing a variety of experimental preparations, permitting iterative model development and experimental tests of model predictions. This review will specifically consider experimental results that led to development of various brainstem respiratory network models, and/or were motivated by modeling results or were performed to test modeling predictions. This iterative approach has

advanced our understanding of respiratory network architecture and connectivity, mechanisms of rhythmic motor pattern generation and its modulation by afferent systems, and circuit reconfiguration for different breathing-related behaviors. The original modeling papers cited should be consulted for theoretical underpinnings and rationales for model development, including historical perspectives and model advantages/limitations for understanding respiratory network behaviors, only some of which are delineated here.

Respiratory Neurons and Respiratory Network Architecture

The respiratory pattern

The eupneic respiratory motor pattern is commonly divided into three phases: (i) inspiration, (ii) postinspiration (post-I) or stage 1 expiration (E1), and (iii) stage 2 expiration (E2) (262, 263). The inspiratory phase is typically identified by the "ramp" or "step-ramp" discharge pattern of phrenic motor neurons. The post-I interval is often recognized by the decrementing (dec, Dec) discharge pattern in brainstem post-I neurons (Fig. 2) and expiratory (E) laryngeal (thyroarytenoid adductor, TA) motor neurons; a dec low-amplitude "residual" phrenic nerve discharge pattern may also be apparent. E2 is characterized by augmenting (aug, Aug) activity of some E neurons (E-AUG or aug-E; see Section "Respiratory neuron classification") reaching a peak or plateau by the end of expiration. Under conditions of elevated respiratory drive (e.g., hypercapnia), expiration may also have a late-expiratory (late-E) component that represents forced expiration as often assessed by recordings of the lumbar nerve activity associated with abdominal muscle contraction (3, 86, 95, 128, 132, 133, 200, 271).

Respiratory neuron classification

Brainstem respiratory neurons are commonly classified according to the phase in the respiratory cycle when they are most active as determined by simple visual inspection of neural recordings (e.g., extracellular recording traces in Figure 2) or, following "spike sorting," by measures of average neuronal firing rate (probability) in respiratory cycle-triggered histograms (Fig. 2). Statistical tests are also used to identify the presence of respiratory-modulated activity (37, 202, 220, 234, 263, 340).

Neurons classified as I or E are often further subdivided into categories such as aug/Aug or dec/Dec, early or late, or "phase-spanning" (IE, EI) depending on their temporal pattern of firing rate modulation during the respiratory cycle. Additional descriptors include "phasic" and "tonic," with the former designation indicating that the cell spiking pattern exhibits one or more intervals during the respiratory cycle with a low firing probability where spiking rarely occurs. Table 1 (adapted from 279) lists common categories or "types" of neurons distinguished by discharge pattern and other properties, including location, axonal projection, and proposed or inferred synaptic action. Table 1 also provides a glossary, key to abbreviations, and alternative nomenclatures that have been used by various investigators. Some neuron types in the table are grouped for simplicity or because different terminology has been used for neurons with similar discharge patterns and proposed functions by different laboratories.

Classification schemes based on spike discharge pattern do not specify the intrinsic or synaptic mechanisms that contribute to the generation of a particular pattern, and usually do not by themselves define a specific function (e.g., I or E) within the network. Heterogeneity due to variation of intrinsic properties or time varying fluctuations of synaptic input patterns that affect spiking profiles within such classes of respiratory neurons must be considered. Neurons with axons confined to the brainstem are termed *propriobulbar* interneurons, while *bulbospinal* neuron populations transmit excitatory or inhibitory signals to spinal

interneurons and motor neurons that innervate muscles of the respiratory pump. Some bulbospinal neurons have axon collaterals within the brainstem (18, 72).

Other properties used to characterize neurons include their ion channels, some of which could be involved in generation of endogenous bursting activities, membrane receptors and neurotransmitter(s) (5) and other molecular phenotypes (24, 103), responses to stimulation of afferent systems, and short-time scale correlations of their spike trains with those of other neurons or with nerve or electromyogram (EMG) signals [reviewed in reference (279)]. Some of these properties may change over the course of development, during different behaviors involving network reconfiguration, and with disorders and diseases.

Spatially arrayed brainstem compartments involved in generation and control of the respiratory rhythm and motor pattern

The bilaterally distributed brainstem "respiratory network" is considered essential for the generation and control of the motor pattern for breathing. This section briefly considers key regions or "compartments" of the medulla and pons containing respiratory network components; the boundaries between and the functions of each compartment as currently understood are based on results of many experiments employing diverse methodologies (Fig. 1). Further details and issues in the delineation of brainstem neuroanatomy relevant to the respiratory network can be found elsewhere (5, 8, 18, 36, 82, 200, 278, 279, 285, 310, 311, 340).

Ventral respiratory column—The VRC includes the core circuitry of the respiratory CPG. VRC extends bilaterally, in the rostral-to-caudal direction, starting from the retrotrapezoid nucleus (RTN) and includes the Bötzinger (BötC) and pre-Bötzinger (pre-BötC) complexes and the rostral (rVRG) and caudal (cVRG) ventral respiratory groups (Fig. 1) (4, 5, 19, 278, 310, 313). Other adjacent ventral medullary regions of interest include the subretrofacial region (187), other parts of the lateral tegmental field (235), and nonrespiratory modulated (NRM) "pericolumnar" areas (297).

The BötC, with predominately expiratory neurons (post-I, dec-E or E-DEC, and aug-E or E-AUG types), is considered to be a major source of E activity patterns in the system during normal breathing (72, 76, 136, 169, 311, 336). This function of the BötC through its interactions with other VRC compartments has been extensively investigated. BötC E-AUG neurons have widespread inhibitory actions upon I neuron populations in the brainstem and spinal cord (78, 80, 238). Mutual inhibitory interactions between E-AUG and E-DEC neurons modulate their respective discharge patterns. Inhibitory actions between E-AUG neurons have also been identified, and it has been suggested that this network property could modulate late expiratory phase E-AUG neuron activity and thus affect post-I rebound properties of I target neurons (72, 74, 76, 80, 136, 169, 174, 307, 336). The absence or paucity of evidence for excitatory actions of BötC neurons in the referenced studies is noteworthy.

Recent work indicates that the BötC contains critical respiratory network elements generating two major forms of E activity (310), which is consistent with a basic role of the BötC in expiratory pattern generation. This role arises from the presence of rhythmic expiratory inhibitory neurons making widely distributed interconnections with other compartments. The BötC neurons are critically involved in control of the transition between inspiratory and expiratory activities in the network, which is fundamental for the rhythmic I-E alternation essential for normal breathing.

The pre-BötC compartment contains interneuron circuitry essential for generating I activity (86, 153, 259, 312, 313). The pre-BötC has been of intense interest because it is thought to

function as a kernel structure that is a main source of rhythmic inspiratory drive originating from bilateral populations of interconnected glutamatergic neurons (24, 103, 326) that excite premotor and other brainstem circuits (331). Furthermore, pre-BötC circuits can express autorhythmic or pacemaker-like bursting activity that generates a rudimentary pattern of I activity when the brainstem structure, including pre-BötC or its parts (islands), are experimentally isolated *in vitro* [e.g., references (139, 153)]. This activity has been proposed to arise from excitatory synaptic interactions within the pre-BötC and intrinsic cellular mechanisms involving persistent (slowly inactivating) sodium current (I_{NaP}, 28, 29, 152, 257, 283, 286, 312). The intrinsic rhythmic activity of the network may also involve calcium-activated nonselective cationic current (I_{CAN}), which in combination with excitatory synaptic interactions can also provide cellular- and network-level rhythmic bursting (55, 241, 258). Collectively, these (and other) neuronal currents and excitatory synaptic interactions provide mechanisms for regenerative initiation, maintenance, and termination of inspiratory network activity in the isolated pre-BötC *in vitro*. Mechanisms underlying rhythmic inspiratory pattern generation in the pre-BötC under more physiological conditions (i.e., when the pre-BötC is embedded in the intact brainstem) are more complex, because there is a dynamic overlay of rhythmic inhibitory, tonic excitatory, and other modulatory inputs that converge on the pre-BötC excitatory network [e.g., references (255, 310, 312)]. Furthermore, the cellular composition of the pre-BötC is heterogeneous, containing different electrophysiological phenotypes (53, 54, 56, 152, 258, 293, 312, 326), including populations of rhythmically active γ-Aminobutyric acid (GABA) containing (159) and glycinergic inhibitory neurons (201, 344). The local microcircuit organization of this region has not been established in detail, as is the case with other VRC areas.

The rVRG compartment contains the main bilateral clusters of bulbospinal inspiratory [ramp-inpiratory (ramp-I) or (I-AUG)] excitatory neurons that project to spinal phrenic and intercostal inspiratory motor neurons and shape the inspiratory motor output pattern (17, 18, 79, 81, 190, 263, 340). These neurons are driven by the pre-BötC excitatory neurons and are inhibited during expiration by the BötC inhibitory neurons (18, 72, 299); both of these inputs along with other modulatory drives shape and control the characteristic ramping pattern of inspiratory rVRG activity. Thus, the rVRG is also a compartment with multiple convergent input drives essential for inspiratory pattern formation but in contrast to the pre-BötC, this neuronal population as a whole does not appear to have intrinsic rhythmogenic capability (310) although neurons with intrinsic rhythmic bursting properties have been identified in this region (322).

The cVRG compartment contains excitatory bulbospinal expiratory neurons that project to spinal thoracic and lumbar expiratory motor neurons and are concentrated in the retroambiguus area (72). This compartment is presumed to be the expiratory counterpart to the inspiratory rVRG. Convergent inputs, including those from BötC that are synaptically integrated in the cVRG, locally shape the patterns of excitatory and inhibitory expiratory bulbospinal drives.

The retrotrapezoid nucleus/parafacial respiratory group—A source of rhythmic respiratory-related activity independent of the pre-BötC was discovered by Onimaru et al. (227) in the isolated brainstem-spinal cord preparation from neonatal rats. This structure supposedly located more rostral to the BötC was subsequently associated with the so-called parafacial respiratory group (pFRG), spatially overlapping with the RTN (5, 40, 86, 213, 231, 232). The RTN, originally described by Smith et al. (315), is a site of central chemoreception (109, 173), containing chemoresponsive neurons (217), including cells with intrinsic chemosensitive properties (102, 112, 213, 218, 330). These neurons are gluta-matergic and have widespread projections to the respiratory network providing excitatory

drive to the VRC and pons (2). Lesions, including genetic deletions of the large subpopulation of RTN neurons expressing the *Phox2b* transcription factor (62), or experimental perturbations decreasing neuronal activity in this region, reduce or eliminate phrenic activity, alter respiratory cycle frequency (323), and decrease CO_2 sensitivity (2, 102, 111, 219). Some RTN neurons respond to peripheral chemoreceptor inputs and many have respiratory-modulated firing patterns (40, 110, 248), attributable to inputs from more caudal regions of the VRC (239, 330).

The pFRG (231, 233), consists of rhythmically active neurons including cells with intrinsic bursting properties (233), and has been proposed to constitute the primary rhythm generator by Onimaru's group (227, 228). The RTN/pFRG region includes neurons that burst twice per respiratory cycle: in late expiration and in the post-I phase. Neurons with this discharge pattern are common in neonatal preparations (233), but less frequently observed in adults, and have been described as a type of preinspiratory (pre-I) neuron (86, 134, 189, 226, 227, 229, 231, 232) or as "biphasic-E" (3, 200, 276, 278, 310–312). It has been noted that BötC E-Aug neurons may become biphasic during hypercapnic anoxia (94, 276) or hypoxia (279). Biphasic neurons active in late expiration and late inspiration have also been found, albeit rarely, *in vivo* and in simulations (10).

It has been proposed that rhythmically active RTN/pFRG neurons are elements of a separate expiratory oscillator that is coupled with a pre-BötC inspiratory oscillator for generation of the coordinated I-E pattern *in vivo* (86, 132–134, 189). Subsequent work employing *in situ* rat brainstem-spinal cord preparations, and more recently targeted photostimulation experiments in anesthetized rats *in vivo* (243) suggests that RTN/pFRG neurons provide or relay a late expiratory drive to bulbospinal premotor expiratory neurons and upper airway adductor motor neurons activated under critical metabolic conditions producing high respiratory drive such as hypercapnia (3, 86, 132–134, 184, 200).

Pontine regions involved in control of breathing pattern—Pontine neurons are also essential for generation of the normal resting breathing pattern (18, 32, 33, 96, 137, 138, 177, 211, 297, 298, 320, 321). The PRG includes neurons of the dorsolateral pons (dlP) with either phasic, or more commonly, tonic respiratory-modulated discharge patterns. Phase-spanning activity profiles are frequently observed (297) and the pattern of respiratory modulation may vary, depending on the presence of vagal afferent or pulmonary afferent feedback signals (60).

Functional connectivity within the ponto-medullary network [reviewed in references (73, 297)] suggests circuits for the critical role of respiratory phase switching and hence respiratory pattern generation (212, 279, 285). For example, stimulation of the medial parabrachial or Kölliker-Fuse nucleus in dlP induces a premature I-E transition and extended expiratory phase. These effects are similar to the effects of vagal stimulation (36, 121, 340). Also, it appears that the perturbations of respiratory pattern with both vagal and pontine stimulation are mediated by the same medullary circuits that control the onset and termination of inspiration (114, 115, 225, 285).

Since the experiments of Lumsden (177), many studies have shown that ponto-medullary transections in the vagotomized cat (36, 321) and rat (211, 342) convert the normal three-phase pattern (eupnea) to apneusis (a two-phase pattern with prolonged inspiratory durations), whereas the complete removal of the pons (transection at the ponto-medullary junction) results in a gasping breathing pattern (36, 177, 321). In perfused rat brainstem-spinal cord preparations *in situ*, transverse sections through the brainstem starting at the pontine level and progressing caudally have revealed similar characteristic transformations of the respiratory motor pattern (310, 311) (see later).

Medullary raphé—Medullary raphé nuclei, which contain serotonergic neurons, also have multiple functions in the control of breathing. Multisite recordings and spike train analysis of functional connectivity support a model of brainstem respiratory network architecture with medullary raphé circuits constituting a parallel system of "intermediate relays" for breathing-related signaling between the pons and VRC (222). Reciprocal interactions with an efferent copy of respiratory drive and phase information from the VRC to midline raphé circuits may contribute to raphé modulation of the respiratory motor pattern (167, 255). Conversely, raphé serotonergic neurons provide a fundamental permissive excitatory drive to the respiratory CPG circuits (58, 125, 255, 261, 267).

These and other studies have led to the concept that midline medullary circuits maintain particular states or levels of neuronal activity that are subject to adjustment by several afferent systems (6, 161–165, 205, 222, 255). Rostral and other medullary raphé sites include chemoresponsive neurons (223, 261), and local CO_2 and/or pH perturbations evoke state-dependent changes in breathing (216). Similar experimental perturbations in more caudal raphé regions modulate the responses of other central chemoreceptive sites such as the RTN. Stimulation of peripheral chemoreceptors also evokes changes in raphé neuron activity (59, 202, 203, 205, 209, 223). Moreover, repeated stimulation of carotid body receptors or medullary raphé neurons can induce the aforementioned persistent increase in inspiratory drive termed LTF (193, 204, 206, 209).

The nucleus of the solitary tract—The DRG is located in the NTS and is composed of I neurons inhibited (α) or excited (β neurons) by lung inflation (18). Both types of neurons receive central inspiratory drive, presumably from the VRC (335). I-β neurons also receive input from pulmonary stretch receptors (PSRs). In cats, these populations are bulbospinal and excite phrenic and intercostal motor neurons (18); axon collaterals within the medulla have also been identified (237).

The NTS contains second-order neurons for several reflex circuits that profoundly influence breathing. Lung afferents include slowly adapting PSRs sensitive to changes in airway volume. These PSRs project to second-order "pump cells" (P-cells) in the NTS, so called because their rhythmic activity is entirely dependent on periodic lung inflation by a ventilator (pump) in some fictive breathing animal model systems (14, 22). In the rat, P-cells are modulated by a variety of central respiratory modulated influences that contribute to their discharge pattern (199). P-cells mediate the Hering-Breuer inflation reflex (see later in Section "Feedback control of the respiratory CPG") (77, 121, 157, 236).

Carotid body chemoreceptor afferent projections terminate in the medial and lateral subnuclei of the NTS (42, 61, 91, 104) and in the ventrolateral medulla (42, 91, 104). Peripheral chemoreceptors contribute to the drive to breathe and are stimulated by a decrease in blood oxygen tension or rise in $PaCO_2$. Selective stimulation of peripheral chemoreceptors evokes an increase in phrenic nerve discharge amplitude and alterations in respiratory frequency through distributed actions in the respiratory network (223).

The NTS also contains CO_2- and pH-sensitive neurons and local perturbations of CO_2 in the NTS stimulate breathing (49). A new theory proposes that solitary complex central chemoreceptors may also contribute to the control of gastric CO_2 ventilation during respiratory acidosis (48).

NTS neurons receive and transform inputs from carotid and aortic baroreceptors (61, 157, 172, 269). Baroreceptors play an important role in the regulation of cardiovascular function through the baroreflex. They also modulate breathing. Perturbations that transiently elevate arterial blood pressure or carotid sinus pressure can reduce inspiratory drive hence affecting

phrenic discharge amplitude and respiratory frequency (20, 27, 108, 124, 162, 221, 268). Baroresponsive NTS neurons project to regions of the rostral and caudal ventrolateral medulla and toward the pons (8, 75).

Feedback control of the respiratory CPG

The NTS is the site of termination of various populations of lung afferents and other sensory inputs that influence the motor pattern for breathing and the regulation of lung volume by coordination of diaphragmatic, intercostal, abdominal, laryngeal, and other muscle activities (18, 157). The two main receptor types that monitor airway volume or pressure are termed slowly adapting PSRs and rapidly adapting receptors (290, 292, 348).

The PSRs activated during inspiration and lung inflation have a prominent role in the Hering-Breuer reflex in which lung inflation inhibits inspiration and prolongs expiration (157). Through the P-cells, PSR-originating signals alter the activity of CPG neurons in manners consistent with their proposed roles in regulation of rhythmic pattern generation. E-DEC (post-I) neurons display reductions in the rate of decline in firing frequency, and the prolonging of their discharge mirrors the increase in expiratory duration (83, 121, 156, 179, 245). Conversely, lung inflation accelerates the rate at which I-DEC [early-inspiratory (early-I)] neurons decrease their firing frequency, corresponding to the reduction of inspiratory duration (156). The firing frequency of another class of neurons that fire late in inspiration, I-AUG (ramp-I) neurons, does not appear to be affected by lung inflation, but the onset of their firing is advanced by the duration of inspiratory shortening, supporting the suggestion that they are involved in I-E phase switching. Furthermore, vagal stimulation/ lung inflation was shown to excite post-I and ramp-I neurons and inhibit early-I neurons (38, 113–115, 225, 260).

Thus, PSR inputs, through their second-order neurons in the NTS, are a major component of the peripheral afferent loop, and must be accounted for in models of this system when considering control of phase switching and phase durations. As noted earlier, the effects of both vagal and pontine stimulation appear to be mediated by the same medullary circuits that control the onset and termination of inspiration (114, 115, 225). Finally, the respiratory pattern in vagotomized animals with an intact pons is similar to that in animals without the pons and vagi intact. The earlier observations support the idea that the pontine nuclei mediate a function similar to that of the Hering-Breuer reflex.

Brainstem circuits also represent targets mediating feedback regulation of the respiratory motor pattern by afferents from respiratory pump muscles (301), peripheral and central chemoreceptors (92, 223), and other afferent systems that influence breathing and cardio-respiratory coupling (e.g., baroreceptor reflexes 20, 162, 188, 338).

Computational Models of the Respiratory CPG

Early network models

Computational models of the respiratory network have been in development for several decades, with the objective of explaining mechanisms of respiratory rhythm and pattern generation. Although the alternative concepts of pacemaker and network mechanisms for respiratory rhythmogenesis had been introduced [e.g., reference (289)], most early computational models focused on the network interactions between different types of respiratory neurons and did not consider possible contributions of the intrinsic biophysical properties of neurons, which were essentially unknown during that period [e.g., references (10, 23, 63, 66, 84, 85, 98, 101, 186, 224, 277)]. These network models were based on simple, activity-based models of neurons, which did not simulate the neuronal spike-generating mechanism. The output activity of a neuron (or neural population) was usually

described by a single continuous variable representing the neuronal firing rate. Synaptic interactions in these models were also simplified whereby neuronal input was represented as a weighted sum of output variables of all source neurons projected to the given neuron. Generation of the respiratory rhythm in these models was based on a pure network concept suggesting that the respiratory rhythm results from sequential phase switching, such as an inspiratory off-switch (IOS, transition from inspiration to expiration) and an expiratory off-switch (EOS, transition from expiration to inspiration). The phase switching mechanisms were suggested to operate via the reciprocal (mostly inhibitory) interactions among different types of respiratory neurons or neuronal populations. For example, Duffin (63) proposed a network model consisting of one excitatory (I-AUG) and two inhibitory (I-DEC and E-BÖT) neurons that generated two-phase (inspiration-expiration) oscillations due to mutual inhibition between the I-DEC and E-BÖT neurons. Both phase-switching mechanisms (IOS and EOS) in this model were based on the adaptive properties (i.e., time-dependent decline of activity) of the I-DEC neuron and the reciprocal interactions between the two inhibitory neurons.

A series of three-phase pattern-generating network models were developed based on a conceptual schematic proposed by Richter and his collaborators (264, 265) postulating that the respiratory cycle consists of three phases: inspiration, post-I, and stage-2 (late) expiration. As a representative example, Figure 3A and B shows the schematic of the Ogilvie et al. (224) model and its performance. Other similar models were also developed [e.g., references (23, 101)]. The IOS mechanism in these models involved the late-I neurons that started firing by the end of inspiration, reached the peak of activity at the transition from inspiration to expiration, and provided the initial inhibition of I neurons. These early three-phase models also usually consisted of nonspiking activity-based models for simulating single neurons or neural populations. The model proposed by Botros and Bruce (23) included five neuron populations: I (inspiratory with a ramp-I pattern), early-I, late-I, and post-I and E (expiratory). Interconnections among these populations were assigned in accordance with the Richter schematic (264, 265). The model generated a stable respiratory rhythm and reproduced realistic activity profiles of all five neuron populations incorporated. Some effects of pulmonary feedback on the respiratory pattern were also reproduced.

Balis et al. (10) developed the first model of interacting populations of respiratory neurons that incorporated simplified, "spiking" (integrate-and-fire type) models of single neurons. These models allow calculation of the timing of "generated spikes." It is considered that the action potential (spike) is generated when the neuronal membrane potential reaches a threshold, but the changes in the membrane voltage itself are not associated with, and are not described based on, kinetics of the fast ionic conductances driving the action potential generation. Nevertheless, such models enable, in many instances, realistic neuron simulation and require much less computational power than more complicated models of the H-H type. Specifically, they allow an investigator to perform simulations of interactions among the large populations of spiking neurons (with numbers of neurons in populations close to their numbers in the real system). Synaptic processes in these models can be realistically modeled via changes in the corresponding postsynaptic conductances. The model of Balis et al. contained six neuron populations: one excitatory of I-AUG type, four inhibitory [I-DEC, E-AUG (SYM), E-AUG (LATE), and E-DEC], and an additional I-E/I (pre-I/I, see Table 1) excitatory population. Some key connections in the model network were assigned from a spike-train analysis of multiple, simultaneous neuronal recordings performed by the same group (168–170, 299). Simulated perturbations of the activity of various populations and changes in their connection strengths led to several predictions on control of phase durations and patterns that guided subsequent experiments. Interestingly, depending on the model parameters, the respiratory pattern could be generated with or without involvement of the I-E/I population.

Rybak et al. (280–282, 284) built a series of network models with more complicated, ionic conductance-based models of single neurons described in the H-H style, which allowed analysis of possible roles of intrinsic neuronal properties in the genesis of the respiratory rhythm. Several distinct network schematics were comparatively investigated. The basic model included six respiratory neurons: early-I, ramp-I, late-I, post-I, aug-E (or E2), and pre-I, the latter of which was proposed as a potentially important class of neurons for E-I phase switching as suggested from experimental recording of this cell type(s) (263, 293). The IOS mechanism in these models operated via the late-I neuron as proposed by the Richter scheme (see earlier text). The EOS mechanism involved the pre-I neuron, which was inhibited during expiration and gradually released from this inhibition, allowing neuronal spiking that provided an initial activation of early-I and ramp-I neurons; the early-I neuron then inhibited post-I and aug-E neurons hence completing the switch to inspiration. The model also included a simplified model of the lungs and PSRs that provided pulmonary feedback to the respiratory network. This feedback was excitatory to the late-I and post-I neurons and inhibitory to the early-I neuron allowing expression of the Hering-Breuer reflex. Disconnecting the vagal feedback (vagotomy) caused a prolongation of inspiration and an increase in the amplitude of integrated phrenic nerve discharges. The model was shown to generate a realistic respiratory pattern, reproduce membrane potential trajectories of individual respiratory neurons, and exhibited proper changes in the respiratory pattern and firing activities of individual respiratory neurons under different conditions, including vagotomy and various afferent input stimulations. However, this model (as well as other purely network models) could not reproduce some important behaviors obtained from *in vitro* studies of the respiratory network, specifically the persistence of rhythmic activity after synaptic inhibition in the network was blocked (see Section "Generation of respiratory oscillations *in vitro*, the pre-Bötzinger complex, and the role of intrinsic cellular mechanisms").

Generation of respiratory oscillations *in vitro*, the pre-Bötzinger complex, and the role of intrinsic cellular mechanisms

A fundamentally distinct concept of respiratory rhythm generation, at least for the generation of inspiratory activity, was derived from studies conducted with isolated neonatal rodent brainstem-spinal cord and slice preparations that generate rhythmic respiratory activity *in vitro* (313, 314). The important discovery has been that a functionally specialized region within the VRC, called the pre-BötC complex, contains a population of interneurons that can intrinsically generate a rudimentary inspiratory rhythm (313). This rhythm was shown to persist after disrupting GABAergic and glycinergic synaptic inhibition (90, 139, 306), consistent with the experimental finding that the pre-BötC contains a subpopulation of specialized "pacemaker" cells with intrinsic oscillatory bursting properties (Fig. 4) and mutually excitatory interconnections that can synchronize their activity to generate coherent population-wide rhythmic bursting (153, 313). The possible contributions of neuronal pacemaker properties to respiratory rhythm generation had long been speculated upon in the field and these findings provided initial evidence for the existence of such properties. Butera et al. (28, 29, 53) developed and analyzed a series of computational models of bursting pacemaker neurons and heterogeneous populations of these neurons with mutual excitatory synaptic connections that captured features of the rhythmic behavior of pre-BötC neurons and circuits.

These models proposed biophysically minimal mechanisms for intrinsic rhythmic bursting activity at the cellular-level (in the absence of excitatory interactions) based on H-H style descriptions of a persistent sodium current (I_{NaP}) with a subthreshold, voltage-dependent activation as the essential burst-generating, inward cationic current. In one of the model formulations (model 1), the rhythmic bursting cycle was controlled by the hypothesized

slow kinetics of I_{NaP} inactivation and recovery from inactivation, as defined by the H-H inactivation variable h (Fig. 4B), and the dynamic interactions of I_{NaP} with a K^+-dominated, outward leak current [for a mechanistically different model 2 formulation not discussed here see Butera et al. (29)]. In the simulations performed, the slow kinetics of h in model 1 was shown sufficient to orchestrate burst termination, regulate the dynamics of the interburst period, and generate voltage-dependent oscillations with the bursting frequency spanning the frequency range observed experimentally *in vitro* (Fig. 4D) (16, 29, 30, 53); this voltage-dependent behavior provided a rudimentary mechanism for burst frequency control when these neurons were subjected to tonic depolarizing excitatory synaptic drive. Furthermore, these neuron models, as found experimentally, had multiple activity states (Fig. 4A): quiescence at hyperpolarized membrane voltages where I_{NaP} was not activated, oscillatory bursting in the voltage regimes where I_{NaP} underwent rhythmic activation and inactivation, and tonic spiking activity at more depolarized voltages where I_{NaP} was essentially inactivated. As a consequence of this voltage-dependent behavior, I_{NaP}-dependent bursting is conditional, and the neuronal models can be tuned to be either conditional intrinsic bursters (rhythmic bursting emerging for some level of depolarizing input) or nonintrinsically bursting cells that cannot rhythmically burst for any level of input, for example, due to a low level of I_{NaP} conductance relative to the leak conductance.

The model 1 formulation of oscillatory bursting dynamics with voltage-dependent slow inactivation of I_{NaP}, which is consistent with experimental observations of I_{NaP} kinetic behavior and bursting characteristics of pre-BötC neurons (Fig. 4B), has been widely adopted. This model has been utilized in extensive modeling studies investigating the dynamical behavior of heterogeneous excitatory networks consisting of subpopulations of intrinsically bursting and nonintrinsically bursting cells as a basic model for the pre-BötC excitatory network (28–30, 53, 257, 272, 286, 287) including recent studies exploring how different connection topologies contribute to network burst synchrony and shape network activity (97).

Modeling heterogeneous networks of such intrinsic and nonintrinsically bursting neurons with mutually excitatory interactions has shown that the excitatory synaptic interactions coupled with I_{NaP} activation can readily synchronize cellular activity bursts and produce population-wide rhythmic bursting (Fig. 5) over a broad range of frequencies, including a situation when only a small fraction (5%–10%) of the neurons within the network are intrinsically bursting cells. Moreover, synchronized emergent population rhythms can occur at the network level in these models even if none of the cells are in the intrinsic bursting state or exhibit conditional bursting at some level of depolarizing input (i.e., as characterized in the absence of excitatory interactions among the cells) (28, 68, 257, 274, 286, 287) due to the ability of I_{NaP} to dynamically orchestrate population-wide burst initiation and synchronous termination in a mutual excitatory network. The oscillatory dynamics are controlled in complex ways, even in small symmetrical networks (Fig. 5A), by the strengths of excitatory drive inputs, excitatory synaptic coupling strengths, and in large networks by connection probabilities (sparse vs. densely connected networks) (28) and different network topologies (97). Interestingly, this network modeling (257) has shown that the oscillatory frequency range is a function of the fraction of neurons with intrinsic bursting properties within the network. Inclusion of such pacemaker neurons in the network increases the robustness of rhythm generation by substantially augmenting the operational range of oscillation frequencies (as controlled by tonic excitatory drive) compared with networks containing no intrinsically bursting neurons. A feature of these heterogeneous networks is that there is a temporal dispersion of neuronal spiking activity within the population (28, 53) with a subset of (pre-I/I) neurons generating pre-I spiking activity (Fig. 5B) that produces early excitatory synaptic activity in the network contributing to inspiratory burst initiation.

The presence of I_{NaP} in pre-BötC intrinsic bursters and also nonintrinsically bursting I neurons predicted by these models was confirmed experimentally (54, 152, 256, 286). As predicted by these models, the critical difference found between the experimentally characterized pre-BötC I neurons with and without intrinsic bursting properties was the higher level of I_{NaP} conductance relative to the conductance of K^+-dominated leak current in the intrinsic bursters (54, 152). Various conditions for the generation of I_{NaP}-dependent oscillations in the pre-BötC were intensively studied using computational modeling. These studies found and described the dependence of I_{NaP}-dependent bursting on the extracellular potassium concentration $[K^+]_o$ and leak conductances; this modeling has provided explanations for several experimental results obtained *in vitro,* including control of bursting by neuronal "background" leak channel conductances (151, 152, 287).

Generation of I_{NaP}-dependent population oscillations does not require neuronal inhibitory interactions, which as noted earlier, can explain the persistence of rhythmic activity in the pre-BötC *in vitro* after inhibitory synaptic transmission was blocked—the phenomenon that the earlier network models could not reproduce. Interestingly, the pre-BötC network modeling studies have shown that, similar to the voltage-dependent behavior of individual pre-BötC conditional bursters noted earlier, progressive elevation of tonic excitatory drive to an excitatory population of cells with I_{NaP}-dependent bursting properties sequentially produces switching from an inactive state to population rhythmic bursting with burst frequency increasing with the level of drive and, finally, to a regime of sustained asynchronous tonic spiking activity (Fig. 5A and E, see also references (28, 286, 287)]. This multistate behavior of the isolated pre-BötC network has figured prominently in the development of extended models of the respiratory network in which the pre-BötC network interacts dynamically with other CPG components providing multiple state-dependent mechanisms for respiratory rhythm generation (see upcoming sections).

The models of the isolated pre-BötC network based on populations of neurons with I_{NaP}-dependent bursting properties could explain a number of experimentally observed features of pre-BötC neuron and network rhythmic behavior. Moreover, experimental studies confirmed that I_{NaP} is ubiquitous in pre-BötC neurons and endows both individual neurons and the network as a whole with intrinsic oscillatory bursting properties. Nevertheless, the necessity of I_{NaP} for rhythm generation in the pre-BötC network *in vitro* has been questioned and is now under debate (55, 86, 242). One of the issues is whether other mechanisms intrinsic to the pre-BötC network predominate, particularly those giving rise to network-level emergent rhythms. This debate has been driven by a suggestion of another intrinsic rhythmogenic mechanism that can involve a Ca^{2+}-activated nonspecific cationic current (I_{CAN}); I_{CAN}-dependent intrinsic bursting behavior of individual pre-BötC I neurons has been extensively studied (55, 240, 241, 251, 258, 334, 339). Thus, currently both Na^+- and Ca^{2+}-based mechanisms are considered to contribute to inspiratory rhythm generation in the pre-BötC network and the degree of their involvement may depend on the age of the animal and experimental conditions.

A computational model of pre-BötC bursting activity based on I_{CAN} was proposed by Rubin et al. (275) to represent a so-called "group-pacemaker" mechanism for inspiratory rhythm generation (86, 259), which emphasizes a critical role of synaptic mechanisms and network interactions in the production of emergent network rhythms that in principle cannot be generated by mechanisms operating at the single neuron level. In this model, the excitatory synaptic inputs to each neuron via mutual synaptic interconnections within the population, which involve 2-amino-3-(5-methyl-3-oxo-1,2-oxazol-4-yl)propanoic acid (AMPA) and metabotropic glutamate receptors, were proposed to evoke a release of Ca^{2+} from intracellular stores. The Ca^{2+} accumulated from intracellular stores activates I_{CAN}, which underlies the burst phase of neuronal and network activity. Robust depolarization due to

I_{CAN} was postulated to cause voltage-dependent spike inactivation (depolarization block of sodium channel activation), which diminishes mutual excitation in the network and thus attenuates postsynaptic Ca^{2+} accumulation. Consequently, the depression of synaptic activity within the network along with cellular activation of Na^+/K^+ ATPase pumps, Na^+-dependent K^+ currents (K_{Na+}) (155), or other ionic mechanisms, can terminate the inspiratory burst followed by a transient quiescent state in the network (275). Thus in this model, network-wide burst termination is critically based on transient Na^+ current-dependent spike inactivation and the activation of outward currents, rather than on I_{NaP} inactivation (51).

Synthesizing the concepts of Na^+- and Ca^{2+}-based mechanisms for intrinsic cellular bursting, Toporikova and Butera (337) have proposed a two-compartment (somatic-dendritic) model of pre-BötC neurons incorporating I_{NaP} and I_{CAN} as two independent burst-generating mechanisms. Bursting in the somatic compartment is produced by I_{NaP} activation-inactivation as in the earlier Butera et al. models, and a separate burst-generation mechanism operating in a dendritic compartment involves Ca^{2+} oscillations arising from inositol triphosphate (IP3)-regulated intracellular Ca^{2+} release that activates I_{CAN}. The inclusion of a dendritic compartment was motivated in part by the intriguing experimental observations of Mironov (194) that activation of I_{CAN} may involve propagating Ca^{2+} waves originating from dendritic intracellular Ca^{2+} release due to metabotropic glutamate receptor activation, although electrotonic propagation of dendritic Ca^{2+} current may be particularly important (52). As modeled, voltage-dependent I_{NaP} as well as Ca_2^+ oscillation-dependent I_{CAN} burst-generation mechanisms are regenerative, and thus can explain the existence of the two different types of intrinsic neuronal oscillatory bursting observed experimentally in the pre-BötC *in vitro* (334). Importantly, this model explicitly incorporates kinetic descriptions of cytoplasmic signaling pathways and associated Ca^{2+} dynamics, expanding the pre-BötC neuronal modeling enterprise to include somaticdendritic processes with intracellular biochemical signaling involved in ion channel gating. Modeling studies of excitatory networks incorporating such hybrid neurons are in progress. Such network modeling should provide understanding of different regimes of pre-BötC network rhythm generation associated with distinct or combinations of Na^+- and Ca^{2+}-based mechanisms.

A major conclusion from these experimental and modeling results is that the pre-BötC network alone may incorporate multiple, potentially coexisting rhythmogenic mechanisms involving complex dynamic interactions of various intrinsic cellular and network properties that give rise to a rich set of oscillatory properties. While extensive effort has been devoted to understanding mechanisms operating in the pre-BötC network isolated *in vitro*, a major problem in the field has been to understand how and when these properties operate with the pre-BötC embedded in the intact nervous system. More complete models of the CPG network have been formulated to begin to address some of these issues and are considered later.

Inhibitory network-based versus excitatory pacemaker-network-driven mechanisms for respiratory rhythmogenesis and a hybrid pacemaker-network model

The early network models of respiratory rhythm generation described earlier (Section "Early network models") that incorporated inhibitory circuit interactions reproduced many characteristics of respiratory CPG behavior including the generation of realistic respiratory neuron and motor patterns under different conditions. These models were formulated before the detailed analyses of the pre-BötC's excitatory and autorhythmic properties and thus did not incorporate biophysical mechanisms underlying intrinsic cellular and network bursting behavior. On the other hand, the excitatory network models incorporating subsets of neurons with pacemaker-like intrinsic bursting behavior (pacemaker network), developed to explain data on the intrinsic bursting properties of some I neurons within the pre-BötC network

isolated *in vitro*, could not explain many features of respiratory network activity observed *in vivo*. These features include the various temporal patterns of inspiratory and expiratory population activities, independent regulation of the duration of each respiratory phase, the Hering-Breuer and other respiratory reflexes. These models could also not reproduce apneusis, a breathing pattern characterized by a significantly prolonged inspiration (lasting up to several seconds) alternating with short expiratory intervals. Even the basic pattern of rhythmic I activity generated by the reduced *in vitro* preparations and pacemaker-based network models, which typically exhibit decrementing inspiratory discharges (e.g., see Fig. 5), differs fundamentally from the augmenting shape of rVRG population and phrenic nerve discharges observed during normal (eupneic) breathing *in vivo*. The isolated pre-BötC network usually generates a more primitive pattern of I activity that resembles in some respects the decrementing inspiratory bursts observed during gasping *in vivo* (247), which has led to extensive debate [reviewed in reference (322)] about the functional significance of the rhythmic activity generated by the isolated pre-BötC network.

The contradiction between the inhibitory network-based and excitatory pacemaker-network concepts and models can be resolved by postulating that (i) the rhythmogenic behavior of the pre-BötC when embedded in a larger brainstem respiratory network becomes dependent on the dynamic interactions with other respiratory neural populations including inhibitory neurons and that (ii) respiratory rhythmogenesis *per se* is state dependent, and therefore the rhythm may be generated predominantly by either inhibitory network-based or excitatory pacemaker-network driven mechanisms, or their specific combinations depending on the conditions.

Based on these ideas, Smith et al. (312) proposed a hybrid pacemaker-network model in which the pre-BötC network functions as an excitatory "kernel" that receives convergent synaptic inputs from a number of other neuronal populations, including neurons generating tonic excitation, tonic inhibition, and rhythmic expiratory-phase inhibition that dynamically regulate the behavior of the pre-BötC network when embedded in the larger brainstem respiratory network (Fig. 6). This model was proposed to account for rhythm-generation mechanisms with the embedded kernel as well as for network mechanisms generating temporal patterns of I and E activities. The model contained several populations of I and E neurons (pre-I/I, early-I, ramp-I, late-I, post-I, and aug-E) simulated as populations of H-H style, conductance-based single-compartment neuron models. It was shown that this model could operate in multiple rhythm-generating regimes depending on the expression of voltage- and I_{NaP}-dependent bursting properties in the pre-BötC excitatory network, and also on the inhibitory network interactions regulating the dynamic evolution and transitions of I and E phases. Thus, the model represented a hybrid of excitatory pacemaker-network- and inhibitory network-based mechanisms for rhythm generation. In the excitatory pacemaker-network driven mode of rhythm generation, which occurs when I_{NaP} is not inactivated (e.g., at relatively low levels of tonic excitatory input to the pre-BötC network), inspiratory bursting activity involved neuronal I_{NaP}-dependent bursting pacemaker properties that contributed importantly to inspiratory burst onset within the heterogeneous pre-BötC excitatory network. With the system operating in this mode, oscillation frequency was controlled by tonic excitation/inhibition, and the kinetics of recovery of I_{NaP} inactivation, as in models for the isolated kernel *in vitro*. Phasic inhibitory network inputs (e.g., from the post-I neurons) contributed to inspiratory phase termination and were required for evolution of the expiratory phase. The inhibitory hyperpolarization resets I_{NaP} in the pre-BötC kernel cells, allowing recovery from partial current inactivation; the next inspiration is initiated when the inhibition declined and the subthreshold-voltage activation of I_{NaP}, including importantly in pre-I/I spiking neurons, promoted the E-I phase transition. In the inhibitory network driven mode, the pre-BötC excitatory neurons operated in the regime of sustained spiking activity with I_{NaP} essentially inactivated due to high levels of

tonic excitation, so that the network-based phasic expiratory inhibition is critically required for inspiratory phase termination. In this case the recovery dynamics of I_{NaP} inactivation play a much smaller role in controlling the onset of pre-I/I spiking and inspiratory burst initiation, which is now predominantly controlled by the decline of post-I inhibition and the high tonic excitatory drive to the pre-BötC network.

The analysis demonstrated that this hybrid model could be transformed dynamically between the different modes of rhythm generation with specific changes in model parameters. For example, reducing the average level of tonic excitatory postsynaptic conductance in the pre-BötC network could transform the system from the inhibitory network-driven to the excitatory kernel-driven mode. Explicit in the model was also the concept that conditions may occur *in vivo* in which the pre-BötC kernel could become functionally unembed-ded due to reduced phasic inhibitory network interactions, analogous to the *in vitro* conditions. In this case, the kernel would provide rudimentary I_{NaP}-dependent pacemaker-network mechanisms for rhythmic inspiratory pattern generation via excitatory synaptic drive to bulbospinal and cranial premotor inspiratory drive transmission circuits. The hybrid pacemaker-network model set the stage for development of more elaborate CPG models exploring state-dependent mechanisms of rhythm and pattern generation.

State-dependent generation of the respiratory rhythm: Ponto-medullary models

The functional state of pre-BötC neurons can be controlled by excitatory and inhibitory tonic drives and phasic synaptic inhibition. Specifically, a relatively high excitatory drive can depolarize these neurons, producing inactivation without recovery of I_{NaP}, and maintain these neurons in the state of tonic spiking. In addition, phasic inhibition can entrain a rhythmic rebound bursting resulting from the periodical disinhibition of pre-BötC neurons. Hence, tonic drives from different brainstem regions (e.g., from the pons, RTN/pFRG, NTS, and raphé) may control the functional state of the pre-BötC directly, via excitatory drive, as well as indirectly through the activation of BötC post-I neurons that phasically inhibit the pre-BötC neurons. Accordingly, pontine and other inputs to both the pre-BötC and BötC may change the operating rhythmogenic mechanism by transforming the functional state of pre-BötC neurons.

Rybak et al. (285) developed a model of the ponto-medullary respiratory network that employed the earlier-stated switching mechanisms. Figure 7A shows the schematic of this model and its performance under different conditions. The model consisted of interacting populations of neurons described using conductance-based (H-H type) neuron models. An attempt was made to integrate known cellular, network, and systems level mechanisms contributing to respiratory rhythm generation and control, and accumulate all advantages of the previous models. In contrast to previous models, this model for the first time considered the spatial organization of respiratory compartments within the medullary VRC and in the pons by incorporating separate compartments such as rVRG, pre-BötC, BötC, as well as separate rostral (rPons) and caudal (cPons) pontine components. These compartments included neural populations known to be dominantly present in each region. Postulated synaptic connections between populations within the VRC [i.e., between the ramp-I, early-I, late-I, post-I, aug-E, and pre-I (pre-I/I) populations] defined the basic circuitry for IOS and EOS mechanisms, which were similar to those operating in the earlier network models (23, 101, 224, 281, 282). At the same time, the pre-I (pre-I/I) population of pre-BötC contained neurons with I_{NaP}-dependent pacemaker properties. Reciprocal excitatory connections between the medullary ramp-I and the pontine I-mod and IE-mod populations, and between the medullary post-I and the pontine IE-mod and E-mod populations, provided I-, IE-, or E-modulation of the activity of the corresponding pontine populations. This model incorporated reticular neurons in the caudal pons (the tonic population) to provide excitatory tonic drive to the majority of medullary respiratory neurons. The model also included PSR-

like feedback that controlled activity of the key neural populations involved in IOS and EOS mechanisms (via activation of the late-I, post-I, and ramp-I populations and inhibition of the early-I population). This enabled regulation of the durations of respiratory phases through the Hering-Breuer reflex. In addition, this feedback suppressed the activity of the pontine neural populations that receive excitation from the medullary populations (I-mod, IE-mod, and E-mod). Importantly, consistent with experimental observations, the IOS and EOS mechanisms in this model operated under control of both pontine input and pulmonary feedback, both of which were excitatory to the late-I, ramp-I, and post-I populations (115, 225).

The performance of the model under different conditions is shown in Figure 7B-E. With the pons intact, the model generated a stable three-phase "eupneic" respiratory rhythm with realistic spiking patterns and membrane potential trajectories of respiratory neurons (see Fig. 7B). Specifically, the bursts of ramp-I neurons as well as the simulated phrenic nerve discharges exhibited augmenting patterns. The pulmonary feedback to the medulla provided the Hering-Breuer reflex, therefore a disconnection of this feedback (vagotomy) produced an increase in the amplitude and duration of phrenic discharges (Fig. 7C) reflecting the loss of the reflex circuit interactions.

Disconnection of vagal feedback also eliminated the suppressing influence of vagal afferents upon the pontine I-mod, IE-mod, and E-mod populations (Fig. 7A) and hence enabled a role of these pontine populations in the control of respiratory phase switching. This control was provided via the same medullary IOS and EOS circuits that were controlled by pulmonary vagal feedback when the latter was intact.

As shown previously in cats and rats, removal of the rPons or chemical blockade of respiratory-related structures within this region produced apneusis, and a complete removal of the pons produced gasping-like phrenic nerve bursts with decrementing discharge patterns (137, 177, 211, 321, 342). Similarly, a removal of rPons in this model converted the normal breathing pattern to apneusis (Fig. 7D). A complete removal of the pons (eliminating the cPons) produced gasping-like (or *in vitro*-like) oscillations originating in the pre-BötC and characterized by decrementing phrenic discharges (Fig. 7E).

This model was able to reproduce many experimental observations. Specifically, mild continuous vagal stimulation in the model shortened inspiration and prolonged expiration [as was previously shown experimentally, see references (36, 82, 121, 340)], whereas strong continuous stimulation arrested the rhythm in the post-I phase ["postI apnea" see references (121, 160, 260)]. Short stimuli applied to the simulated vagal afferent inputs during inspiration could terminate the ongoing inspiration, and the threshold for this inspiratory termination decreased during inspiration (35, 36, 340). Stimuli delivered during post-I prolonged expiration, whereas vagal stimulation during the late part of expiration had no effect on expiratory duration (82, 148, 260). Short duration stimulation of the pontine IE-mod population in the model terminated inspiration. Experimentally, a similar effect of inspiratory termination by stimulation of the rPons [e.g., the nucleus parabrachialis medialis/Kölliker-Fuse (NPBM/KF) region that contains many I- and IE-modulated neurons)] had been previously demonstrated in both cats and rats [e.g., references (15, 36, 82, 115, 137, 177, 225, 343)]. Also in this model, a continuous stimulation of the pontine IE-mod population shortened inspiration and prolonged expiration, whereas the same stimulation applied to the E-mod pontine population prolonged expiration without altering inspiration. The latter had also been experimentally demonstrated by stimulation of the ventrolateral pons, which is known to contain mainly expiratory-modulated neurons (138).

Similar to the Smith et al. hybrid pacemaker-network model described earlier, the Rybak et al. (285) model has suggested that the operating rhythm-generating mechanism (inhibitory network-based, pacemaker-network driven, or hybrid) engaged under particular conditions depends on the functional states of the pre-BötC and other VRC compartments (e.g., BötC), which in turn are controlled by multiple network interactions within the medulla as well as by various supramedullary circuits (e.g., pontine and afferent inputs carrying information on the functional state and metabolic needs of the system).

A more complicated ponto-medullary model (279) was developed based on the previously mentioned and other earlier (10) models to simulate interactions of medullary and pontine neurons with more details. This model used integrate-and-fire descriptions for both the nonpacemaker neurons (10) and I_{NaP}-dependent pre-BötC bursters (25). In contrast to the Rybak et al. (285) model, which included only a minimal set of pontine populations that did not interact with each other and had only hypothetical interconnections with the medullary populations, this model explicitly incorporated the types of pontine populations and their interconnections within the pons and with medullary populations that were identified by the analysis of many multielectrode recordings made in a series of coordinated *in vivo* studies in cats (297).

The schematic of the model is shown in Figure 8. Similar to the model of Rybak et al. (285), the IOS and EOS mechanisms in this model were controlled by pontine inputs and vagal feedback via the key medullary populations involved in phase switching. The model also included the pre-BötC's I-E/I (I-Driver) population consisting of neurons with conditional pacemaker properties [simulated as in reference (25)] that, under certain conditions, allowed this population to generate intrinsic inspiratory oscillations in the network. The model reproduced all experimental observations that the model of Rybak et al. (285) did, including the changes in the respiratory pattern following simulated vagotomy (Fig. 9A and B) as well as those evoked by pontine transections and various afferent and pontine stimulations. The model also reproduced characteristic changes in neuronal activity and motor patterns observed *in vivo* during fictive cough (302) and during hypoxia in nonrapid eye movement sleep (176).

One of the objectives of this model was to investigate specific relationships between inhibitory network and excitatory pacemaker-network-based rhythm-generating mechanisms. As in the model of Rybak et al. (285), removal of pontine circuits produced a gasping-like activity with decrementing phrenic nerve bursts (Fig. 9C). However, the simulations showed that, with a subsequent tonic re-excitation of the VRC network, the model could generate pacemaker-network-driven gasp-like bursts superimposed upon a network-generated augmenting inspiratory ramp, resulting in a "burst-ramp" phrenic pattern (Fig. 9D, enlarged in Figure 9E). In this connection, during severe brain hypoxia *in vivo*, the eupneic pattern of inspiratory motor output is also replaced by gasping (321, 322). These simulation results allowed the suggestion that hypoxia-induced gasps are generated by a dynamically "reduced" network, involving a I_{NaP}-dependent intrinsic mechanism in the pre-BötC [see also reference (247)]. In addition, simulations performed with this model predicted that recovery from hypoxia-induced gasping might go through transitional states, in which gasp-like bursts are superimposed on a reemerging network-generated ramp-like inspiratory pattern (Fig. 9F). These modeling results motivated *in vivo* experiments to address this hypothesis.

To test this prediction, activity of different respiratory neurons within the VRC and efferent phrenic motor patterns were monitored *in vivo* during fictive breathing, followed by hypoxia (gas mixture of 5% O_2–95% N_2) and then by reoxygenation (316, 318) in vagotomized, decerebrate, neuromuscularly blocked, thoracotomized, and artificially ventilated cats.

Simultaneous recordings of multiple single neuron spike trains were made with a multielectrode array (Fig. 10). In these experiments (279), the patterns of phrenic nerve activity during severe brain hypoxia and recovery were similar to those from the model simulations: the recorded phrenic activity progressed from fictive gasp-like bursts to ramp activity with superimposed bursts, and then to augmenting discharge patterns similar to those observed during the control period (Fig. 10). The firing patterns of ten simultaneously monitored single neurons and phrenic nerve activity recorded during a control period are shown in Figure 10A. Hypoxic exposure in this carotid body-intact preparation first produced an excitatory response with augmented inspiratory discharge amplitude and frequency followed by hypoxic depression (not shown), typical of the response of the intact network (318). Subsequently, during recovery from the depression, gasp-like phrenic bursts were observed, which were associated with the corresponding activity in the I-EI neurons and a subset of I neurons (Fig. 10B). The posthypoxic "recovery" was first associated with the reemergence of E-Aug neuron activity (Fig. 10C) followed by spiking in the E-Dec neurons (Fig. 10D and F). After recovery, an augmenting eupneic-like phrenic pattern was fully reestablished (Fig. 10F). However, this recovery of the eupneic phrenic activity pattern went through intermediate stages in which gasp-like decrementing bursts were superimposed with reemergent augmenting bursts (Fig. 10D and F). The evolution of integrated phrenic discharge profiles is shown in Figure 10F, which demonstrates that during the recovery phase distinct phrenic motor patterns occurred, alternating in successive cycles during some intervals. The phrenic pattern marked by a dashed red ellipse was similar to the phrenic activity profile from the model simulations shown in Figure 9D and E. As predicted by the model, this sequence of simultaneously recorded discharge patterns suggests that components of a distributed neural network active during eupnea can be coordinated with a functionally "simplified" and distinct mechanism that generates gasping and augmented burst activity during recovery from severe brain hypoxia.

Spatial and functional architecture of the mammalian brainstem respiratory network: Circuit building blocks, state dependency, and hierarchy of oscillatory mechanisms

A major problem in the field has been to determine the structural-functional organization of the brainstem respiratory network including how specific network components and their functions are distributed anatomically. The concept of pontine and VRC structural "compartments" with functionally distinct network components was postulated in the models of Rybak et al. (279, 285) as discussed earlier. This compartmentalization has been inferred in part from recordings of neuron population activity, suggesting that each region contains one or more predominant type of neuron population postulated to contribute to network operation in particular ways, as considered in Section "Spatially arrayed brainstem compartments involved in generation and control of the respiratory rhythm and motor pattern," and from anatomical studies that suggest regional specialization (5). This compartmentalized network organization has been studied recently by exploiting *in situ* arterially perfused rat brainstem-spinal cord preparations (246, 252). These preparations allowed sequential rostral-to-caudal microtransections through the brainstem while recording cranial and spinal motor outflows, as well as regional neuronal population activity, to observe transformations of network behavior (278, 310, 311). It was hypothesized that there is a rostral-to-caudal array of network "building blocks" subserving distinct circuit functions that can be revealed as particular compartments are physically removed.

The major results obtained from these studies have been that sequential reduction of the network progressively reorganizes network dynamics, resulting in the emergence of new rhythmogenic mechanisms (Fig. 11) that involve various network components. Specifically, with sequential brainstem transection starting from one at the pontine-medullary junction

and continuing in the caudal direction, the normal three-phase respiratory pattern (Fig. 11B1) is transformed to a two-phase rhythmic pattern lacking the post-I phase (Fig. 11B2), which persisted as long as the BötC compartment was present. With more caudal transections made close to, or at the rostral boundary of pre-BötC, the respiratory activity transforms to a "one-phase" of active inspiratory oscillations originating within the pre-BötC (Fig. 11B3) and generated without critical involvement of phasic expiratory inhibition (278, 310). These results led to the conclusions that: (i) generation of the normal three-phase rhythmic pattern requires the presence of the pons, specifically the excitatory drive from pontine neurons to the VRC; (ii) generation of the two-phase pattern is intrinsic to reciprocal inhibitory synaptic interactions between BötC and pre-BötC neurons, and may also involve the RTN to provide excitatory drive to generate stable behavior; and (iii) the one-phase inspiratory oscillations are generated within the pre-BötC, analogous to those generated by the isolated pre-BötC *in vitro*, and rely on intrinsic bursting mechanisms operating within the pre-BötC excitatory network. These authors inferred the latter conclusion by systematically probing for I_{NaP}-dependent properties by the application of riluzole, a pharmacological blocker of I_{NaP}, which abolished the one-phase oscillations in contrast to the three-phase and two-phase rhythmic patterns that persisted in the presence of riluzole (278, 310); see Figure 12A1–A3. Remarkably, the disturbances of the pre-BötC inspiratory oscillations by blocking I_{NaP} in the reduced mature rat neuraxis *in situ* (Fig. 12A3) were very similar to those obtained with the pre-BötC compartment isolated *in vitro* within neonatal rat medullary slices (152).

This approach of sequentially reducing the pontine-medullary network, coupled with analysis of network activity patterns and systematic probing for pre-BötC autorhythmic mechanisms, provided a new view on the architecture and operation of the respiratory CPG. Two different computational models—a large-scale network model (278, 310) and subsequently a simplified neural activity model (276)—of the spatially distributed respiratory network were developed to reproduce the above experimental findings. These models suggested explanations for transformations of the rhythm-generating mechanism with sequential reduction of the network.

Large-scale network model—The schematic of the model developed in Smith et al. (310) is shown in Figure 13A. Each neuron type in the model is represented by a population of 50 single-compartment neurons described in the H-H style. The model includes the pons and three major medullary compartments: BötC, pre-BötC, and rVRG. The BötC compartment contains two populations of inhibitory expiratory neurons, aug-E and post-I, which inhibit neuronal populations within the pre-BötC and rVRG and each other, and an excitatory population [post-I(e)] that contributes to the post-I component of cVN motor output. All BötC neurons [post-I, post-I(e), and aug-E] have intrinsic adapting spike frequency properties due to high-voltage activated Ca^{2+} (I_{CaL}) and Ca_2^{+}-dependent potassium ($I_{K,Ca}$) currents in these neurons. The pre-BötC compartment includes two neural populations, pre-I/I and "early-I(1)." The pre-I/I population is the key excitatory population of the pre-BötC network that serves as a major source of rhythmic inspiratory synaptic drive in the network. This population projects to the ramp-I population of premotor I neurons of rVRG and to the hypoglossal motor output (HN). The pre-I/I population, as in previous models described earlier, is composed of excitatory neurons with I_{NaP}, a subset of which have intrinsic bursting properties, and mutual excitatory synaptic connections within the population, similar to previous models described in Section "Generation of respiratory oscillations *in vitro*, the pre-Bötzinger complex, and the role of intrinsic cellular mechanisms." At a relatively low level of neuronal excitability or tonic excitatory drive, this population can operate in an I_{NaP}-dependent bursting mode that drives rhythmic network activity. An increase in the average neuronal excitability or in external excitatory drive produces an increase in the burst frequency and, finally, can switch the population activity to

the mode of tonic (asynchronous) spiking (see Fig. 5E). Under normal conditions, most neurons of this population in the model operate in a tonic-spiking mode due to high tonic excitatory input, and are inhibited by expiratory neurons (post-I, aug-E) during expiration. The early-I(1) population of pre-BötC consists of inhibitory interneurons also with adapting spiking properties defined by I_{CaL} and $I_{K,Ca}$. This population receives excitation from the pre-I/I population and serves as a major source of inhibition of all expiratory neurons during inspiration. The rVRG compartment contains the ramp-I and "early-I(2)" populations. As in other models, the ramp-I population of excitatory premotor I neurons drives phrenic motor neurons and inspiratory motor output (PN) and the inspiratory component of cVN discharge. The major role of the inhibitory early-I(2) population in this model is shaping the augmenting patterns of ramp-I neurons via feed-forward inhibition.

As described earlier, the behavior of the respiratory CPG depends on a variety of afferent inputs to different respiratory neurons that allow breathing to maintain the appropriate homeostatic level and adaptively respond to various metabolic demands. These inputs are modeled as "excitatory drives" that carry state-characterizing information provided by multiple sources distributed within the brainstem (pons, RTN, raphé nuclei, and NTS), including those considered to be major chemoreceptor sites (sensing CO_2/pH), and/or receiving input from peripheral chemoreceptors (sensing CO_2/pH and low O_2) [i.e., RTN, raphé, see reference (110, 216, 261)]. These drives are represented in the model for simplicity by three separate sources located in the pons, RTN, and raphé.

Figure 13C1–D1 shows the performance of the intact model. The activity of each population in Figure 13C1 is represented by an average spike-frequency histogram of population activity. The BötC post-I population exhibits decrementing activity during expiration. With the progressive reduction of post-I inhibition from these adapting neurons the activity of the aug-E population develops later in expiration, forming the late expiratory (E2) phase. At the end of expiration, the pre-I/I population of pre-BötC is released from inhibition and activates the early-I(1) population that in turn inhibits all expiratory populations within the BötC. As a result, the ramp-I and early-I(2) populations of rVRG are released from inhibition (with some delay relative to pre-I/I population activity), which initiates the next inspiratory phase. During the inspiratory phase, the activity of the pre-BötC early-I(1) population declines, providing a slow disinhibition of the BötC post-I population. Once the post-I population starts firing, the I activity is inhibited, completing the IOS. The process is then repeated. Simulated motor output patterns (Fig. 13D1) and population activities in this intact model reproduce all major characteristics of the experimentally recorded three-phase respiratory pattern (for comparison see Fig. 11B1), including: (i) an augmenting profile of PN inspiratory bursts; (ii) a preinspiratory (Pre-I) onset of bursts in HN (relative to PN); and (iii) a prominent post-I component in cVN activity.

In summary, the three-phase respiratory rhythm in the intact model emerges from the mutual inhibitory interactions between early-I(1), post-I, and aug-E populations comprising a three-population, mutual inhibitory ring-like structure, with the pre-I/I excitatory population in the pre-BötC participating in the onset of inspiration (see Fig. 13B1).

To model perturbations caused by a "transection" removing the pons (Fig. 13A), the pontine tonic excitatory drive in the model was set to zero, reducing the intact model to a "medullary model." The performance of the medullary model is illustrated in Figure 13B2–D2. Based on experimental evidence that stimulation of the dlP (PB/KF region) provides strong activation of post-I neurons (69, 285), post-I neurons in the model, as in previous models, received relatively strong pontine excitatory tonic drive. In contrast, the aug-E population in the model was assumed to be less dependent on pontine drive but received a major excitatory drive from the RTN and other medullary sources. Thus, removal of the pons

reduced the excitability of post-I neurons relative to aug-E neurons so that the post-I population becomes fully inhibited by the aug-E population, which then exhibits a decrementing spiking frequency pattern (defined by I_{CaL} and $I_{K,Ca}$ as in the other adapting neurons). Therefore, the two-phase rhythm generated in the medullary model was based on an inhibitory half-center circuit of reciprocally interacting inhibitory populations of adapting aug-E and early-I(1) neurons (see Fig. 13B2). In addition, elimination of pontine drive in the model reduces the excitability and firing frequency of the pre-I/I and ramp-I populations, reducing the amplitude of all motor outputs (see Fig. 13D2). Thus the medullary model reproduced all major characteristics of the respiratory pattern recorded experimentally in the corresponding reduced *in situ* brainstem-spinal cord preparations (see Fig. 11B2): (i) the loss of post-I activity in the network and cVN; (ii) a reduced amplitude, square-wave-like/ slightly decrementing activity profile of all inspiratory populations and motor outputs; and (iii) synchronized onset of activity in all motor outputs.

A critical prediction of this model is that with the transformation of the intact three-phase respiratory pattern to a two-phase pattern lacking the post-I phase (e.g., after the pontine transection), some aug-E neurons of BötC should change their firing pattern from an augmenting to a decrementing (post-I/dec-E-like) pattern due to the absence of post-I phase inhibition. This prediction has no explicit experimental support so far and requires experimental testing. However, this transformation has been observed with progressive attenuation of Cl$^-$-mediated synaptic inhibition (310), suggesting asymmetries of the strengths of Cl$^-$-mediated reciprocal inhibition between post-I and aug-E neurons, which should also be further explored experimentally and in the modeling.

The result of a second "transection" in the model is shown in Figure 13B3–D3. The resulting "pre-BötC model" was obtained by removing all model components "rostral" to the pre-BötC compartment (Fig. 13A). This transformation resulted in a further reduction in tonic excitatory drive to the pre-I/I population of pre-BötC and loss of expiratory-related phasic inhibition due to the removal of the BötC populations (see Fig. 13A). These alterations switch the operating state of the pre-I/I population, which starts generating rhythmic bursting activity based on the expression of I_{NaP}-dependent bursting and mutual excitatory interactions within the population (Fig. 13B3 and C3). This rhythmic endogenous bursting drives the activity of the rVRG, and all motor outputs, which now exhibit the one-phase inspiratory oscillations with a decrementing burst shape (Fig. 13D3), similar to that recorded experimentally from the *in situ* pre-BötC preparation (see Fig. 11B3).

To investigate the role of I_{NaP} and compare model behaviors to experimental data obtained with the I_{NaP} blocker riluzole (Fig. 12A1–A3), the mean maximal conductance of persistent sodium channels ($\bar{g}_{NaP}$) was progressively reduced (to zero) in all pre-I/I neurons of pre-BötC. As shown in Figure 12B1, a progressive reduction of $\bar{g}_{NaP}$ in the intact network model caused only a small reduction in the amplitude and frequency of PN inspiratory bursts. In the medullary model generating the two-phase rhythm, the oscillatory frequency and PN amplitude became more sensitive to I_{NaP} block because after removing the pontine excitatory drive, the mean level of I_{NaP} inactivation was reduced, enabling some participation of the pre-I/I population's intrinsic burst-generating properties in the E-I cycle dynamics. However, the two-phase rhythm persisted in the model even at $\bar{g}_{NaP} = 0$ (Fig. 12B2). In the pre-BötC model, the one-phase inspiratory oscillations were generated solely by I_{NaP}-dependent bursting activity within the pre-I/I population. Therefore, reducing $\bar{g}_{NaP}$ progressively decreased PN inspiratory burst frequency and finally abolished the rhythm when $\bar{g}_{NaP}$ became less than a critical value (2.5 nS in Fig. 12B3). These modeling results were also fully consistent with the experimental data (Fig. 12A1–A3).

Activity-based network model—The minimal core network that can reproduce the above three rhythmogenic mechanisms should include the post-I and aug-E neurons of the BötC and the pre-BötC early-I neurons, coupled in a ring-like network with mutually inhibitory interactions. This circuit interacts with the excitatory pre-BötC neurons with intrinsic I_{NaP}-dependent bursting properties that can in some states dynamically participate in the E-I phase transition and inspiratory phase generation (see Fig. 13B1). The state and behavior of this network are also postulated to depend on excitatory drives (see Fig. 13A). Rubin et al. (276) developed a reduced model of this core network to theoretically investigate the functional states and corresponding oscillatory regimes inherent in the network. The schematic of this model is shown in Figure 14A and consists of four neurons: pre-I/I, early-I, post-I, and aug-E, connected according to the scheme shown in Figure 13B1, and three sources of excitatory drive, representing inputs from the pons, RTN and raphé nuclei. Neurons in this circuit were described by activity-based (nonspiking) single neuron models. The formulations of the pre-I/I neuron model also included an explicit representation of the slow inactivation mechanism of I_{NaP} to permit consideration of the role of this conductance mechanism. These simplified descriptions allowed the authors to apply analytic techniques (70) such as fast-slow variable decomposition methods and perform bifurcation analysis of transitions between different oscillatory regimes (states) and between different phases within each regime. The model reproduced all three regimes described earlier resulting from simulated transections. Figure 14B shows the performance of the intact model under basal conditions where activity of all four neurons represents the three-phase respiratory pattern.

This model was used to investigate the effects of variations in the total excitatory drive to each neuron on the oscillation period (T) and on the durations of inspiration (T_I) and expiration (T_E). This analysis of the control of oscillation frequency and phase durations had not been performed with the large-scale network model and was facilitated by the reduced complexity of the activity-based model. Some of the results are shown in Figure 14C and D. An increase in total drive to the pre-I/I neuron produced monotonic shortening in the durations of both expiration and, to a lesser degree, inspiration, with the maximal value of T equal to 4.4 times its minimal value (Fig. 14C). An increase in total drive to the aug-E neuron produces a strong increase in T_E and a small increase in T_I, leading to an overall large increase in T (Fig. 14D).

In the experimental and modeling studies of Rybak et al. (278) and Smith et al. (310) brainstem transections as described earlier were used to uncover different rhythmogenic mechanisms embedded in the network. Such dramatic perturbations, however, do not occur under natural conditions. Nonetheless, similar transformations of rhythmogenic mechanisms may occur in the intact network under different physiological and/or metabolic conditions associated with alterations of excitatory drives to particular neural populations. Therefore Rubin et al. (276) investigated possible transformations of mechanisms induced by gradual changes of the various drives incorporated in the intact model. Figure 15 shows the sequential transformation of the respiratory pattern occurring with gradual reduction of total excitatory drive to the post-I neuron from all external sources (D_3). This total drive represents a weighted sum of drives (d1–d3) from three different sources in the model (pons, d_1; RTN, d_2; and raphé, d_3; see Figure 14A) to the neuron 3 (post-I) in the model ($D_3 = c_{13}d_1+c_{23}d_2+c_{33}d_3$). With the reduction of D_3 to about 0.62, the intact model continued generating oscillations with a regular (called "biological" or "bio") three-phase pattern (Figures 15A and A1). Further reduction of D_3 resulted in the emergence of high-amplitude late-E activity in the aug-E neuron (at the end of expiration) expressed in every third cycle, then (with further D_3 reduction) this late-E activity was expressed in every second cycle (Fig. 15B and B1), and finally (approximately at $D_3 = 0.58$) in each cycle (Fig. 15C and C1). This latter pattern was called a "mathematical" or "math" three-phase pattern, because it

involved three fast jumps between surfaces of fast subsystem equilibrium points (see 273). Further reduction of D_3 (approximately below 0.46) produced multiple oscillations during expiration, with alternating activity of aug-E and post-I neurons (not shown), and with D_3 below about 0.42, a biphasic-E activity (with post-I and late-E components) emerged in the aug-E neuron output (Fig. 15D and D1). With further reduction of D_3 (below about 0.34), the post-I neuron became fully inhibited during expiration by the aug-E neuron and the intact model switched to the generation of two-phase oscillations with lack of post-I activity (see Fig. 15E and E1). Therefore, the model demonstrated that a gradual reduction of excitatory drive to the post-I neuron can sequentially transform the network state (and output oscillations) from a state producing a regular (bio) three-phase oscillatory pattern to a state generating oscillations with enhanced late-E activity ("math" three-phase regime), and then to a state producing two-phase oscillation patterns. The latter are similar to those generated by the medullary model described earlier after complete removal of pontine drive.

In summary, the models described in this section have suggested that the pontine-medullary respiratory network has a specific spatial and functional organization extending from the rPons to the caudal VRC. Although some respiratory neuron types (e.g., post-I, aug-E, and early-I) incorporated in the models are not strictly localized within particular medullary compartments, but rather are distributed throughout the VRC (18, 72), each compartment nevertheless contains dominant populations that may define a specific functional role of each compartment. A basic principle suggested by the modeling and experimental results is that each compartment operates under control of more rostral compartments, constituting a rostro-caudal functional hierarchy of interacting circuit building blocks (310, 311). Specifically, I activity of rVRG bulbospinal premotor neurons is formed by rhythmic excitatory synaptic drive from the pre-BötC I neurons and phasic inhibition from BötC expiratory neurons. In turn, the pre-BötC is controlled by the more rostrally positioned BötC that inhibits the pre-BötC during expiration, whereas the RTN and pontine nuclei provide excitatory drives to BötC, pre-BötC and rVRG. The pontine activation of expiratory BötC populations (especially post-I neurons) provides a widely distributed inhibition within the network during expiration that appears critical for rhythm and pattern generation under normal conditions.

As noted by Smith et al. (310), the behavioral repertoire of the respiratory CPG likely necessitates a flexible organization of respiratory circuits, permitting multiple state-dependent modes of operation under different physiological and pathophysiological conditions. Changes in metabolic conditions such as levels of carbon dioxide/pH, or oxygen that alter the balance of excitatory and inhibitory drives (295, 296), as well as excitability of pontine, RTN, BötC and pre-BötC neuronal populations can change network interactions, producing transformations from the normal three-phase rhythmic state to the other rhythmogenic states inherent in the system. For example, hypocapnia can convert the network three-phase to a two-phase rhythmic pattern (328). Severe hypoxia transforms the system to generate a one-phase, I_{NaP}-dependent inspiratory gasping rhythm (247), which represents a functional unembedding of I_{NaP}-dependent oscillatory mechanisms intrinsic to the pre-BötC.

Thus an emerging view (311), which has been bolstered by the modeling, is that the respiratory CPG architecture incorporates multiple rhythmogenic mechanisms within the spatial and functional organization of the brainstem respiratory network. This network has rhythmogenic capabilities at multiple levels of cellular and network organization with oscillatory mechanisms ranging from inhibitory network-based synaptic interactions, to neuronal conductance-based endogenous mechanisms. The emergence of each oscillatory mechanism depends on the metabolic and functional state of the system and is controlled by multiple sources of drives located within the medulla and pons. Some of these drives are

sensitive to the levels CO_2/pH and O_2 that provide for homeostatic regulation, while others arise from multiple descending systems involved in sensorimotor integration. The architecture of the core circuitry including an embedded pre-BötC excitatory kernel provides multiple nodes for external control of respiratory oscillation frequency and phase durations as well as for functionally transforming the mode of CPG operation.

Coupled oscillators concept and "active" expiration

As reviewed earlier, the respiratory rhythm and coordinated motor pattern during breathing is generated within the medullary VRC with the pre-BötC and BötC complexes containing core circuits of the CPG. The respiratory oscillations generated within this core circuitry are defined by the intrinsic biophysical properties of respiratory neurons involved, the architecture of network interactions between I and E neural populations, and input drives from other brainstem compartments, including the pons, RTN, and raphé nuclei. Information on the metabolic state of the system, such as levels of CO_2/pH, or O_2 provided by the RTN, raphé, and peripheral chemoreceptors (via the NTS), can reorganize the respiratory network and operating rhythmogenic mechanisms depending on metabolic conditions.

A distinct site of neural oscillations, namely, the pFRG, putatively involved in respiratory function was initially identified *in vitro*, in the isolated neonatal rat brainstem-spinal cord preparation (226, 227). The pFRG seems to reside within, or to overlap with, RTN. It has been proposed that RTN/pFRG oscillations drive abdominal motor activity, expressing preI (or late-E) or biphasic-E discharges (with pre-I and post-I components) in the abdominal motor output when the system operates in the active expiration state to force exhalation (86, 132, 133). Several competing concepts concerning the physiological role of RTN/pFRG oscillations have been suggested and debated (87). These include the suggestion that the pFRG represents the primary inspiratory oscillator (231, 232) and the dual oscillator concept that considers the RTN/pFRG to be an independent expiratory rhythm generator that is coupled with a distinct inspiratory rhythm generator in the pre-BötC (86, 132, 133). However, the exact physiological role of pFRG oscillations, the specific conditions for their emergence, and the nature and mechanisms of the interactions between the BötC-pre-BötC and RTN/pFRG oscillators are not yet understood. Several computational models with various levels of complexity have been developed to explore these issues.

Two relatively simple computational models were initially proposed to simulate coupling between pre-BötC and RTN/pFRG oscillators and suggest possible mechanisms governing their interactions. Joseph and Butera (140) used an abstract canonical model composed of two identical phase oscillators. Wittmeier et al. (345) simulated both oscillators as single neurons with I_{NaP}-dependent bursting properties as originally described for the pre-BötC by Butera et al. (29). The connections between the oscillators proposed in both models were: (i) an excitatory input from the RTN/pFRG oscillator to the pre-BötC oscillator, providing entrainment of the latter by the former and (ii) an inhibitory input from the pre-BötC oscillator to the RTN/pFRG oscillator, providing inhibition of the latter during inspiration. These connections were sufficient to reproduce the regime of "quantal slowing" of the pre-BötC oscillator exhibiting phase relationships as observed experimentally under conditions of reduced excitability of pre-BötC neurons (189), which was considered as a test for these models.

Molkov et al. (200) and Rubin et al. (271) extended the models of Smith et al. (310) and Rubin et al. (276), respectively, to investigate: (i) the metabolic state-dependent conditions for the emergence of RTN/pFRG oscillations, (ii) the neural mechanisms underlying interactions between the BötC-pre-BötC and RTN/pFRG oscillators, and (iii) the role of these interactions in shaping the coordinated pattern of respiratory motor outputs under different conditions. In this connection, Molkov et al. (200) analyzed previously published

results (3) and additional experimental data to find critical regimes of coupling between RTN/pFRG and BötC-pre-BötC oscillations, including a regime of "quantal acceleration" of late-E oscillations with the development of hypercapnia, described later and shown in Figure 16.

The experimental observations modeled were obtained from studies using the *in situ* arterially perfused rat brainstem-spinal cord preparations, in which under baseline normocapnic metabolic conditions (95% O_2, 5% CO_2), the abdominal nerve motor output (AbN) typically exhibits a low-amplitude expiratory (post-I) activity (3, 200). Switching to hypercapnic (7%–10% CO_2) and/or hypoxic conditions evoked large amplitude late-E (also called pre-I) bursts in the AbN (3). Figure 16 (200) shows that these late-E discharges emerge in AbN at 7% CO_2 followed by a progressive increase in their frequency as the CO_2 concentration in the perfusate of the experimental preparation is incremented to 10%. Importantly, although the frequency of late-E bursts increases with CO_2 these bursts remained coupled (phase-locked) with inspiratory bursts in the PN, cVN, and HN (Fig. 16A2–A4). With the development of hypercapnia, the ratio of late-E burst frequency to the PN burst frequency showed a step-wise (quantal) increase from 1:5 and 1:4 (seen in Fig. 16B) to 1:3, 1:2, and, finally, to 1:1 (Fig. 16A2–A4 and B). On returning CO_2 to the control levels, the ratio showed a step-wise reversal. Similar hypercapnia-evoked AbN late-E discharges phase-locked to PN with a step-wise increase of their frequency with increasing CO_2 levels were demonstrated *in vivo* by Iizuka and Fregosi (128). This process was called quantal acceleration of late-E activity with development of hypercapnia (200, 271).

Based on a series of *in vitro* and *in vivo* studies, Feldman and collaborators (86, 132–134, 243) hypothesized that the source of pre-I (late-E) oscillations in AbN is located within RTN/pFRG. Consistent with this suggestion, Abdala et al. (3) demonstrated that a population of neurons becomes rhythmically active in this region during hypercapnia, suggesting that the AbN oscillation may be an indicator of the corresponding RTN/pFRG oscillations, although a causal role of these oscillations remains to be established. Modeling studies (345) have hypothesized that RTN/pFRG oscillations involve an intrinsic I_{NaP}-dependent mechanism. This suggestion was consistent with the observation that the I_{NaP} blocker riluzole abolishes rhythmic embryonic parafacial (e-pF) neuronal activity (93, 333). Similarly, it has been shown that riluzole abolished the AbN late-E activity evoked by hypercapnia *in situ* (200), while rhythmic respiratory activity persisted in other nerves. This result was consistent with the *in vivo* and *in situ* studies showing that respiratory rhythm generation in the intact brainstem under normal conditions was not critically dependent on I_{NaP} (247, 278, 310), as discussed earlier.

The schematic of the model developed by Molkov et al. (200) by applying the earlier experimental findings as prerequisites is shown in Figure 17A. In extending the Smith et al. model (Fig. 13A), an additional late-E neuronal population was included in RTN/pFRG compartment to represent a pFRG oscillator. Also, a bulbospinal-E population of cVRG was added to provide excitatory bulbospinal drive generating the abdominal motor output. The late-E population in the model was biophysically identical to the pre-BötC pre-I/I population and consisted of neurons containing I_{NaP} and mutual excitatory interactions within the population. Importantly, although the pre-I/I and late-E populations were identical, their behaviors were different due to differences in their excitability in the model. Specifically, under normal conditions, the pre-I/I population received a strong total excitatory drive that kept this population in the state of sustained spiking activity essentially independent of I_{NaP} until phasic external inhibition terminated its activity [see references (278, 310)] In contrast, a relatively weak "hypercapnic" drive could evoke I_{NaP}-dependent bursting behavior in the late-E population.

The following connections between the late-E population and other neural populations were incorporated in the model (Fig. 17A): (i) excitatory connection from the RTN/pFRG late-E to the excitatory pre-I/I population of pre-BötC, allowing entrainment of the pre-BötC oscillations by late-E oscillations; (ii) inhibitory connection from the inhibitory inspiratory population [early-I(1) of pre-BötC] to provide inhibition of late-E neurons during inspiration; (iii) excitatory connection from the late-E to the cVRG compartment to drive the AbN motor output; (iv) excitatory connections from the late-E to the inhibitory populations aug-E (of BötC) and early-I(2) (of rVRG), which both inhibit the premotor ramp-I population to produce an additional delay in the onset of PN discharge by the preceding late-E burst; and finally (v) inhibitory connection from the post-I population of BötC to the late-E population.

The performance of the model under normal metabolic conditions simulated (i.e., when the late-E population in the RTN/pFRG is not active) is shown in Figure 17B-D. Panel B shows the integrated activities of key respiratory populations, panel C exhibits the traces of membrane potential of single respiratory neurons (randomly selected from each population), and panel D shows the dynamics of motor outputs (PN, cVN, and HN). The model generates the three-phase eupneic-like respiratory pattern similar to that observed in the *in situ* preparations under control conditions.

The behavior of the model during hypercapnia is shown in Figure 18. Progressive hypercapnia was simulated as a linear increase of a "hypercapnic" excitatory drive to the lateE population (see Figures 17A). The behavior of the model late-E neurons depends on: (i) their I_{NaP}-dependent intrinsic properties, (ii) the phasic inhibition that these neurons receive from the post-I population of BötC during expiration and from the early-I(1) population of pre-BötC during inspiration, and (iii) the hypercapnic excitatory drive. The late-E population begins generating bursts when hypercapnic drive exceeds some threshold (see Fig. 18B) that is mostly defined by the post-I inhibition. This post-I inhibition progressively reduces during expiration, allowing the late-E bursts to appear only close to the end of expiration. The post-I and early-I inhibition of late-E neurons, together with late-E excitation of pre-BötC pre-I/I neurons, provide the coupling of RTN/pFRG (late-E) and BötC-pre-BötC oscillations. Similar to the experimental results with progressive hypercapnia (see Fig. 16 and also 128), the progressive increase of hypercapnic drive in the model evokes a step-wise increase in AbN burst frequency (quantal acceleration) with a ratio to PN burst frequency sequentially jumping from 1:4 to 1:3, then to 1:2 and, finally, to 1:1 (see Fig 18A1–A3, B and compare with Figure 16A2–A4,B). Figure 18C shows the activity of a single pre-BötC pre-I/I neuron and a single late-E RTN/pFRG neuron when the ratio of late-E:pre-I/I discharge frequencies is equal to 1:2. A more detailed analysis of this quantal acceleration behavior using dynamical systems theory methods applied to a simplified mathematical model can be found in Rubin et al. (271).

Figure 18D shows the result of modeling of the effect of riluzole, the I_{NaP} blocker, on the system behavior during hypercapnia. The effect of riluzole was simulated by reducing the I_{NaP} maximal conductance to zero in all late-E and pre-I/I neurons. The figure shows that the suppression of I_{NaP} during hypercapnia (1:1 coupling regime) silenced activity of the late-E AbN (and RTN/pFRG late-E neurons) but did not abolish BötC, pre-BötC, and PN oscillations.

It is important to notice critical differences between the model of Molkov et al. (200) and the earlier model of Wittmeier et al. (345). In the Wittmeier et al. model, bursting in the pre-BötC is I_{NaP}-dependent. This means, for example, that application of I_{NaP} blocker riluzole should eliminate both rhythms. This is not consistent with the behavior of the intact system *in vivo* under normal conditions. In contrast, in the Molkov et al. model (Fig. 20), as well as

in the preceding models of Rybak et al. (278) and Smith et al. (310), respiratory oscillations generated by the BötC/pre-BötC core do not critically depend on I_{NaP} under normal conditions. In addition, the Wittmeier et al. model did not consider the post-I inhibition of the RTN/pFRG oscillator. Moreover, in the Wittmeier et al. model both oscillators (pre-BötC and RTN/pFRG) operate under normal conditions, whereas in the Molkov et al. model this can only occur during hypercapnia or hypercapnic hypoxia.

The model of Molkov et al. (200) was able to reproduce several experimentally observed phenomena, including the quantal slowing of the pre-BötC and PN oscillations with the reduction of excitability of pre-BötC circuits that had been previously demonstrated experimentally using administration of opioid agonists (132, 133, 189) as well as transformation of the late-E activity to a biphasic pre-I/post-I pattern with the development of hypoxic hypercapnia (3). Furthermore, the model suggested that RTN/pFRG oscillations are not observed under normal metabolic conditions because of inhibition of the RTN/pFRG oscillator by inhibitory feedback from the BötC–pre-BötC core network, so that a suppression of synaptic inhibition in the late-E population should evoke bursing activity in both the RTN/pRFG late-E population and in the AbN under normal conditions (Fig. 19A). Consistent with this prediction, blocking/attenuating GABAergic synaptic transmission bilaterally within the ventrolateral RTN by microinjection of the GABA$_A$ receptor antagonist bicuculline (10 μmol/L) under normal metabolic conditions (5% CO_2) evoked a low-amplitude late-E activity, which then disappeared with washout of the antagonist (Fig. 19B and C) (244). Other recent experimental studies report similar results of disinhibiting the RTN/pFRG region (243).

Interactions between the BötC-pre-BötC and RTN/pFRG suggested by the model of Molkov et al. (200) are summarized in Figure 20. In this schematic, the BötC-pre-BötC oscillator controls the emergence of RTN/pFRG oscillations, their frequency, and coupling to BötC-pre-BötC oscillations, which is evident by the regime of quantal acceleration of late-E activity with the development of hypercapnia (Figures 16 and 18). Therefore, the late-E activity in AbN (and probably in RTN/pFRG) is not generated under normal metabolic conditions. The excitability of the late-E population in RTN/pFRG, however, as suggested by the experimental observations noted earlier, is highly sensitive to hypercapnia. Therefore, progressive hypercapnia producing depolarization of late-E neurons can overcome the inhibition of RTN/pFRG by BötC-pre-BötC circuits and initiate late-E rhythmic activity that goes through quantal acceleration until the late-E activity reaches 1:1 coupling with the BötC-pre-BötC oscillations. In contrast, strong hypoxia or anoxia can evoke the RTN/pFRG oscillations through a reduction of inhibition, specifically the post-I inhibition, and produce an effect similar to hypercapnia by shifting the balance between inhibition and excitation at the level of RTN/pFRG late-E neurons.

Other network models

Several other models of respiratory circuits have been developed employing different approaches to explore potential mechanisms of rhythm generation. Matsugu et al. (186) studied the dynamical behavior of a "compound" CPG model consisting of a simple mutual inhibitory (I-E) half-center neural network oscillator as a minimal model of the respiratory rhythm generator, driven by either a constant or periodic source of inputs of varying amplitudes, frequencies, and phases, such as occur with chemoreceptor drives, afferent feedback from the lungs, and other oscillatory inputs (e.g., cardiac- or locomotor-related). In particular, the half-center inhibitory network oscillated spontaneously only when both neurons received adequate and proportionate constant excitation, and in the presence of a periodic input, this spontaneous rhythm was stably entrained by: (i) antiphase periodic inputs with alternating drives to both interacting inhibitory neurons and (ii) a single periodic drive to only one of the inhibitory neurons. In-phase inputs of similar magnitude and phase

relationships to both neurons disrupted the entrained oscillations in various ways, including harmonic and phase distortions, and the emergence of chaotic-like behavior. The "apneic" episodes with repetitive alternation of active (intrinsic oscillation) and inactive (cessation of oscillation) states were exhibited when the network was driven by a moderate periodic input of low frequency. Similar results were demonstrated in other, more complex oscillator models including a three-phase activity respiratory network model adapted from Gottschalk et al. (101). In general, these simulation results demonstrated how a simple CPG model with a minimum number of neural elements and "mild" nonlinear properties of the elements could reproduce many complex dynamical behaviors under various inputs including periodic drive.

Dunin-Barkowski et al. (67) proposed a model of the respiratory CPG incorporating at the neuronal level interactions between Ca^{+2}-dependent K^+ channels in respiratory neurons (191) and Ca^{+2}-induced Ca^{+2}-release from intracellular stores (123, 197, 198, 294) as a potential dynamic mechanism for rhythm generation at cellular and network levels. Addressing the debate about pacemaker versus inhibitory network mechanisms for rhythm generation, these investigators sought to define Ca^{2+}-dependent mechanisms that could simultaneously underlie neuronal bursting pacemaker properties as well as support inhibitory-based network oscillations due to neuron activity adaptation arising from the modeled Ca^{2+}-dependent processes. The model, consisting of integrate-and-fire neurons, demonstrated that individual neurons with these Ca^{2+}-dependent mechanisms could exhibit conditional bursting pacemaker properties when subjected to steady excitatory inputs. With the addition of reciprocal inhibitory interactions between two neuronal populations composed of these cells, different regimes of rhythmic activity emerged. Weak inhibitory synaptic interactions between the two populations could synchronize their activity, but as the strength of inhibitory synaptic connections was increased, the model simulations produced unsynchronized bursting pacemaker activity of individual neurons, then synchronous periodic bursts, and finally reciprocal (I- and E-like) rhythmic activity of the populations. The authors proposed that both pacemaker and coordinated rhythmic network behaviors could manifest from basic Ca^{2+}-dependent mechanisms operating at the cellular level.

A model for the pre-BötC network *in vitro* was developed by Kosmidis et al. (154) to investigate if rhythms could be generated by an excitatory network composed of nonpacemaker neuron models without inhibitory interactions, thus addressing the question of potential mechanisms supporting emergent network rhythms. The key neuronal membrane conductances implemented in the neuron models were low- and high-threshold Ca^{2+} currents and the Ca^{2+}-dependent K^+ current, which under certain excitability conditions could collectively generate cellular-level periodic bursting activity. At the network level, the simulations showed that an increase of external K^+ concentration induced rhythmic activity attributable to cellular rhythmic bursting or emergent network rhythms, depending on model parameters. Gaussian noise also induced rhythmic activity dependent solely on network properties, since individual neurons subjected to similar noisy stimulation did not exhibit rhythmic bursting capability. In all cases in this model, the Ca^{2+}-dependent K^+ current played a central role in burst termination and control of interburst duration. Network dynamics with simulated periodic inhibition was also investigated with the model, suggesting that activation of the Ca^{2+}-dependent K^+ current during the repolarization phase following inhibition contributed to a ramping population activity of the emergent rhythm. This model demonstrated emergent excitatory network rhythms and a possible role of the Ca^{2+}-dependent K^+ current in rhythm generation in the presence and absence of network inhibition.

Modeling of Other Reflexes and Respiratory-Related Behaviors

Pontine and vagal control of the respiratory pattern

Vagotomy or withholding lung inflation during fictive "neural inspiration" in anesthetized or decerebrate animals results in an increased rhythmic respiratory modulation of PRG neurons. This change has been attributed to a loss of PSR-mediated inhibitory gating of an inspiratory efferent copy mechanism that modulates PRG activity (Fig. 21A and B) (38) to partially compensate for the loss of PSR effects on the IOS mechanism (see previous sections). Although this view is supported by the appearance of apneustic breathing (prolonged inspiratory periods) in vagotomized animals with pontine lesions (177, 211, 321, 324, 342), the activity profiles of some pontine neurons following vagotomy are not simply accounted for by this standard gating model (60, 208). This observation and the concept of an integrated raphé-pontomedullary network (222) motivated a test of the hypotheses that raphé neurons can also have altered firing patterns during withheld lung inflation or vagotomy leading to the development of an alternative to the PSR inhibitory gating model (208).

The new model was suggested by earlier observations on VRC-raphé functional connectivity (167) and respiratory phase-dependent firing synchrony among raphé neurons even when their individual firing rates had no respiratory modulation (164). In the model (Fig 21C), a tonic population receives two inputs: an excitatory inspiratory efferent copy from the VRC I-Aug population and a balancing feed-forward inhibitory input from neurons also driven by the I-Aug neurons. Tonic neurons without respiratory modulated firing rates in the model circuit exhibited phase-dependent synchrony due to shared excitation and delayed inhibition (60). Next, the excitability of the inhibitory population was set to be less than the tonic target population, based on differential excitability found in the raphé [e.g., reference (145)]. Under these conditions, the number of tonic neurons with respiratory modulation increased following the simulated loss of PSR input (vagotomy) (Fig. 21D), reproducing altered firing patterns similar to those recorded *in vivo* with vagotomy (Fig. 21E) (60, 208). These results suggest that such a circuit can transform NRM tonic neurons into different categories of respiratory modulated neurons potentially involved in phase-switching and pattern tuning functions under conditions of altered efferent copy drive or with changes in other inputs to embedded feed-forward inhibitory populations.

Baroreceptor modulation of breathing

As noted in Section "The nucleus of the solitary tract," a substantial body of evidence has established that changes in arterial blood pressure modulate breathing (188). *In vivo* experiments that included perturbations of baroreceptors and blood pressure together with multisite neuron recordings and spike train analysis have detected functional interactions between the medullary raphé and VRC E-Dec neurons consistent with roles in the baroreflex-mediated reduction of inspiratory drive and prolongation of expiratory duration (162). Neuron responses and correlation linkage maps suggested that raphé circuits promote parallel excitatory and disinhibitory influences on VRC E-Dec neurons, including a "tonic" E-Dec population with inhibitory actions on premotor bulbospinal or phrenic motor neurons (Fig. 22A). Incorporating these additional raphé populations and inferred connectivity to the ponto-medullary network model of Rybak et al. (279) reproduced experimentally observed changes in the phrenic motor pattern during simulated baroreceptor stimulation (Fig. 22B) (166). These results also support the hypothesis that a tonic expiratory neuron population within the VRC can have significant inhibitory and disinhibitory modulatory influences on inspiratory populations during the inspiratory phase of the respiratory cycle (168).

Other related work has modeled baroreceptor influences on respiratory-sympathetic interactions and their contributions to cardio-respiratory coupling (8).

Modeling of cough

The cough reflex is an important airway defensive mechanism. An early network model and simulations led to predicted roles for, and the reconfiguration of, the VRC network during cough (303). Multisite *in vivo* neuron recordings during mechanical evocation of fictive cough in cats and activity correlation analysis supported many of the model's predictions and suggested specific network interactions involved in cough motor pattern generation (302). A subsequent model (279) incorporated the earlier hypotheses and later experimental results, including measurements of pontine neuron activity during fictive cough (304). The model proposed that stimulation of airway cough receptors evokes impulses in second-order neurons that act directly or indirectly on specific VRC and PRG populations (Fig. 8), causing reconfiguration of the respiratory network to produce the cough motor pattern. The cough motor pattern is generated, at least in part, through VRC neurons providing drive to muscles during normal breathing. The model generated realistic cough-like motor patterns (Fig. 23) in phrenic, lumbar, and laryngeal motor neurons, and functionally antecedent VRC and pontine neuron populations in the model had activity profiles similar to those observed *in vivo* (9, 302, 305). Details of the model may be found in Rybak et al. (279).

Perspectives and Some Future Directions

Some caveats and limitations of current models

Modeling neurobiological processes at all levels of respiratory circuit and system organization undoubtedly becomes critically important for understanding the complex, multi-scale dynamical operation of the respiratory control system. While certain key brainstem respiratory structures, containing local microcircuits with the specific features of cellular/circuit electrophysiological behavior, and their general functional roles have been identified to some extent as highlighted here, the current models discussed in this review remain in many respects speculative. The modeling, by necessity, relies heavily on simplifications and assumptions about many aspects of structural-functional organization. This reflects not only the lack of detailed experimental data necessary to constrain the models, but also as noted at the beginning of this article, decisions made by the modelers on the degree of neurobiological detail and computational complexity to be incorporated in attempting to address specific issues.

As with all other neural systems, there are numerous unknowns about cellular properties, including the identity and biophysical details of ionic conductances and cytoplasmic signaling cascades involved as well as various other phenotypic properties of different respiratory neuronal types such as cellular somatodendritic architectures. Likewise, there are many uncertainties regarding network topology and interactions, including details of patterns of axonal projections, somatodendritic distributions of synaptic inputs and connection strengths between different respiratory neuronal phenotypes with potentially plastic adjustments under various conditions. In general, the spatial organization of respiratory microcircuits and their interconnections are currently not known in any detail. Furthermore, as we have attempted to delineate, debates are ongoing about the basic processes involved in respiratory rhythm generation, spatiotemporal pattern formation, and other aspects of neural system operation. The more "realistic" models described here that have attempted to address these issues are in fact relatively simple, despite the large relatively unconstrained parameter sets incorporated, and ultimately such models may have to become more detailed both structurally and biophysically to accurately represent the complex processes underlying neural control of breathing. At present, the minimum set of

features/parameters required to accurately model particular respiratory network processes have not been clearly defined—a general problem in network modeling [for insightful perspectives on problems connected with variability in neuronal and network properties, parameter set selection/tuning and constraints in neural network modeling see references (1, 46, 182, 183)].

Integrated multiscale respiratory control system models

Ultimately, large-scale models of the respiratory system with full integration of neural and peripheral respiratory components are required for understanding breathing and respiratory control. Several integrated models incorporating both a neural control component, represented with varying levels of complexity, and other elements, including various respiratory and cardiovascular non-neural subsystem components, have been developed over the years in parallel with models of the respiratory neural network. Integrative models have enhanced our understanding of mechanisms and conditions that contribute to ventilatory instability and variability. Models have considered the effects of controller gain, delays, and response lags in chemoreflex loops, optimization, and changes due to fluctuations in system state and blood pressure (13, 65, 144, 254).

A recent example incorporating a hierarchy of subsystem components is a model of respiratory and cardiovascular control in sleep-disordered breathing (34). This study includes a succinct summary of the history of the integrated modeling approach. Other recent examples include models dealing with homeostasis during exercise (57, 253) and models coupling neural dynamics to peripheral gas exchange and transport with feedback control mechanisms regulating blood and brain CO_2 and O_2 levels based on dynamic control theory (Fig. 24) (12, 13, 175).

Models addressing the role of the brainstem network in coordinating laryngeal and diaphragmatic motor activities that typify eupneic and adaptive patterns of breathing involving upper airway control will benefit from extending the models to include representations of the airways, lungs, and associated respiratory muscles. "Physiome-style" multiscale models (e.g., 41, 126) that include detailed structural-dynamical models of peripheral respiratory system components are needed to permit virtual experiments and simulations of system behavior under various perturbations and states.

Incorporation of network plasticity and respiratory network control by neuromodulators

The respiratory CPG is functionally plastic for state-dependent behavioral control [e.g., reference (158)], which is likely achieved in part through neuromodulatory mechanisms, including regulatory systems such as the medullary raphé nuclei (89). In general, neuromodulators such as monoamines and neuropeptides modify intrinsic properties of neurons and/or the strengths of synaptic connections and can orchestrate different neural activity patterns in motor pattern generation networks [e.g., references (107, 120, 143)]. As indicated earlier, there is already a large body of experimental data on interactions among neurons of the medullary raphé nuclei, which coexpress serotonin and neuropeptides, and the ponto-medullary respiratory circuits (6, 58, 161, 162, 167, 222, 223, 255).

The raphé has been proposed as a site for transforming and transmitting information from various external and internal sensory systems. This includes roles in cardio-respiratory coupling (207), and contributions to the induction and expression of respiratory LTF induced by repeated intermittent hypoxia, raphé stimulation, or carotid chemoreceptor stimulation (89, 185, 192, 196, 204).

Disruption of vagal feedback by repeated obstructive apneas can trigger another form of LTF that is independent of hypoxia and that differentially modulates hypoglossal motor

neuron activity and genioglossus muscle tone (329). Multiscale network models that incorporate modifiable cellular properties and synaptic connections in the context of mechanisms generating respiratory LTF and other aspects of neuronal and circuit plasticity are needed.

Emerging technologies: Large-scale parallel computing; interactive computational models; computationally based neuroanatomy and circuit architecture

Various modeling approaches and software packages have been used to simulate brainstem networks for breathing and breathing-related behavior. An important direction for future research will be the integration of increasingly refined multiscale neural network models with other subsystem modules and the tools that facilitate their interconnection, visualization of states, and analysis of their dynamic behavior. As network components and modeled subsystems with associated model parameter sets increase in complexity, large-scale modeling is required and the trend of distributing individual simulations over many processors [e.g., reference (210)] is likely to accelerate. Interactive modeling and visualization tools are also needed. For example, the modeling environment used by Rybak et al. (279) permits visualization of simulated population dynamics in an atlas-based three-dimensional (3D) coordinate system and transection lesions through arbitrary planes. In general, the detailed representation of local and distributed networks in 3D space will allow further model development and simulations of various brainstem lesions and other regional and population-specific physiological and pharmacological perturbations that generate various reproducible alterations of the respiratory motor pattern. Simulation and visualization tools developed for other data-driven physiological [e.g., reference (41)] and neural system modeling [e.g., references (99, 100)] enterprises, and available in the public domain, will likely be applied to respiratory system modeling.

Connections in most of the respiratory network models considered in this review have been based on data from many laboratories and complementary experimental approaches guided by antecedent anatomical and perturbative (lesion, inactivation, and microstimulation) studies. Many specific connections between model populations have been inferred from measurements of phase-dependent synaptic activity in single neurons [e.g., reference (264)], spike-triggered averaging of synaptic potentials [e.g., reference (72)], and spike-train correlation methods [e.g., reference (10)]. Predictive models have also included more speculative connections (the reader is referred to papers cited herein for details). Clearly new experimental strategies and technologies for mapping circuit connections and functional interactions are required to further advance understanding of network connectivity.

Correlation linkage maps generated from neuronal activity measured at many sites simultaneously with electrode arrays [e.g., reference (222)], together with optical (270) and optogenetic methods (2, 50, 58, 243) for monitoring and perturbing individual neurons and populations with specific phenotypes, are increasingly providing insights into respiratory network architecture. The emergence of new computationally based technologies to reconstruct quantitatively neuronal morphology and circuit architecture, including the "connectome" initiatives that involve mapping neural circuits at unprecedented levels of structural resolution [e.g., references (26, 122, 300)] will likely have impact on future efforts to define structure-function relationships in respiratory circuits. The large body of computational neuroscience theory and approaches, some of which are noted in this review, will undoubtedly continue to provide impetus accelerating further data-driven model development.

Conclusion

Computational models of the respiratory network have provided explicit theoretical and conceptual frameworks for synthesizing experimental data from various experimental approaches and understanding neurophysiological mechanisms generating respiratory movements. The models reviewed in this article describe neural mechanisms controlling breathing at different degrees of abstraction and span several levels of neurobiological organization and time scales. Models are most valuable when they explain observed phenomena, highlight gaps in knowledge, lead to experimentally testable predictions, and define constraints on system organization. The models described here in most cases were developed iteratively with coordinated experimental studies. This data-driven modeling approach has advanced our understanding of respiratory network architecture and neural mechanisms underlying generation of the respiratory rhythm and pattern, including state-dependent expression of different pattern generation mechanisms that enable a wide repertoire of respiratory and breathing-related behaviors under various physiological conditions.

Acknowledgments

References

1. Abbott LF. Theoretical neuroscience rising. Neuron. 2008; 60:489–495. [PubMed: 18995824]

2. Abbott SBG, Stornetta RL, Fortuna MG, Depuy SD, West GH, Harris TE, Guyenet PG. Photostimulation of retrotrapezoid nucleus Phox2b-expressing neurons *in vivo* produces long-lasting activation of breathing in rats. J Neurosci. 2009; 29:5806–5819. [PubMed: 19420248]

3. Abdala APL, Rybak IA, Smith JC, Paton JFR. Abdominal expiratory activity in the rat brainstem-spinal cord *in situ*: Patterns, origins and implications for respiratory rhythm generation. J Physiol. 2009; 587:3539–3559. [PubMed: 19491247]

4. Alheid GF, Gray PA, Jiang MC, Feldman JL, McCrimmon DR. Parvalbumin in respiratory neurons of the ventrolateral medulla of the adult rat. J Neurocytol. 2002; 31:693–717. [PubMed: 14501208]

5. Alheid GF, McCrimmon DR. The chemical neuroanatomy of breathing. Respir Physiol Neurobiol. 2008; 164:3–11. [PubMed: 18706532]

6. Arata A, Hernandez YM, Lindsey BG, Morris KF, Shannon R. Transient configurations of baroresponsive respiratory-related brainstem neuronal assemblies in the cat. J Physiol. 2000; 525:509–530. [PubMed: 10835051]

7. Ashmore RC, Wild JM, Schmidt MF. Brainstem and forebrain contributions to the generation of learned motor behaviors for song. J Neurosci. 2005; 25:8543–8554. [PubMed: 16162936]

8. Baekey DM, Molkov YI, Paton JFR, Rybak IA, Dick TE. Effect of baroreceptor stimulation on the respiratory pattern: Insights into respiratory-sympathetic interactions. Respir Physiol Neurobiol. 2010; 174:135–145. [PubMed: 20837166]

9. Baekey DM, Morris KF, Gestreau C, Li Z, Lindsey BG, Shannon R. Medullary respiratory neurones and control of laryngeal motoneurones during fictive eupnoea and cough in the cat. J Physiol. 2001; 534(2):565–581. [PubMed: 11454973]

10. Balis UJ, Morris KF, Koleski J, Lindsey BG. Simulations of a ventrolateral medullary neural network for respiratory rhythmogenesis inferred from spike train cross-correlation. Biol Cybern. 1994; 70:311–327. [PubMed: 8148410]

11. Barillot JC, Grelot L, Reddad S, Bianchi AL. Discharge patterns of laryngeal motoneurones in the cat: An intracellular study. Brain Res. 1990; 509:99–106. [PubMed: 2306643]

12. Ben-Tal A, Smith JC. A model for control of breathing in mammals: Coupling neural dynamics to peripheral gas exchange and transport. J Theor Biol. 2008; 251:480–497. [PubMed: 18262570]

13. Ben-Tal A, Smith JC. Control of breathing: Two types of delays studied in an integrated model of the respiratory system. Respir Physiol Neurobiol. 2010; 170:103–112. [PubMed: 19853063]

14. Berger AJ, Dick TE. Connectivity of slowly adapting pulmonary stretch receptors with dorsal medullary respiratory neurons. J Neurophysiol. 1987; 58:1259–1274. [PubMed: 3437333]

15. Bertrand F, Hugelin A. Respiratory synchronizing function of nucleus parabrachialis medialis: Pneumotaxic mechanisms. J Neurophysiol. 1971; 34:189–207. [PubMed: 5545937]

16. Best J, Borisyuk A, Rubin J, Terman D, Wechselberger M. The dynamic range of bursting in a model respiratory pacemaker network. SIAM J Appl Dyn Syst. 2005; 4:1107–1139.

17. Bianchi AL. Modalités de décharge et propriétés anatomofonctionnelles des neurones respiratoires bulbaires. J Physiol (Paris). 1974; 68:555–587. [PubMed: 4377671]

18. Bianchi AL, Denavit-Saubie M, Champagnat J. Central control of breathing in mammals: Neuronal circuitry, membrane properties, and neurotransmitters. Physiol Rev. 1995; 75:1–45. [PubMed: 7831394]

19. Bianchi AL, Gestreau C. The brainstem respiratory network: An overview of a half century of research. Respir Physiol Neurobiol. 2009; 168:4–12. [PubMed: 19406252]

20. Bishop B. Carotid baroreceptor modulation of diaphragm and abdominal muscle activity in the cat. J Appl Physiol. 1974; 36:12–19. [PubMed: 4358833]

21. Bolser DC, Poliacek I, Jakus J, Fuller DD, Davenport PW. Neurogenesis of cough, other airway defensive behaviors and breathing: A holarchical system? Respir Physiol Neurobiol. 2006; 152:255–265. [PubMed: 16723284]

22. Bonham AC, McCrimmon DR. Neurones in a discrete region of the nucleus tractus solitarius are required for the Breuer-Hering reflex in rat. J Physiol. 1990; 427:261–280. [PubMed: 2213599]

23. Botros SM, Bruce EN. Neural network implementation of a three-phase model of respiratory rhythm generation. Biol Cybern. 1990; 63(2):143–153. [PubMed: 2375940]

24. Bouvier J, Thoby-Brisson M, Renier N, Dubreuil V, Ericson J, Champagnat J, Pierani A, Chedotal A, Fortin G. Hindbrain interneurons and axon guidance signaling critical for breathing. Nat Neurosci. 2010; 13:1066–1074. [PubMed: 20680010]

25. Breen BJ, Gerken WC, Butera RJ. Hybrid integrate-and-fire model of a bursting neuron. Neural Comput. 2003; 15:2843–2862. [PubMed: 14629870]

26. Briggman KL, Denk W. Towards neural circuit reconstruction with volume electron microscopy techniques. Curr Opin Neurobiol. 2006; 16:562–570. [PubMed: 16962767]

27. Brunner MJ, Sussman MS, Greene AS, Kallman CH, Shoukas AA. Carotid sinus baroreceptor reflex control of respiration. Circ Res. 1982; 51:624–636. [PubMed: 7139881]

28. Butera RJ, Rinzel J, Smith JC. Models of respiratory rhythm generation in the pre-Bötzinger complex. II. Populations of coupled pacemaker neurons. J Neurophysiol. 1999a; 82(1):398–415. [PubMed: 10400967]

29. Butera RJ, Rinzel J, Smith JC. Models of respiratory rhythm generation in the pre-Bötzinger complex. I. Bursting pacemaker neurons. J Neurophysiol. 1999b; 82(1):382–397. [PubMed: 10400966]

30. Butera, RJ.; Rubin, J.; Terman, D.; Smith, JC. Oscillatory bursting mechanisms in respiratory pacemaker neurons and networks. In: Coombes, S.; Bresloff, PC., editors. Bursting: The Genesis of Rhythm in the Nervous System. London: World Scientific Press; 2005. p. 303-347.

31. Buzsáki, G. Rhythms of the Brain. New York: Oxford University Press; 2006.

32. Chamberlin N, Saper C. Topographic organization of respiratory responses to glutamate microstimulation of the parabrachial nucleus in the rat. J Neurosci. 1994; 14:6500–6510. [PubMed: 7965054]

33. Chamberlin NL, Saper CB. A brainstem network mediating apneic reflexes in the rat. J Neurosci. 1998; 18:6048–6056. [PubMed: 9671689]

34. Cheng L, Ivanova O, Fan H-H, Khoo MCK. An integrative model of respiratory and cardiovascular control in sleep-disordered breathing. Respir Physiol Neurobiol. 2010; 174:4–28. [PubMed: 20542148]

35. Clark FJ, von Euler C. On the regulation of depth and rate of breathing. J Physiol. 1972; 222:267–295. [PubMed: 5033464]

36. Cohen MI. Neurogenesis of respiratory rhythm in the mammal. Physiol Rev. 1979; 59:1105–1173. [PubMed: 227004]

37. Cohen MI, Piercey MF, Gootman PM, Wolotsky P. Synaptic connections between medullary inspiratory neurons and phrenic motoneurons as revealed by cross-correlation. Brain Res. 1974; 81:319–324. [PubMed: 4373128]

38. Cohen MI, Shaw C-F. Role in the inspiratory off-switch of vagal inputs to rostral pontine inspiratory-modulated neurons. Respir Physiol Neurobiol. 2004; 143:127–140. [PubMed: 15519550]

39. Coles SK, Dick TE. Neurones in the ventrolateral pons are required for post-hypoxic frequency decline in rats. J Physiol. 1996; 497(1):79–94. [PubMed: 8951713]

40. Connelly CA, Ellenberger HH, Feldman JL. Respiratory activity in retrotrapezoid nucleus in cat. Am J PhysiolLung Cell Mol Physiol. 1990; 258:L33–L44.

41. Crampin EJ, Halstead M, Hunter P, Nielsen P, Noble D, Smith N, Tawhai M. Computational physiology and the physiome project. Exp Physiol. 2004; 89:1–26. [PubMed: 15109205]

42. Davies RO, Edwards MW Jr. Medullary relay neurons in the carotid body chemoreceptor pathway of cats. Respir Physiol. 1975; 24:69–79. [PubMed: 1197947]

43. Dayan, P.; Abbott, LF. Theoretical Neuroscience: Computational and Mathematical Modeling of Neural Systems. Cambridge, MA: MIT Press; 2001.

44. de Almeida ATR, Al-Izki S, Denton ME, Kirkwood PA. Patterns of expiratory and inspiratory activation for thoracic motoneurones in the anaesthetized and the decerebrate rat. J Physiol. 2010; 588:2707–2729. [PubMed: 20530111]

45. De Schutter E. Why are computational neuroscience and systems biology so separate? PLoS Comput Biol. 2008; 4:e1000078. [PubMed: 18516226]

46. De Schutter E, Ekeberg Ö, Kotaleski JH, Achard P, Lansner A. Biophysically detailed modelling of microcircuits and beyond. Trends Neurosci. 2005; 28:562–569. [PubMed: 16118023]

47. De Troyer A, Kirkwood PA, Wilson TA. Respiratory action of the intercostal muscles. Physiol Rev. 2005; 85:717–756. [PubMed: 15788709]

48. Dean JB. Theory of gastric CO_2 ventilation and its control during respiratory acidosis: Implications for central chemosensitivity, pH regulation, and diseases causing chronic CO_2 retention. Respir Physiol Neurobiol. 2011; 175:189–209. [PubMed: 21144912]

49. Dean JB, Nattie EE. Central CO_2 chemoreception in cardiorespiratory control. J Appl Physiol. 2010; 108:976–978. [PubMed: 20150571]

50. Deisseroth K. Optogenetics. Nature Methods. 2011; 8:26–29. [PubMed: 21191368]

51. Del Negro, CA.; Hayes, JA.; Pace, RW.; Brush, BR.; Teruyama, R.; Feldman, JL. Synaptically activated burst-generating conductances may underlie a group-pacemaker mechanism for respiratory rhythm generation in mammals. In: Gossard, J-P.; Dubuc, R.; Kolta, A., editors. Progress in Brain Research. Amsterdam The Netherlands: Elsevier; 2010. p. 111-136.

52. Del Negro CA, Hayes JA, Rekling JC. Dendritic calcium activity precedes inspiratory bursts in pre-Bötzinger complex neurons. J Neurosci. 2011; 31:1017–1022. [PubMed: 21248126]

53. Del Negro CA, Johnson SM, Butera RJ, Smith JC. Models of respiratory rhythm generation in the pre-Bötzinger complex. III. Experimental tests of model predictions. J Neurophysiol. 2001; 86:59–74. [PubMed: 11431488]

54. Del Negro CA, Koshiya N, Butera RJ Jr, Smith JC. Persistent sodium current, membrane properties and bursting behavior of pre-Bötzinger complex inspiratory neurons *in vitro*. J Neurophysiol. 2002; 88:2242–2250. [PubMed: 12424266]

55. Del Negro CA, Morgado-Valle C, Hayes JA, Mackay DD, Pace RW, Crowder EA, Feldman JL. Sodium and calcium current-mediated pacemaker neurons and respiratory rhythm generation. J Neurosci. 2005; 25:446–453. [PubMed: 15647488]

56. Del Negro CA, Wilson CG, Butera RJ, Rigatto H, Smith JC. Complex neural activity patterns in the network responsible for respiratory rhythm in mammals. Biophys J. 2002; 82:206–214. [PubMed: 11751309]

57. Dempsey JA. Challenges for future research in exercise physiology as applied to the respiratory system. Exerc Sport Sci Rev. 2006; 34:89–141.

58. DePuy SD, Kanbar R, Coates MB, Stornetta RL, Guyenet PG. Control of breathing by raphé obscurus serotonergic neurons in mice. J Neurosci. 2011; 31:1981–1990. [PubMed: 21307236]

59. Dias MB, Li A, Nattie E. Focal CO_2 dialysis in raphé obscurus does not stimulate ventilation but enhances the response to focal CO_2 dialysis in the retrotrapezoid nucleus. J Appl Physiol. 2008; 105:83–90. [PubMed: 18450988]

60. Dick TE, Shannon R, Lindsey BG, Nuding SC, Segers LS, Baekey DM, Morris KF. Pontine respiratory-modulated activity before and after vagotomy in decerebrate cats. J Physiol. 2008; 586:4265–4282. [PubMed: 18599543]

61. Donoghue S, Felder RB, Jordan D, Spyer KM. The central projections of carotid baroreceptors and chemoreceptors in the cat: A neurophysiological study. J Physiol. 1984; 347:397–410. [PubMed: 6707961]

62. Dubreuil V, Barhanin J, Goridis C, Brunet J-F. Breathing with Phox2b. Philos Trans R Soc Lond B Biol Sci. 2009; 364:2477–2483. [PubMed: 19651649]

63. Duffin J. A model of respiratory rhythm generation. NeuroReport. 1991; 2:623–626. [PubMed: 1756244]

64. Duffin J. Functional organization of respiratory neurons: A brief review of current questions and speculations. Exp Physiol. 2004; 89:517–529. [PubMed: 15258123]

65. Duffin J. The role of the central chemoreceptors: A modeling perspective. Respir Physiol Neurobiol. 2010; 173:230–243. [PubMed: 20227528]

66. Duffin J, Ezure K, Lipski J. Breathing rhythm generation: Focus on the rostral ventrolateral medulla. News Physiol Sci. 1995; 10:133–140.

67. Dunin-Barkowski W, Escobar AL, Lovering AT, Orem JM. Respiratory pattern generator model using Ca++-induced Ca++ release in neurons shows both pacemaker and reciprocal network properties. Biol Cybern. 2003; 89:274–288. [PubMed: 14605892]

68. Dunmyre J, Rubin J. Optimal intrinsic dynamics for bursting in a three-cell network. SIAM J Appl Dyn Syst. 2010; 9:154–187.

69. Dutschmann M, Herbert H. The Kolliker-Fuse nucleus gates the postin-spiratory phase of the respiratory cycle to control inspiratory off-switch and upper airway resistance in rat. Eur J Neurosci. 2006; 24:1071–1084. [PubMed: 16930433]

70. Ermentrout, GB.; Terman, DH. Mathematical Foundations of Neuroscience. New York: Springer; 2010.

71. Evans KC. Cortico-limbic circuitry and the airways: Insights from functional neuroimaging of respiratory afferents and efferents. Biolo Psychol. 2010; 84:13–25.

72. Ezure K. Synaptic connections between medullary respiratory neurons and considerations on the genesis of respiratory rhythm. Prog Neurobiol. 1990; 35:429–450. [PubMed: 2175923]

73. Ezure K. Respiration-related afferents to parabrachial pontine regions. Respir Physiol Neurobiol. 2004; 143:167–175. [PubMed: 15519553]

74. Ezure K, Manabe M. Decrementing expiratory neurons of the Bötzinger complex II. Direct inhibitory synaptic linkage with ventral respiratory group neurons. Exp Brain Res. 1988; 72:159–166. [PubMed: 3169183]

75. Ezure K, Tanaka I. Contralateral projections of barosensitive neurons of the nucleus tractus solitarii. Neurosci Lett. 1996; 219:37–40. [PubMed: 8961298]

76. Ezure K, Tanaka I, Saito Y. Activity of brainstem respiratory neurones just before the expiration-inspiration transition in the rat. J Physiol. 2003; 547:629–640. [PubMed: 12562954]

77. Ezure K, Tanaka I, Saito Y, Otake K. Axonal projections of pulmonary slowly adapting receptor relay neurons in the rat. J Comp Neurol. 2002; 446:81–94. [PubMed: 11920722]

78. Fedorko L, Duffin J, England S. Inhibition of inspiratory neurons of the nucleus retroambigualis by expiratory neurons of the Bötzinger complex in the cat. Exp Neurol. 1989; 106:74–77. [PubMed: 2792299]

79. Fedorko L, Hoskin RW, Duffin J. Projections from inspiratory neurons of the nucleus retroambigualis to phrenic motoneurons in the cat. Exp Neurol. 1989; 105:306–310. [PubMed: 2475362]

80. Fedorko L, Merrill EG. Axonal projections from the rostral expiratory neurones of the Bötzinger complex to medulla and spinal cord in the cat. J Physiol. 1984; 350:487–496. [PubMed: 6747857]

81. Fedorko L, Merrill EG, Lipski J. Two descending medullary inspiratory pathways to phrenic motoneurones. Neurosci Lett. 1983; 43:285–291. [PubMed: 6672694]

82. Feldman, JL. Neurophysiology of breathing in mammals. In: Bloom, FE., editor. Handbook of Physiology. The Nervous System. Intrinsic Regulatory Systems of the Brain. Vol. 1. Bethesda, MD: American Physiological Society; 1986. p. 463-524.

83. Feldman JL, Cohen MI. Relation between expiratory duration and rostral medullary expiratory neuronal discharge. Brain Res. 1978; 141:172–178. [PubMed: 624073]

84. Feldman JL, Cowan JD. Large-scale activity in neural nets I: Theory with application to motoneuron pool responses. Biol Cybern. 1975a; 17:29–38. [PubMed: 1115818]

85. Feldman JL, Cowan JD. Large-scale activity in neural nets II: A model for the brainstem respiratory oscillator. Biol Cybern. 1975b; 17:39–51. [PubMed: 1115819]

86. Feldman JL, Del Negro CA. Looking for inspiration: New perspectives on respiratory rhythm. Nat Rev Neurosci. 2006; 7:232–241. [PubMed: 16495944]

87. Feldman JL, Janczewski WA. The Last Word: Point: Counterpoint authors respond to commentaries on "The parafacial respiratory group (pFRG)/pre-Bötzinger complex (preBötC) is the primary site of respiratory rhythm generation in the mammal". J Appl Physiol. 2006; 101:689. [PubMed: 16709655]

88. Feldman, JL.; McCrimmon, DR. Neural control of breathing. In: Zigmond, MJ.; Bloom, FE.; Landis, SC.; Roberts, JL.; Squire, LR., editors. Fundamental Neuroscience. San Diego, CA: Academic Press; 1998. p. 1063-1090.

89. Feldman JL, Mitchell GS, Nattie EE. Breathing: Rhythmicity, plasticity, chemosensitivity. Annu Rev Neurosci. 2003; 26:239–266. [PubMed: 12598679]

90. Feldman JL, Smith JC. Cellular mechanisms underlying modulation of breathing pattern in mammals. Ann N Y Acad Sci. 1989; 563:114–130. [PubMed: 2476055]

91. Finley JC, Katz DM. The central organization of carotid body afferent projections to the brainstem of the rat. Brain Res. 1992; 572:108–116. [PubMed: 1611506]

92. Forster HV, Smith CA. Contributions of central and peripheral chemoreceptors to the ventilatory response to $CO_2/H+$ J Appl Physiol. 2010; 108:989–994. [PubMed: 20075260]

93. Fortin G, Thoby-Brisson M. Embryonic emergence of the respiratory rhythm generator. Respir Physiol Neurobiol. 2009; 168:86–91. [PubMed: 19560563]

94. Fortuna MG, West GH, Stornetta RL, Guyenet PG. Bötzinger expiratory-augmenting neurons and the parafacial respiratory group. J Neurosci. 2008; 28:2506–2515. [PubMed: 18322095]

95. Fregosi RF. Influence of hypoxia and carotid sinus nerve stimulation on abdominal muscle activities in the cat. J Appl Physiol. 1994; 76:602–609. [PubMed: 8175570]

96. Fung ML, St John WM. Neuronal activities underlying inspiratory termination by pneumotaxic mechanisms. Respir Physiol. 1994; 98:267–281. [PubMed: 7899728]

97. Gaiteri C, Rubin JE. The interaction of intrinsic dynamics and network topology in determining network burst synchrony. Front Comput Neurosci. 2011; 5:10. [PubMed: 21373358]

98. Geman S, Miller M. Computer simulation of brainstem respiratory activity. J Appl Physiol. 1976; 41:931–937. [PubMed: 1002648]

99. Gleeson P, Crook S, Cannon RC, Hines ML, Billings GO, Farinella M, Morse TM, Davison AP, Ray S, Bhalla US, Barnes SR, Dimitrova YD, Silver RA. NeuroML: A language for describing data driven models of neurons and networks with a high degree of biological detail. PLoS Comput Biol. 2010; 6:e1000815. [PubMed: 20585541]

100. Gleeson P, Steuber V, Silver RA. neuroConstruct: A tool for modeling networks of neurons in 3D space. Neuron. 2007; 54:219–235. [PubMed: 17442244]

101. Gottschalk A, Ogilvie MD, Richter DW, Pack AI. Computational aspects of the respiratory pattern generator. Neural Comput. 1994; 6:56–68.

102. Gourine AV, Kasymov V, Marina N, Tang F, Figueiredo MF, Lane S, Teschemacher AG, Spyer KM, Deisseroth K, Kasparov S. Astrocytes control breathing through pH-dependent release of ATP. Science. 2010; 329:571–575. [PubMed: 20647426]

103. Gray PA, Hayes JA, Ling GY, Llona I, Tupal S, Picardo MCD, Ross SE, Hirata T, Corbin JG, Eugenin J, Del Negro CA. Developmental origin of pre-Bötzinger complex respiratory neurons. J Neurosci. 2010; 30:14883–14895. [PubMed: 21048147]

104. Grelot L, Barillot JC, Bianchi AL. Central distributions of the efferent and afferent components of the pharyngeal branches of the vagus and glossopharangeal nerves: An HRP study in the cat. Exp Brain Res. 1989; 78:327–335. [PubMed: 2599042]

105. Grelot L, Barillot JC, Bianchi AL. Activity of respiratory-related oropharyngeal and laryngeal motoneurones during fictive vomiting in the decerebrate cat. Brain Res. 1990; 513:101–105. [PubMed: 2350673]

106. Grillner S. The motor infrastructure: From ion channels to neuronal networks. Nat Rev Neurosci. 2003; 4:573–586. [PubMed: 12838332]

107. Grillner S. Biological pattern generation: The cellular and computational logic of networks in motion. Neuron. 2006; 52:751–766. [PubMed: 17145498]

108. Grunstein MM, Derenne JP, Milic-Emili J. Control of depth and frequency of breathing by baroreceptor stimulation in cats. J Appl Physiol. 1975; 39:395–404. [PubMed: 126222]

109. Guyenet PG. The 2008 Carl Ludwig Lecture: Retrotrapezoid nucleus, CO_2 homeostasis, and breathing automaticity. J Appl Physiol. 2008; 105:404–416. [PubMed: 18535135]

110. Guyenet PG, Mulkey DK, Stornetta RL, Bayliss DA. Regulation of ventral surface chemoreceptors by the central respiratory pattern generator. J Neurosci. 2005; 25:8938–8947. [PubMed: 16192384]

111. Guyenet PG, Stornetta RL, Bayliss DA. Central respiratory chemoreception. J Comp Neurol. 2010; 518:3883–3906. [PubMed: 20737591]

112. Guyenet PG, Stornetta RL, Bayliss DA, Mulkey DK. Retrotrapezoid nucleus: A litmus test for the identification of central chemoreceptors. Exp Physiol. 2005; 90.3:247–253. [PubMed: 15728136]

113. Haji A, Okazaki M, Takeda R. $GABA_A$ receptor-mediated inspiratory termination evoked by vagal stimulation in decerebrate cats. Neuropharmacology. 1999a; 38:1261–1272. [PubMed: 10471079]

114. Haji A, Okazaki M, Takeda R. Synaptic interactions between respiratory neurons during inspiratory on-switching evoked by vagal stimulation in decerebrate cats. Neurosci Res. 1999b; 35:85–93. [PubMed: 10616912]

115. Haji A, Okazaki M, Yamazaki H, Takeda R. Physiological properties of late inspiratory neurons and their possible involvement in inspiratory off-switching in cats. J Neurophysiol. 2002; 87:1057–1067. [PubMed: 11826069]

116. Harding R, Hooper SB. Regulation of lung expansion and lung growth before birth. J Appl Physiol. 1996; 81:209–224. [PubMed: 8828667]

117. Harding R, Johnson P, McClelland ME. Respiratory function of the larynx in developing sheep and the influence of sleep state. Respir Physiol. 1980; 40:165–179. [PubMed: 7394367]

118. Harper RM. The cerebellum and respiratory control. Cerebellum. 2002; 1:1–2. [PubMed: 12879968]

119. Harper RM, Frysinger RC, Ni HF, Terreberry RR. Suprapontine influences on respiratory patterning during sleep-waking states. Prog Clin Biol Res. 1990; 345:33–39. [PubMed: 2198594]

120. Harris-Warrick RM, Marder E. Modulation of neural networks for behavior. Annu Rev Neurosci. 1991; 14:39–57. [PubMed: 2031576]

121. Hayashi F, Coles SK, McCrimmon DR. Respiratory neurons mediating the Breuer-Hering reflex prolongation of expiration in rat. J Neurosci. 1996; 16(20):6526–6536. [PubMed: 8815930]

122. Helmstaedter M, Briggman KL, Denk W. 3D structural imaging of the brain with photons and electrons. Curr Opin Neurobiol. 2008; 18:633–641. [PubMed: 19361979]

123. Hernández-Cruz A, Escobar AL, Jiménez N. Ca^{2+}-induced Ca^{2+} release phenomena in mammalian sympathetic neurons are critically dependent on the rate of rise of trigger Ca^{2+} J Gen Physiol. 1997; 109:147–167. [PubMed: 9041445]

124. Heymans C, Bouckaert JJ. Sinus caroticus and respiratory reflexes. I. Cerebral blood flow and respiration. Adrenaline apnoea. J Physiol. 1930; 69:255–266.

125. Hodges MR, Wehner M, Aungst J, Smith JC, Richerson GB. Transgenic mice lacking serotonin neurons have severe apnea and high mortality during development. J Neurosci. 2009; 29:10341–10349. [PubMed: 19692608]

126. Hunter PJ, Borg TK. Integration from proteins to organs: The Physiome Project. Nat Rev Mol Cell Biol. 2003; 4:237–243. [PubMed: 12612642]

127. Hutchison AA, Wozniak JA, Choi HG, Conlon M, Otto RA, Abrams RM, Kosch PC. Laryngeal and diaphragmatic muscle activities and airflow patterns after birth in premature lambs. J Appl Physiol. 1993; 75:121–131. [PubMed: 8376258]

128. Iizuka M, Fregosi RF. Influence of hypercapnic acidosis and hypoxia on abdominal expiratory nerve activity in the rat. Respir Physiol Neurobiol. 2007; 157:196–205. [PubMed: 17292680]

129. Iscoe, SD. Central control of the upper airway. In: Oommen, MP.; Sant'Ambrogio, G., editors. Respiratory Function of the Upper Airway. Marcel Dekker, Inc; New York: Kingston: 1988. p. 125-192.

130. Iscoe SD. Control of abdominal muscles. Prog Neurobiol. 1998; 56:433–506. [PubMed: 9775401]

131. Izhikevich, EM. Dynamical Systems in Neuroscience: The Geometry of Excitability and Bursting. Cambridge, MA: MIT Press; 2007.

132. Janczewski WA, Feldman JL. Distinct rhythm generators for inspiration and expiration in the juvenile rat. J Physiol. 2006a; 570:407–420. [PubMed: 16293645]

133. Janczewski WA, Feldman JL. Novel data supporting the two respiratory rhythm oscillator hypothesis. Focus on "Respiration-related rhythmic activity in the rostral medulla of newborn rats". J Neurophysiol. 2006b; 96:1–2. [PubMed: 16554514]

134. Janczewski WA, Onimaru H, Homma I, Feldman JL. Opioid-resistant respiratory pathway from the preinspiratory neurones to abdominal muscles: *In vivo* and *in vitro* study in the newborn rat. J Physiol. 2002; 545:1017–1026. [PubMed: 12482904]

135. Jean A. Brain stem control of swallowing: Neuronal network and cellular mechanisms. Physiol Rev. 2001; 81:929–969. [PubMed: 11274347]

136. Jiang C, Lipski J. Extensive monosynaptic inhibition of ventral respiratory group neurons by augmenting neurons in the Bötzinger complex in the cat. Exp Brain Res. 1990; 81:639–648. [PubMed: 2226695]

137. Jodkowski JS, Coles SK, Dick TE. A 'pneumotaxic centre' in rats. Neurosci Lett. 1994; 172:67–72. [PubMed: 8084539]

138. Jodkowski JS, Coles SK, Dick TE. Prolongation in expiration evoked from ventrolateral pons of adult rats. J Appl Physiol. 1997; 82(2):377–381. [PubMed: 9049713]

139. Johnson SM, Koshiya N, Smith JC. Isolation of the kernel for respiratory rhythm generation in a novel preparation: The pre-Bötzinger complex "island". J Neurophysiol. 2001; 85:1772–1776. [PubMed: 11287498]

140. Joseph IMP, Butera RJ. A simple model of dynamic interactions between respiratory centers. Conf Proc IEEE Eng Med Biol Soc. 2005; 6:5840–5842. [PubMed: 17281587]

141. Joshi S, Kotecha S. Lung growth and development. Early hum dev. 2007; 83:789–794. [PubMed: 17905543]

142. Jürgens U. Neural pathways underlying vocal control. Neurosci Biobehav Rev. 2002; 26:235–258. [PubMed: 11856561]

143. Katz, PS. Beyond neurotransmission: Neuromodulation and its importance for information processing. New York: Oxford University Press; 1999. p. 406

144. Khoo MCK. Determinants of ventilatory instability and variability. Respir Physiol. 2000; 122:167–182. [PubMed: 10967342]

145. Kirby LG, Pernar L, Valentino RJ, Beck SG. Distinguishing characteristics of serotonin and non-serotonin-containing cells in the dorsal raphé nucleus: Electrophysiological and immunohistochemical studies. Neuroscience. 2003; 116:669–683. [PubMed: 12573710]

146. Kirkwood PA, Schmid K, Sears TA. Functional identities of thoracic respiratory interneurones in the cat. J Physiol. 1993; 461:667–687. [PubMed: 8350279]

147. Kitterman JA. Physiological factors in fetal lung growth. Can J Physiol Pharmacol. 1988; 66:1122–1128. [PubMed: 3052746]

148. Knox CK. Characteristics of inflation and deflation reflexes during expiration in the cat. J Neurophysiol. 1973; 36:284–295. [PubMed: 4706263]

149. Kobayashi S, Fujito Y, Matsuyama K, Aoki M. Spontaneous respiratory rhythm generation in *in vitro* upper cervical slice preparations of neonatal mice. J Physiol Sci. 2010; 60:303–307. [PubMed: 20419361]

150. Koch, C.; Segev, I. Methods in Neuronal Modeling: From Ions to Networks. 2. Cambridge, MA: MIT Press; 1998.

151. Koizumi H, Smerin SE, Yamanishi T, Moorjani BR, Zhang R, Smith JC. TASK channels contribute to the K+-dominated leak current regulating respiratory rhythm generation *in vitro*. J Neurosci. 2010; 30:4273–4284. [PubMed: 20335463]

152. Koizumi H, Smith JC. Persistent Na+ and K+-dominated leak currents contribute to respiratory rhythm generation in the pre-Bötzinger complex *in vitro*. J Neurosci. 2008; 28:1773–1785. [PubMed: 18272697]

153. Koshiya N, Smith JC. Neuronal pacemaker for breathing visualized *in vitro*. Nature. 1999; 400(6742):360–363. [PubMed: 10432113]

154. Kosmidis EK, Pierrefiche O, Vibert J-F. Respiratory-like rhythmic activity can be produced by an excitatory network of non-pacemaker neuron models. J Neurophysiol. 2004; 92:686–699. [PubMed: 15277592]

155. Krey RA, Goodreau AM, Arnold TB, Del Negro CA. Outward currents contributing to inspiratory burst termination in pre-Bötzinger complex neurons of neonatal mice studied *in vitro*. Front Neural Circuits. 2010; 4

156. Krolo M, Tonkovic-Capin V, Stucke AG, Stuth EA, Hopp FA, Dean C, Zuperku EJ. Subtype composition and responses of respiratory neurons in the pre-Bötzinger region to pulmonary afferent inputs in dogs. J Neurophysiol. 2005; 93:2674–2687. [PubMed: 15601729]

157. Kubin L, Alheid GF, Zuperku EJ, McCrimmon DR. Central pathways of pulmonary and lower airway vagal afferents. J Appl Physiol. 2006; 101:618–627. [PubMed: 16645192]

158. Kuwaki T, Li A, Nattie E. State-dependent central chemoreception: A role of orexin. Respir Physiol Neurobiol. 2010; 173:223–229. [PubMed: 20170755]

159. Kuwana, S-i; Tsunekawa, N.; Yanagawa, Y.; Okada, Y.; Kuribayashi, J.; Obata, K. Electrophysiological and morphological characteristics of GABAergic respiratory neurons in the mouse pre-Bötzinger complex. Eur J Neurosci. 2006; 23:667–674. [PubMed: 16487148]

160. Lawson EE. Prolonged central respiratory inhibition following reflex-induced apnea. J Appl Physiol. 1981; 50:874–879. [PubMed: 7263371]

161. Li Z, Morris KF, Baekey DM, Shannon R, Lindsey BG. Multimodal medullary neurons and correlational linkages of the respiratory network. J Neurophysiol. 1999; 82:188–201. [PubMed: 10400947]

162. Lindsey BG, Arata A, Morris KF, Hernandez YM, Shannon R. Medullary raphé neurones and baroreceptor modulation of the respiratory motor pattern in the cat. J Physiol. 1998; 512:863–882. [PubMed: 9769428]

163. Lindsey BG, Hernandez YM, Morris KF, Shannon R. Functional connectivity between brain stem midline neurons with respiratory-modulated firing rates. J Neurophysiol. 1992; 67:890–904. [PubMed: 1588389]

164. Lindsey BG, Hernandez YM, Morris KF, Shannon R, Gerstein GL. Dynamic reconfiguration of brain stem neural assemblies: Respiratory phase-dependent synchrony versus modulation of firing rates. J Neurophysiol. 1992a; 67:923–930. [PubMed: 1588391]

165. Lindsey BG, Hernandez YM, Morris KF, Shannon R, Gerstein GL. Respiratory-related neural assemblies in the brain stem midline. J Neurophysiol. 1992b; 67:905–922. [PubMed: 1588390]

166. Lindsey, BG.; Ross, A.; O'Connor, RE.; Morris, KF.; Nuding, SC.; Segers, LS.; Shannon, R.; Dick, TE.; Dunin-Barkowski, WL.; Orem, JM.; Solomon, IC.; Rybak, IA. FASEB J (Abstract). FASEB; Bethesda, Maryland: 2007. Modulation and reconfiguration of the pontomedullary respiratory network: A computational modeling study. Program No. 610.11

167. Lindsey BG, Segers LS, Morris KF, Hernandez YM, Saporta S, Shannon R. Distributed actions and dynamic associations in respiratory-related neuronal assemblies of the ventrolateral medulla and brain stem midline: Evidence from spike train analysis. J Neurophysiol. 1994; 72(4):1830–1851. [PubMed: 7823104]

168. Lindsey BG, Segers LS, Shannon R. Functional associations among simultaneously monitored lateral medullary respiratory neurons in the cat. II. Evidence for inhibitory actions of expiratory neurons. J Neurophysiol. 1987; 57(4):1101–1117. [PubMed: 3585455]

169. Lindsey BG, Segers LS, Shannon R. Discharge patterns of rostrolateral medullary expiratory neurons in the cat: Regulation by concurrent network processes. J Neurophysiol. 1989; 61(6): 1185–1196. [PubMed: 2746319]

170. Lindsey BG, Shannon R, Gerstein GL. Gravitational representation of simultaneously recorded brainstem respiratory neuron spike trains. Brain Res. 1989; 483:373–378. [PubMed: 2706527]

171. Lipski J, Duffin J. An electrophysiological investigation of propriospinal inspiratory neurons in the upper cervical cord of the cat. Exp Brain Res. 1986; 61:625–637. [PubMed: 3956619]

172. Lipski J, McAllen RM, Trzebski A. Carotid baroreceptor and chemoreceptor inputs onto single medullary neurones. Brain Res. 1976; 107:132–136. [PubMed: 1268716]

173. Loeschcke HH. Central chemosensitivity and the reaction theory. J Physiol. 1982; 332:1–24. [PubMed: 6818338]

174. Long S, Duffin J. The neuronal determinants of respiratory rhythm. Prog Neurobiol. 1986; 27:101–182. [PubMed: 3529237]

175. Longobardo G, Evangelisti CJ, Cherniack NS. Introduction of respiratory pattern generators into models of respiratory control. Respir Physiol Neurobiol. 2005; 148:285–301. [PubMed: 16143285]

176. Lovering AT, Fraigne JJ, Dunin-Barkowski WL, Vidruk EH, Orem JM. Medullary respiratory neural activity during hypoxia in NREM and REM sleep in the cat. J Neurophysiol. 2006; 95:803–810. [PubMed: 16192335]

177. Lumsden T. Observations on the respiratory centres in the cat. J Physiol. 1923; 57:153–160. [PubMed: 16993609]

178. Mahamed, S.; Mitchell, GS. Respiratory long-term facilitation: Too much or too little of a good thing?. In: Poulin, MJ.; Wilson, RJA., editors. Integration in Respiratory Control: From Genes to Systems. Springer; 2008. p. 224-227.

179. Manabe M, Ezure K. Decrementing expiratory neurons of the Bötzinger complex. Exp Brain Res. 1988; 72:150–158. [PubMed: 3169182]

180. Marder E, Abbott LF. Theory in motion. Curr Opin Neurobiol. 1995; 5:832–840. [PubMed: 8805418]

181. Marder E, Calabrese RL. Principles of rhythmic motor pattern generation. Physiol Rev. 1996; 76:687–717. [PubMed: 8757786]

182. Marder E, Taylor AL. Multiple models to capture the variability in biological neurons and networks. Nat Neurosci. 2011; 14:133–138. [PubMed: 21270780]

183. Marder, E.; Tobin, A-E.; Grashow, R. How tightly tuned are network parameters? Insight from computational and experimental studies in small rhythmic motor networks. In: Paul Cisek, TD.; John, FK., editors. Progress in Brain Research. Elsevier; 2007. p. 193-200.

184. Marina N, Abdala AP, Trapp S, Li A, Nattie EE, Hewinson J, Smith JC, Paton JFR, Gourine AV. Essential role of Phox2b-expressing ventrolateral brainstem neurons in the chemosensory control of inspiration and expiration. J Neurosci. 2010; 30:12466–12473. [PubMed: 20844141]

185. Mateika JH, Sandhu KS. Experimental protocols and preparations to study respiratory long term facilitation. Respir Physiol Neurobiol. 2011; 176:1–11. [PubMed: 21292044]

186. Matsugu M, Duffin J, Poon C-S. Entrainment, instability, quasi-periodicity, and chaos in a compound neural oscillator. J Comput Neurosci. 1998; 5:35–51. [PubMed: 9540048]

187. McAllen RM. Identification and properties of sub-retrofacial bulbospinal neurones: A descending cardiovascular pathway in the cat. J Auton Nerv Syst. 1986; 17:151–164. [PubMed: 3782723]

188. McMullan S, Dick TE, Farnham MMJ, Pilowsky PM. Effects of baroreceptor activation on respiratory variability in rat. Respir Physiol Neurobiol. 2009; 166:80–86. [PubMed: 19429523]

189. Mellen NM, Janczewski WA, Bocchiaro CM, Feldman JL. Opioid-induced quantal slowing reveals dual networks for respiratory rhythm generation. Neuron. 2003; 37:821–826. [PubMed: 12628172]

190. Merrill, EG. Finding a respiratory function for the medullary respiratory neurons. In: Bellairs, R.; Gray, EG., editors. Essays on the Nervous System. Oxford: Clarendon Press; 1974. p. 451-486.

191. Mifflin, S.; Ballantyne, D.; Backman, S.; Richter, D. Evidence for a calcium activated potassium conductance in medullary respiratory neurones. In: Bianchi, AL.; Denavit-Saubié, M., editors. Neurogenesis of Central Respiratory Rhythm. Ile de Bendor, Bandol, France: MTP Press Limited, Lancaster Boston, The Hague, Dordrecht; 1985. p. 179-182.

192. Millhorn DE. Stimulation of raphé (obscurus) nucleus causes long-term potentiation of phrenic nerve activity in cat. J Physiol. 1986; 381:169–179. [PubMed: 3114470]

193. Millhorn DE, Eldridge FL, Waldrop TG. Prolonged stimulation of respiration by endogenous central serotonin. Respir Physiol. 1980; 42(3):171–188. [PubMed: 6452673]

194. Mironov SL. Metabotropic glutamate receptors activate dendritic calcium waves and TRPM channels which drive rhythmic respiratory patterns in mice. J Physiol. 2008; 586:2277–2291. [PubMed: 18308826]

195. Mitchell GS, Babb TG. Layers of exercise hyperpnea: Modulation and plasticity. Respir Physiol Neurobiol. 2006; 151:251–266. [PubMed: 16530024]

196. Mitchell GS, Johnson SM. Plasticity in respiratory motor control. Invited review: Neuroplasticity in respiratory motor control. J Appl Physiol. 2003; 94:358–374. [PubMed: 12486024]

197. Mitra P, Slaughter MM. Calcium-induced transitions between the spontaneous miniature outward and the transient outward currents in retinal amacrine cells. J Gen Physiol. 2002; 119:373–388. [PubMed: 11929887]

198. Mitra P, Slaughter MM. Mechanism of generation of spontaneous miniature outward currents (SMOCs) in retinal amacrine cells. J Gen Physiol. 2002; 119:355–372. [PubMed: 11929886]

199. Miyazaki M, Tanaka I, Ezure K. Excitatory and inhibitory synaptic inputs shape the discharge pattern of pump neurons of the nucleus tractus solitarii in the rat. Exp Brain Res. 1999; 129:191–200. [PubMed: 10591893]

200. Molkov YI, Abdala APL, Bacak BJ, Smith JC, Paton JFR, Rybak IA. Late-expiratory activity: Emergence and interactions with the respiratory CPG. J Neurophysiol. 2010; 104:2713–2729. [PubMed: 20884764]

201. Morgado-Valle C, Baca SM, Feldman JL. Glycinergic pacemaker neurons in PreBötzinger complex of neonatal mouse. J Neurosci. 2010; 30:3634–3639. [PubMed: 20219997]

202. Morris KF, Arata A, Shannon R, Lindsey BG. Inspiratory drive and phase duration during carotid chemoreceptor stimulation in the cat: Medullary neurone correlations. J Physiol. 1996a; 491:241–259. [PubMed: 9011617]

203. Morris KF, Arata A, Shannon R, Lindsey BG. Long-term facilitation of phrenic nerve activity in cats: Responses and short time scale correlations of medullary neurones. J Physiol. 1996b; 490:463–480. [PubMed: 8821143]

204. Morris KF, Baekey DM, Nuding SC, Dick TE, Shannon R, Lindsey BG. Plasticity in respiratory motor control. Invited review: Neural network plasticity in respiration control. J Appl Physiol. 2003; 94:1242–1252. [PubMed: 12571145]

205. Morris, KF.; Baekey, DM.; Nuding, SC.; Segers, LS.; Dick, TE.; Shannon, R.; Lindsey, BG. Society for Neuroscience (Abstract). Society for Neuroscience; Washington, D.C: 2001. Integration of cardiorespiratory responses to carotid chemoreceptor stimulation by medullary and pontine neural networks in cats. Program No. 172.8

206. Morris KF, Baekey DM, Shannon R, Lindsey BG. Respiratory neural activity during long-term facilitation. Respir Physiol. 2000; 121:119–133. [PubMed: 10963769]

207. Morris KF, Lindsey BG, Baekey DM, Nuding SC, Segers LS, Shannon R, O'Connor RE, Dick TE. Cardiorespiratory rhythms in spike trains of caudal raphé and pontine neurons in cats: Insights from computational models of acute vagotomy. 2007 Neuroscience Meeting Planner. 2007 online.

208. Morris KF, Nuding SC, Segers LS, Baekey DM, Shannon R, Lindsey BG, Dick TE. Respiratory and Mayer wave related discharge patterns of raphé and pontine neurons change with vagotomy. J Appl Physiol. 2010; 109:189–202. [PubMed: 20360432]

209. Morris KF, Shannon R, Lindsey BG. Changes in cat medullary neurone firing rates and synchrony following induction of respiratory long-term facilitation. J Physiol. 2001; 532(2):483–497. [PubMed: 11306666]

210. Morrison A, Mehring C, Geisel T, Aertsen A, Diesmann M. Advancing the boundaries of high-connectivity network simulation with distributed computing. Neural Comput. 2005; 17:1776–1801. [PubMed: 15969917]

211. Morrison SF, Cravo SL, Wilfehrt HM. Pontine lesions produce apneusis in the rat. Brain Res. 1994; 652:83–86. [PubMed: 7953724]

212. Mörschel M, Dutschmann M. Pontine respiratory activity involved in inspiratory/expiratory phase transition. Philos Trans R Soc Lond B Biol Sci. 2009; 364:2517–2526. [PubMed: 19651653]

213. Mulkey D, Stornetta R, Weston M, Simmons J, Parker A, Bayliss D, Guyenet P. Respiratory control by ventral surface chemoreceptor neurons in rats. Nat Neurosci. 2004; 7:1360–1369. [PubMed: 15558061]

214. Nakazawa K, Granata AR, Cohen MI. Synchronized fast rhythms in inspiratory and expiratory nerve discharges during fictive vocalization. J Neurophysiol. 2000; 83:1415–1425. [PubMed: 10712468]

215. Nakazawa K, Umezaki T, Zheng YU, Miller AD. Behaviors of bulbar respiratory interneurons during fictive swallowing and vomiting. Otolaryngol Head Neck Surg. 1999; 120:412–418. [PubMed: 10064648]

216. Nattie EE. CO_2, brainstem chemoreceptors and breathing. Prog Neurobiol. 1999; 59(4):299–331. [PubMed: 10501632]

217. Nattie EE, Fung ML, Li A, St John WM. Responses of respiratory modulated and tonic units in the retrotrapezoid nucleus to CO_2. Respir Physiol. 1993; 94:35–50. [PubMed: 8272580]

218. Nattie EE, Li A. Retrotrapezoid nucleus (RTN) metabotropic glutamate receptors and long-term stimulation of ventilatory output. RTN glutamate receptors and breathing. Adv Exp Med Biol. 1995; 393:39–45. [PubMed: 8629516]

219. Nattie EE, Li A, St John WM. Lesions in retrotrapezoid nucleus decrease ventilatory output in anesthetized or decerebrate cats. J Appl Physiol. 1991; 71:1364–1375. [PubMed: 1757359]

220. Netick A, Orem J. Erroneous classification of neuronal activity by the respiratory modulation index. Neurosci Lett. 1981; 21:301–306. [PubMed: 7219876]

221. Nishino T, Honda Y. Changes in pattern of breathing following baroreceptor stimulation in cats. Jpn J Physiol. 1982; 32:183–195. [PubMed: 6809994]

222. Nuding SC, Segers LS, Baekey DM, Dick TE, Solomon IC, Shannon R, Morris KF, Lindsey BG. Pontine-Ventral respiratory column interactions through raphé circuits detected using multi-array spike train recordings. J Neurophysiol. 2009; 101:2943–2960. [PubMed: 19297509]

223. Nuding SC, Segers LS, Shannon R, O'Connor R, Morris KF, Lindsey BG. Central and peripheral chemoreceptors evoke distinct responses in simultaneously recorded neurons of the raphé-pontomedullary respiratory network. Philos Trans R Soc Lond B Biol Sci. 2009; 364:2501–2516. [PubMed: 19651652]

224. Ogilvie MD, Gottschalk A, Anders K, Richter DW, Pack AI. A network model of respiratory rhythmogenesis. Am J PhysiolRegul Integr Comp Physiol. 1992; 263:R962–R975.

225. Okazaki M, Takeda R, Yamazaki H, Haji A. Synaptic mechanisms of inspiratory off-switching evoked by pontine pneumotaxic stimulation in cats. Neurosci Res. 2002; 44:101–110. [PubMed: 12204298]

226. Onimaru H, Arata A, Homma I. Localization of respiratory rhythm-generating neurons in the medulla of brainstem-spinal cord preparations from newborn rats. Neurosci Lett. 1987; 78:151–155. [PubMed: 3627556]

227. Onimaru H, Arata A, Homma I. Primary respiratory rhythm generator in the medulla of brainstem-spinal cord preparation from newborn rat. Brain Res. 1988; 445:314–324. [PubMed: 3370466]

228. Onimaru H, Arata A, Homma I. Firing properties of respiratory rhythm generating neurons in the absence of synaptic transmission in rat medulla *in vitro*. Exp Brain Res. 1989; 76:530–536. [PubMed: 2551710]

229. Onimaru H, Arata A, Homma I. Intrinsic burst generation of prein-spiratory neurons in the medulla of brainstem-spinal cord preparations isolated from newborn rats. Exp Brain Res. 1995; 106:57–68. [PubMed: 8542977]

230. Onimaru H, Homma I. Respiratory rhythm generator neurons in medulla of brainstem-spinal cord preparation from newborn rat. Brain Res. 1987; 403:380–384. [PubMed: 3828828]

231. Onimaru H, Homma I. A novel functional neuron group for respiratory rhythm generation in the ventral medulla. J Neurosci. 2003; 23:1478–1486. [PubMed: 12598636]

232. Onimaru H, Homma I. The parafacial respiratory group/pre-Bötzinger complex is the primary site of respiratory rhythm generation in the mammal. J Appl Physiol. 2006; 100:20094–20098.

233. Onimaru H, Ikeda K, Kawakami K. Phox2b, RTN/pFRG neurons and respiratory rhythmogenesis. Respir Physiol Neurobiol. 2009; 168:13–18. [PubMed: 19712902]

234. Orem J, Netick A. Characteristics of midbrain respiratory neurons in sleep and wakefulness in the cat. Brain Res. 1982; 244:231–241. [PubMed: 7116173]

235. Orer HS, Gebber GL, Barman SM. Medullary lateral tegmental field neurons influence the timing and pattern of phrenic nerve activity in cats. J Appl Physiol. 2006; 101:521–530. [PubMed: 16645195]

236. Otake K, Nakamura Y, Tanaka I, Ezure K. Morphology of pulmonary rapidly adapting receptor relay neurons in the rat. J Comp Neurol. 2001; 430:458–470. [PubMed: 11169480]

237. Otake K, Sasaki H, Ezure K, Manabe M. Axonal trajectory and terminal distribution of inspiratory neurons of the dorsal respiratory group in the cat's medulla. J Comp Neurol. 1989; 286:218–230. [PubMed: 2794117]

238. Otake K, Sasaki H, Ezure K, Manube M. Axonal projections from Bötzinger expiratory neurons to contralateral ventral and dorsal respiratory groups in the cat. Exp Brain Res. 1988; 72:167–177. [PubMed: 3169184]

239. Ott MM, Nuding SC, Segers LS, Lindsey BG, Morris KF. Ventrolateral medullary functional connectivity and the respiratory and central chemoreceptor-evoked modulation of retrotrapezoid-parafacial neurons. J Neurophysiol. 2011; 105:2960–2975. [PubMed: 21389310]

240. Pace RW, Del Negro CA. AMPA and metabotropic glutamate receptors cooperatively generate inspiratory-like depolarization in mouse respiratory neurons *in vitro*. Eur J Neurosci. 2008; 28:2434–2442. [PubMed: 19032588]

241. Pace RW, Mackay DD, Feldman JL, Del Negro CA. Inspiratory bursts in the preBötzinger complex depend on a calcium-activated non-specific cation current linked to glutamate receptors in neonatal mice. J Physiol. 2007a; 582:113–125. [PubMed: 17446214]

242. Pace RW, Mackay DD, Feldman JL, Del Negro CA. Role of persistent sodium current in mouse pre-Bötzinger complex neurons and respiratory rhythm generation. J Physiol. 2007b; 580:485–496. [PubMed: 17272351]

243. Pagliardini S, Janczewski WA, Tan W, Dickson CT, Deisseroth K, Feldman JL. Active expiration induced by excitation of ventral medulla in adult anesthetized rats. J Neurosci. 2011; 31:2895–2905. [PubMed: 21414911]

244. Pagliardini S, Ren J, Gray PA, VanDunk C, Gross M, Goulding M, Greer JJ. Central respiratory rhythmogenesis is abnormal in Lbx1-deficient mice. J Neurosci. 2008; 28:11030–11041. [PubMed: 18945911]

245. Parkes MJ, Lara-Munoz JP, Izzo PN, Spyer KM. Responses of ventral respiratory neurones in the rat to vagus stimulation and the functional diversion of expiration. J Physiol. 1994; 476(1):131–139. [PubMed: 8046628]

246. Paton JF. The ventral medullary respiratory network of the mature mouse studied in a working heart-brainstem preparation. J Physiol. 1996; 493:819–831. [PubMed: 8799902]

247. Paton JFR, Abdala APL, Koizumi H, Smith JC, St-John WM. Respiratory rhythm generation during gasping depends on persistent sodium current. Nat Neurosci. 2006; 9:311–313. [PubMed: 16474390]

248. Pearce RA, Stornetta RL, Guyenet PG. Retrotrapezoid nucleus in the rat. Neurosci Lett. 1989; 101:138–142. [PubMed: 2771161]

249. Peever JH, Shen L, Duffin J. Respiratory pre-motor control of hypoglossal motoneurons in the rat. Neuroscience. 2002; 110:711–722. [PubMed: 11934478]

250. Peever JH, Tian G, Duffin J. Bilaterally independent respiratory rhythms in the decerebrate rat. Neurosci Lett. 1998; 247:41–44. [PubMed: 9637405]

251. Peña F, Ramirez J-M. Substance P-mediated modulation of pacemaker properties in the mammalian respiratory network. J Neurosci. 2004; 24:7549–7556. [PubMed: 15329402]

252. Pickering AE, Paton JFR. A decerebrate, artificially-perfused *in situ* preparation of rat: Utility for the study of autonomic and nociceptive processing. J Neurosci Methods. 2006; 155:260–271. [PubMed: 16499970]

253. Poon C-S, Tin C, Yu Y. Homeostasis of exercise hyperpnea and optimal sensorimotor integration: The internal model paradigm. Respir Physiol Neurobiol. 2007; 159:1–13. [PubMed: 17416554]

254. Poon CS, Lin SL, Knudson OB. Optimization character of inspiratory neural drive. J Appl Physiol. 1992; 72:2005–2017. [PubMed: 1601812]

255. Ptak K, Yamanishi T, Aungst J, Milescu LS, Zhang R, Richerson GB, Smith JC. Raphé neurons stimulate respiratory circuit activity by multiple mechanisms via endogenously released serotonin and substance P. J Neurosci. 2009; 29:3720–3737. [PubMed: 19321769]

256. Ptak K, Zummo GG, Alheid GF, Tkatch T, Surmeier DJ, McCrimmon DR. Sodium currents in medullary neurons isolated from the pre-Bötzinger complex region. J Neurosci. 2005; 25:5159–5170. [PubMed: 15917456]

257. Purvis LK, Smith JC, Koizumi H, Butera RJ. Intrinsic bursters increase the robustness of rhythm generation in an excitatory network. J Neurophysiol. 2007; 97:1515–1526. [PubMed: 17167061]

258. Ramirez J-M, Tryba AK, Peña F. Pacemaker neurons and neuronal networks: An integrative view. Curr Opin Neurobiol. 2004; 14:665–674. [PubMed: 15582367]

259. Rekling JC, Feldman JL. PreBötzinger complex and pacemaker neurons: Hypothesized site and kernel for respiratory rhythm generation. Annu Rev Physiol. 1998; 60:385–405. [PubMed: 9558470]

260. Remmers JE, Richter DW, Ballantyne D, Bainton CR, Klein JP. Reflex prolongation of stage I of expiration. Pflügers Archiv Eur J Physiol. 1986; 407:190–198. [PubMed: 3748780]

261. Richerson GB. Serotonergic neurons as carbon dioxide sensors that maintain pH homeostasis. Nat Rev Neurosci. 2004; 5:449–461. [PubMed: 15152195]

262. Richter DW. Generation and maintenance of the respiratory rhythm. J Exp Biol. 1982; 100:93–107. [PubMed: 6757372]

263. Richter, DW. Neural regulation of respiration: Rhythmogenesis and afferent control. In: Gregor, R.; Windhorst, U., editors. Comprehensive Human Physiology. Berlin: Springer-Verlag; 1996. p. 2079-2095.

264. Richter, DW.; Ballantyne, D. A three phase theory about the basic respiratory pattern generator. In: Schlafke, ME.; Koepchen, HP.; See, WR., editors. Central Neurone Environment. Berlin: Springer-Verlag; 1983. p. 164-174.

265. Richter DW, Ballantyne D, Remmers JE. How is the respiratory rhythm generated? A model. News Physiol Sci. 1986; 1:109–112.

266. Richter, DW.; Camerer, H.; Rohrig, N. Monosynaptic transmissions from lung stretch receptors afferents to Rbeta-neurones. In: von Euler, C.; Lagercrantz, H., editors. Central Nervous Control Mechanisms in Breathing: Physiological and Clinical Aspects of Regular, Periodic, and Irregular Breathing in Adults and in the Perinatal Period. Oxford: Pergamon Press; 1979. p. 267-271.

267. Richter DW, Manzke T, Wilken B, Ponimaskin E. Serotonin receptors: Guardians of stable breathing. Trends Mol Med. 2003; 9:542–548. [PubMed: 14659469]

268. Richter DW, Seller H. Baroreceptor effects on medullary respiratory neurones of the cat. Brain Res. 1975; 86(1):168–171. [PubMed: 163666]

269. Rogers RF, Rose WC, Schwaber JS. Simultaneous encoding of carotid sinus pressure and dP/dt by NTS target neurons of myelinated baroreceptors. J Neurophysiol. 1996; 76:2644–2660. [PubMed: 8899635]

270. Ruangkittisakul A, Okada Y, Oku Y, Koshiya N, Ballanyi K. Fluorescence imaging of active respiratory networks. Respir Physiol Neurobiol. 2009; 168:26–38. [PubMed: 19505861]

271. Rubin J, Bacak B, Molkov Y, Shevtsova N, Smith J, Rybak I. Interacting oscillations in neural control of breathing: Modeling and qualitative analysis. J Comput Neurosci. 2011; 30:607–632. [PubMed: 20927576]

272. Rubin J, Terman D. Synchronized activity and loss of synchrony among heterogeneous conditional oscillators. SIAM J Appl Dyn Syst. 2002; 1:146–174.

273. Rubin J, Wechselberger M. The selection of mixed-mode oscillations in a Hodgkin-Huxley model with multiple timescales. Chaos. 2008; 18:015105–015112. [PubMed: 18377086]

274. Rubin JE. Bursting induced by excitatory synaptic coupling in nonidentical conditional relaxation oscillators or square-wave bursters. Phys Rev E. 2006; 74:021917.

275. Rubin JE, Hayes JA, Mendenhall JL, Del Negro CA. Calcium-activated nonspecific cation current and synaptic depression promote network-dependent burst oscillations. Proc Natl Acad Sci U S A. 2009; 106:2939–2944. [PubMed: 19196976]

276. Rubin JE, Shevtsova NA, Ermentrout GB, Smith JC, Rybak IA. Multiple rhythmic states in a model of the respiratory central pattern generator. J Neurophysiol. 2009; 101:2146–2165. [PubMed: 19193773]

277. Rubio JE. A new mathematical model of the respiratory center. Bull Math Biophys. 1972; 34:467–481. [PubMed: 4659273]

278. Rybak IA, Abdala APL, Markin SN, Paton JFR, Smith JC, Paul Cisek TD, John FK. Spatial organization and state-dependent mechanisms for respiratory rhythm and pattern generation. Prog Brain Res. 2007; 165:201–220. [PubMed: 17925248]

279. Rybak IA, O'Connor R, Ross A, Shevtsova NA, Nuding SC, Segers LS, Shannon R, Dick TE, Dunin-Barkowski WL, Orem JM, Solomon IC, Morris KF, Lindsey BG. Reconfiguration of the pontomedullary respiratory network: A computational modeling study with coordinated *in vivo* experiments. J Neurophysiol. 2008; 100:1770–1799. [PubMed: 18650310]

280. Rybak IA, Paton JFR, Schwaber JS. Modeling neural mechanisms for genesis of respiratory rhythm and pattern. I. Models of respiratory neurons. J Neurophysiol. 1997a; 77:1994–2006. [PubMed: 9114250]

281. Rybak IA, Paton JFR, Schwaber JS. Modeling neural mechanisms for genesis of respiratory rhythm and pattern. II. Network models of the central respiratory pattern generator. J Neurophysiol. 1997b; 77:2007–2026. [PubMed: 9114251]

282. Rybak IA, Paton JFR, Schwaber JS. Modeling neural mechanisms for genesis of respiratory rhythm and pattern. III. Comparison of model performances during afferent nerve stimulation. J Neurophysiol. 1997c; 77:2027–2039. [PubMed: 9114252]

283. Rybak IA, Ptak K, Shevtsova NA, McCrimmon DR. Sodium currents in neurons from the rostroventrolateral medulla of the rat. J Neurophysiol. 2003; 90:1635–1642. [PubMed: 12761275]

284. Rybak IA, Shevtsova NA, Paton JF, Pierrefiche O, St John WM, Haji A. Modelling respiratory rhythmogenesis: Focus on phase switching mechanisms. Adv Exp Med Biol. 2004; 551:189–194. [PubMed: 15602963]

285. Rybak IA, Shevtsova NA, Paton JFR, Dick TE, St-John WM, Morschel M, Dutschmann M. Modeling the ponto-medullary respiratory network. Respir Physiol Neurobiol. 2004; 143:307–319. [PubMed: 15519563]

286. Rybak IA, Shevtsova NA, Ptak K, McCrimmon DR. Intrinsic bursting activity in the pre-Bötzinger complex: Role of persistent sodium and potassium currents. Biol Cybern. 2004; 90:59–74. [PubMed: 14762725]

287. Rybak IA, Shevtsova NA, St John WM, Paton JFR, Pierrefiche O. Endogenous rhythm generation in the pre-Bötzinger complex and ionic currents: Modelling and *in vitro* studies. Eur J Neurosci. 2003; 18:239–257. [PubMed: 12887406]

288. Saito Y, Ezure K, Tanaka I. Swallowing-related activities of respiratory and non-respiratory neurons in the nucleus of solitary tract in the rat. J Physiol. 2002; 540:1047–1060. [PubMed: 11986389]

289. Salmoiraghi GC, Burns BD. Notes on mechanism of rhythmic respiration. J Neurophysiol. 1960; 23:14–26. [PubMed: 14441049]

290. Sant'Ambrogio G, Widdicombe J. Reflexes from airway rapidly adapting receptors. Respir Physiol. 2001; 125:33–45. [PubMed: 11240151]

291. Saywell SA, Ford TW, Meehan CF, Todd AJ, Kirkwood PA. Electrophysiological and morphological characterization of propriospinal interneurons in the thoracic spinal cord. J Neurophysiol. 2011; 105:806–826. [PubMed: 21106900]

292. Schelegle ES, Green JF. An overview of the anatomy and physiology of slowly adapting pulmonary stretch receptors. Respir Physiol. 2001; 125:17–31. [PubMed: 11240150]

293. Schwarzacher SW, Smith JC, Richter DW. Pre-Bötzinger complex in the cat. J Neurophysiol. 1995; 73(4):1452–1461. [PubMed: 7643160]

294. Scornik FS, Merriam LA, Parsons RL. Number of K_{Ca} channels underlying spontaneous miniature outward currents (SMOCs) in mudpuppy cardiac neurons. J Neurophysiol. 2001; 85:54–60. [PubMed: 11152705]

295. Sears TA. Central rhythm generation and spinal integration. Chest. 1990; 97:45S–51S. [PubMed: 2407462]

296. Sears TA, Berger AJ, Phillipson EA. Reciprocal tonic activation of inspiratory and expiratory motoneurones by chemical drives. Nature. 1982; 299:728–730. [PubMed: 6811952]

297. Segers LS, Nuding SC, Dick TE, Shannon R, Baekey DM, Solomon IC, Morris KF, Lindsey BG. Functional connectivity in the pontomedullary respiratory network. J Neurophysiol. 2008; 100:1749–1769. [PubMed: 18632881]

298. Segers LS, Shannon R, Lindsey BG. Interactions between rostral pontine and ventral medullary respiratory neurons. J Neurophysiol. 1985; 54:318–334. [PubMed: 4031991]

299. Segers LS, Shannon R, Saporta S, Lindsey BG. Functional associations among simultaneously monitored lateral medullary respiratory neurons in the cat. I. Evidence for excitatory and inhibitory actions of inspiratory neurons. J Neurophysiol. 1987; 57:1078–1100. [PubMed: 3295135]

300. Seung HS. Reading the book of memory: Sparse sampling versus dense mapping of connectomes. Neuron. 2009; 62:17–29. [PubMed: 19376064]

301. Shannon, R. Reflexes from the respiratory muscles and controvertebral joints. In: Cherniack, NS.; Widdicombe, JG., editors. Handbook of Physiology. The Respiratory System. Control of Breathing, Part 1. Vol. 3. Washington, D.C: American Physiological Society; 1986. p. 431-447.

302. Shannon R, Baekey DM, Morris KF, Li Z, Lindsey BG. Functional connectivity among ventrolateral medullary respiratory neurones and responses during fictive cough in the cat. J Physiol. 2000; 525(1):207–224. [PubMed: 10811738]

303. Shannon R, Baekey DM, Morris KF, Lindsey BG. Ventrolateral medullary respiratory network and a model of cough motor pattern generation. J Appl Physiol. 1998; 84(6):2020–2035. [PubMed: 9609797]

304. Shannon R, Baekey DM, Morris KF, Nuding SC, Segers LS, Lindsey BG. Pontine respiratory group neuron discharge is altered during fictive cough in the decerebrate cat. Respir Physiol Neurobiol. 2004a; 142:43–54. [PubMed: 15351303]

305. Shannon R, Baekey DM, Morris KF, Nuding SC, Segers LS, Lindsey BG. Production of reflex cough by brainstem respiratory networks. Pulm Pharmacol Ther. 2004b; 17:369–376. [PubMed: 15564078]

306. Shao XM, Feldman JL. Respiratory rhythm generation and synaptic inhibition of expiratory neurons in pre-Bötzinger complex: Differential roles of glycinergic and GABAergic neural transmission. J Neurophysiol. 1997; 77:1853–1860. [PubMed: 9114241]

307. Shen L, Li Y, Duffin J. Inhibitory connections among rostral medullary expiratory neurones detected with cross-correlation in the decerebrate rat. Pflügers Archiv Eur J Physiol. 2003; 446:365. [PubMed: 12687375]

308. Shepherd, GM.; Grillner, S. Handbook of Brain Microcircuits. New York: Oxford University Press; 2010.

309. Siniaia MS, Young DL, Poon CS. Habituation and desensitization of the Hering-Breuer reflex in rat. J Physiol. 2000; 523:479–491. [PubMed: 10699090]

310. Smith JC, Abdala APL, Koizumi H, Rybak IA, Paton JFR. Spatial and functional architecture of the mammalian brain stem respiratory network: A hierarchy of three oscillatory mechanisms. J Neurophysiol. 2007; 98:3370–3387. [PubMed: 17913982]

311. Smith JC, Abdala APL, Rybak IA, Paton JFR. Structural and functional architecture of respiratory networks in the mammalian brainstem. Philos Trans R Soc Lond B Biol Sci. 2009; 364:2577–2587. [PubMed: 19651658]

312. Smith JC, Butera RJ, Koshiya N, Del Negro C, Wilson CG, Johnson SM. Respiratory rhythm generation in neonatal and adult mammals: The hybrid pacemaker-network model. Respir Physiol. 2000; 122:131–147. [PubMed: 10967340]

313. Smith JC, Ellenberger HH, Ballanyi K, Richter DW, Feldman JL. Pre-Bötzinger complex: A brainstem region that may generate respiratory rhythm in mammals. Science. 1991; 254:726–729. [PubMed: 1683005]

314. Smith JC, Greer JJ, Liu G, Feldman JL. Neural mechanisms generating respiratory pattern in mammalian brain stem-spinal cord *in vitro* I. Spatiotemporal patterns of motor and medullary neuron activity. J Neurophysiol. 1990; 64:1149–1169. [PubMed: 2258739]

315. Smith JC, Morrison DE, Ellenberger HH, Otto MR, Feldman JL. Brainstem projections to the major respiratory neuron populations in the medulla of the cat. J Comp Neurol. 1989; 281:69–96. [PubMed: 2466879]

316. Solomon IC. Modulation of gasp frequency by activation of pre-Bötzinger complex *in vivo.* J Neurophysiol. 2002; 87:1664–1668. [PubMed: 11877539]

317. Solomon IC, Edelman NH, Neubauer JA. Pre-Bötzinger complex functions as a central hypoxia chemosensor for respiration *in vivo.* J Neurophysiol. 2000; 83:2854–2868. [PubMed: 10805683]

318. Solomon IC, Edelman NH, O'Neal MH III. CO_2/H+ chemoreception in the cat pre-Bötzinger complex *in vivo.* J Appl Physiol. 2000; 88:1996–2007. [PubMed: 10846011]

319. Song G, Poon C-S. Functional and structural models of pontine modulation of mechanoreceptor and chemoreceptor reflexes. Respir Physiol Neurobiol. 2004; 143:281–292. [PubMed: 15519561]

320. Spyer KM. Central nervous mechanisms contributing to cardiovascular control. J Physiol. 1994; 474:1–19. [PubMed: 8014887]

321. StJohn WM. Neurogenesis of patterns of automatic ventilatory activity. Prog Neurobiol. 1998; 56:97–117. [PubMed: 9723132]

322. St John WM. Noeud vital for breathing in the brainstem: Gasping –yes, eupnoea – doubtful. Philos Trans R Soc Lond B Biol Sci. 2009; 364:2625–2633. [PubMed: 19651662]

323. St John WM, Hwang Q, Nattie EE, Zhou D. Functions of the retrofacial nucleus in chemosensitivity and ventilatory neurogenesis. Respir Physiol. 1989; 76(2):159–171. [PubMed: 2749022]

324. St John WM, Paton JFR. Characterizations of eupnea, apneusis and gasping in a perfused rat preparation. Respir Physiol. 2000; 123:201–213. [PubMed: 11007987]

325. Stein, PSG.; Grillner, S.; Selverston, AI.; Stuart, DG. Computational Neuroscience: A Bradford Book Series. Cambridge, MA: MIT Press; 1997. Neurons, networks, and motor behavior; p. 1-305.

326. Stornetta RL, Rosin DL, Wang H, Sevigny CP, Weston MC, Guyenet PG. A group of glutamatergic interneurons expressing high levels of both neurokinin-1 receptors and somatostatin identifies the region of the pre-Bötzinger complex. J Comp Neurol. 2003; 455:499–512. [PubMed: 12508323]

327. Subramanian HH, Balnave RJ, Holstege G. The midbrain periaqueductal gray control of respiration. J Neurosci. 2008; 28:12274–12283. [PubMed: 19020021]

328. Sun Q-J, Goodchild AK, Pilowsky PM. Firing patterns of pre-Bötzinger and Bötzinger neurons during hypocapnia in the adult rat. Brain Res. 2001; 903:198–206. [PubMed: 11382403]

329. Tadjalli A, Duffin J, Peever J. Identification of a novel form of noradrenergic-dependent respiratory motor plasticity triggered by vagal feedback. J Neurosci. 2010; 30:16886–16895. [PubMed: 21159960]

330. Takakura AC, Moreira TS, Colombari E, West GH, Stornetta R, Guyenet PG. Peripheral chemoreceptor inputs to retrotrapezoid nucleus (RTN) CO_2-sensitive neurons in rats. J Physiol. 2006; 572:503–523. [PubMed: 16455687]

331. Tan W, Pagliardini S, Yang P, Janczewski WA, Feldman JL. Projections of preBötzinger complex neurons in adult rats. The J Comp Neurol. 2010; 518:1862–1878.

332. Teppema LJ, Dahan A. The ventilatory response to hypoxia in mammals: Mechanisms, measurement, and analysis. Physiol Rev. 2010; 90:675–754. [PubMed: 20393196]

333. Thoby-Brisson M, Karlén M, Wu N, Charnay P, Champagnat J, Fortin G. Genetic identification of an embryonic parafacial oscillator coupling to the preBötzinger complex. Nat Neurosci. 2009; 12:1028–1035. [PubMed: 19578380]

334. Thoby-Brisson M, Ramirez JM. Identification of two types of inspiratory pacemaker neurons in the isolated respiratory neural network of mice. J Neurophysiol. 2001; 86:104–112. [PubMed: 11431492]

335. Tian GF, Duffin J. The role of dorsal respiratory group neurons studied with cross-correlation in the decerebrate rat. Exp Brain Res. 1998; 121:29–34. [PubMed: 9698187]

336. Tian GF, Peever JH, Duffin J. Mutual inhibition between Bötzinger-complex bulbospinal expiratory neurons detected with cross-correlation in the decerebrate rat. Exp Brain Res. 1999; 125(4):440–446. [PubMed: 10323290]

337. Toporikova N, Butera R. Two types of independent bursting mechanisms in inspiratory neurons: An integrative model. J Comput Neurosci. 2010:1–14.

338. Trelease RB, Sieck GC, Marks JD, Harper RM. Respiratory inhibition induced by transient hypertension during sleep in unrestrained cats. Exp Neurol. 1985; 90:173–186. [PubMed: 4043291]

339. Tryba AK, Pena F, Lieske SP, Viemari J-C, Thoby-Brisson M, Ramirez J-M. Differential modulation of neural network and pacemaker activity underlying eupnea and sigh-breathing activities. J Neurophysiol. 2008; 99:2114–2125. [PubMed: 18287547]

340. von Euler, C. Brain stem mechanism for generation and control of breathing pattern. In: Cherniack, NS.; Widdicombe, JG., editors. Handbook of Physiology. The Respiratory System. Control of Breathing, Part 1. Vol. 3. Washington, D.C: American Physiological Society; 1986. p. 1-67.

341. Waldrop TG, Iwamoto GA, Haouzi P. Point: Counterpoint: Supraspinal locomotor centers do/do not contribute significantly to the hyperpnea of dynamic exercise. J Appl Physiol. 2006; 100:1077–1083. [PubMed: 16467394]

342. Wang W, Fung ML, Darnall RA, St John WM. Characterizations and comparisons of eupnoea and gasping in neonatal rats. J Physiol. 1996; 490:277–292. [PubMed: 8745295]

343. Wang W, Fung ML, St John WM. Pontile regulation of ventilatory activity in the adult rat. J Appl Physiol. 1993; 74(6):2801–2811. [PubMed: 8365984]

344. Winter S, Fresemann J, Schnell C, Oku Y, Hirrlinger J, Hülsmann S. Glycinergic interneurons are functionally integrated into the inspiratory network of mouse medullary slices. Pflügers Archiv Eur J Physiol. 2009; 458:459–469. [PubMed: 19238427]

345. Wittmeier S, Song G, Duffin J, Poon C-S. Pacemakers handshake synchronization mechanism of mammalian respiratory rhythmogenesis. Proc Natl Acad Sci U S A. 2008; 105:18000–18005. [PubMed: 19008356]

346. Xu F, Frazier DT. Role of the cerebellar deep nuclei in respiratory modulation. Cerebellum. 2002; 1:35–40. [PubMed: 12879972]

347. Yoshida Y, Yatake K, Tanaka Y, Imamura R, Fukunaga H, Nakashima T, Hirano M. Morphological observation of laryngeal motoneurons by means of cholera toxin B subunit tracing technique. Acta Otolaryngol Suppl. 1998; 539:98–105. [PubMed: 10095873]

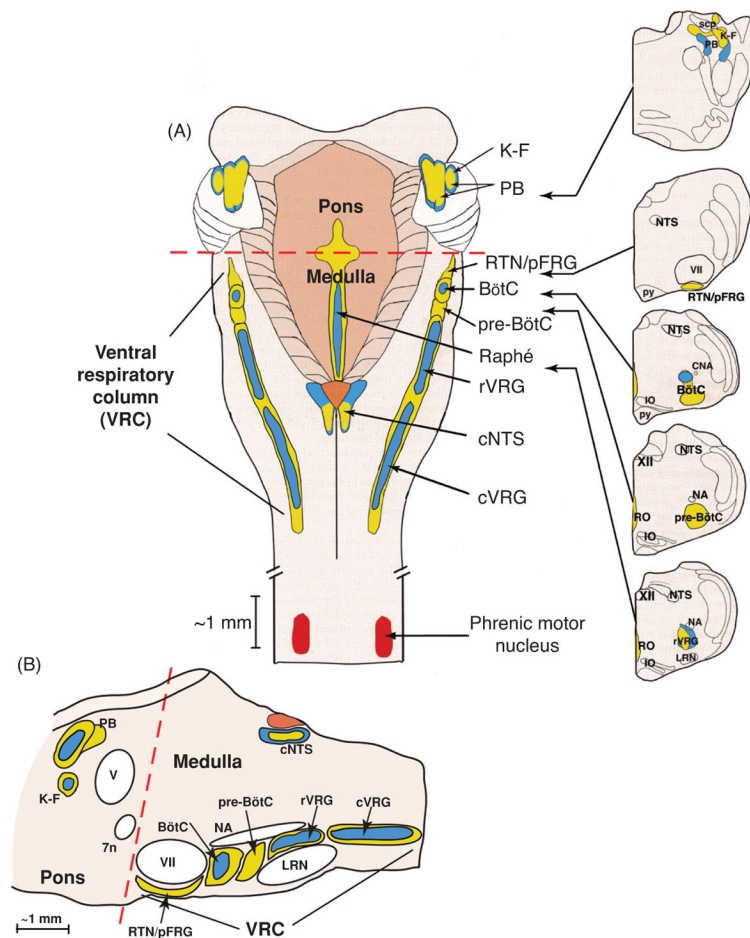348. Yu J. Airway mechanosensors. Respir Physiol Neurobiol. 2005; 148:217–243. [PubMed: 16143281]

Figure 1.
Overview of the mammalian brainstem illustrating major features of the anatomical distribution of pontine and medullary respiratory-related regions/compartments in dorsal (A, left), coronal (A, right), and parasagittal (B) planes. Dorsal view of brainstem in A with respiratory structures projected onto horizontal plane and the serial coronal sections at levels indicated show the dorsolateral pontine regions (K-F and PB) of the pontine respiratory group (PRG), and more caudally medullary regions of the ventral respiratory column (VRC) [retrotrapezoid nucleus (RTN)/parafacial respiratory group (pFRG), Bötzinger (BötC), pre-Bötzinger (pre-BötC), and rostral (rVRG) and caudal (cVRG) ventral respiratory groups]. Dorsomedial regions with the nucleus tractus solitarius (NTS), the caudal parts of which (cNTS) contain the DRG are indicated in A (left) and B, and the midline raphé nuclei are also shown. Distributions of respiratory premotoneurons (with direct connections to motoneurons, blue) and interneurons (with propriobulbar connections, yellow) are indicated. Locations of these neurons as depicted are highly schematic and provide only a general perspective of spatial distributions of some respiratory premotor and interneurons as determined from a variety of experimental approaches, including transsynaptic labeling with a viral tracer injected into the phrenic nerve. The spatial organization of respiratory microcircuits has not been determined in detail for any region, although general patterns of input and output axonal projections from various regions have been established in many cases. The VRC extends from the level of the rostral facial nucleus (VII) to caudally near the spino-medullary junction. The main clusters of rhythmically active VRC respiratory neurons are in the BötC, pre-BötC, rVRG, and cVRG. The RTN/pFRG at the rostral end of the VRC

contains tonically active neurons with direct projections to the rest of the VRC and dorsolateral pons and also contains neurons with respiratory-modulated activity under some conditions, particularly at elevated levels of carbon dioxide (see text for full explanation). The raphé nuclei, with connections to the VRC as well as cranial and spinal motoneurons, also contain tonically active neurons, subsets of which can exhibit respiratory modulation. Dimensions indicated are typical for an adult rat. Other abbreviations: IO, inferior olivary nucleus; K-F, Kölliker-Fuse nucleus; V, trigeminal motor nucleus; NA, nucleus ambiguus; CNA, compact division of NA; PB, parabrachial nucleus; py, pyramidal tract; RO, raphé obscurus; scp, superior cerebellar peduncle; 7n, facial nerve. Dorsal and coronal views in A are modified, with permission, from reference (88) (Fig. 40.4, with permission from Academic Press).
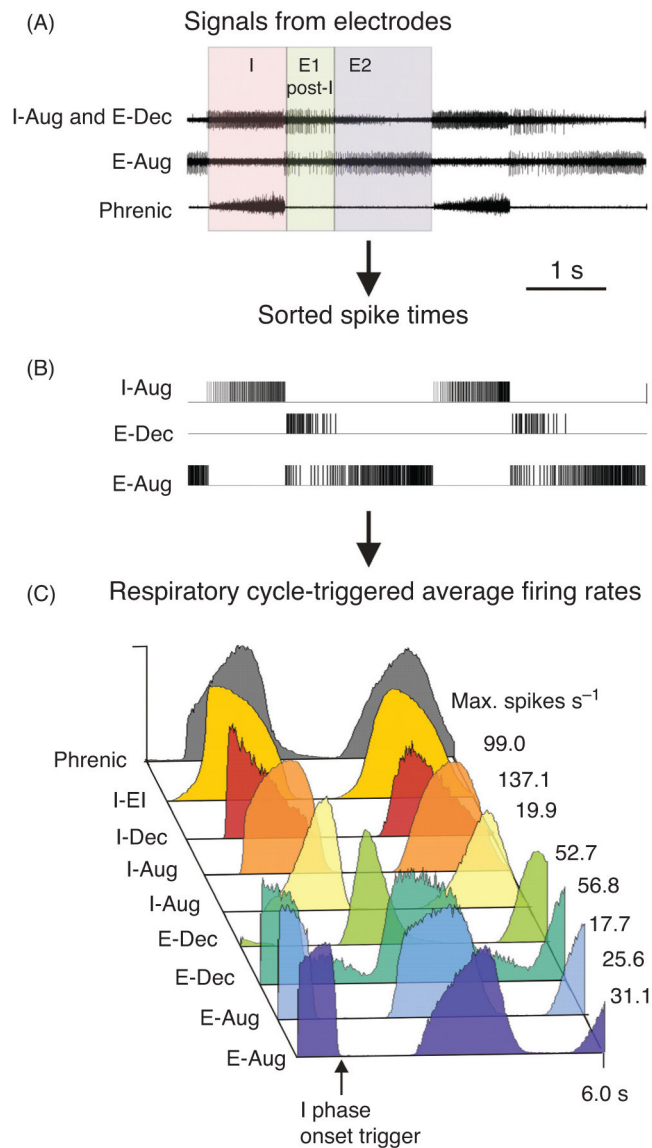
Figure 2.
Spiking patterns of ventral respiratory column (VRC) respiratory neurons. (A) Illustration of representative signals recorded simultaneously from three types of neurons with an extracellular recording electrode array and efferent phrenic nerve activity (data from a decerebrate cat). Color shaded overlays indicate the three "phases" of the respiratory cycle (see text). (B) Times of occurrence of individual spikes extracted from top traces by spike sorting. Adapted, with permission, from reference (297) (Fig. 1). (C) Average firing rates of eight simultaneously monitored VRC neurons and phrenic nerve activity. Temporal patterns of neuron spiking are represented by respiratory cycle-triggered spike frequency histograms obtained by triggering histogram computation at the onset of phrenic nerve activity signal (labeled arrow). Data are from a different animal than top traces. Adapted, with permission, from reference (222) (Fig. 1).
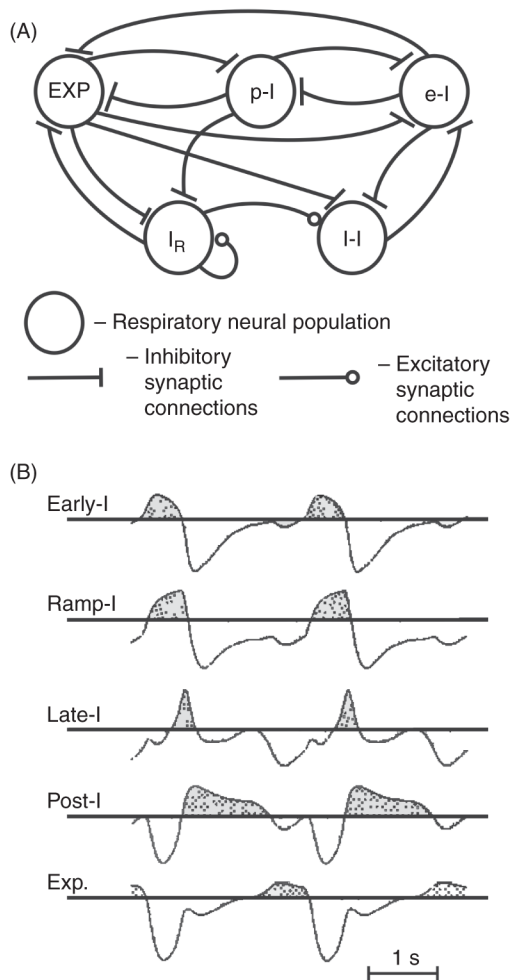
Figure 3.
An early respiratory network model proposed to generate a three-phase pattern of neural activity. (A) Model schematics indicating excitatory and inhibitory synaptic interactions among respiratory neuron populations including expiratory (EXP), postinspiratory (post-I), early-inspiratory (e-I), late-inspiratory (l-I), and ramp-inspiratory (I_R) populations. Note that I_R represents an excitatory and inhibitory population lumped in the schematic as a single component for simplicity. Not shown are excitatory inputs to each component from the reticular activating system that are reduced when p-I cells fire. (B) Patterns of activity for the model components (two cycles are shown). For each component, the period of active firing is indicated by the stippled region above threshold (horizontal line). Adapted, with permission, from reference (224) (Figures 3 and 4).
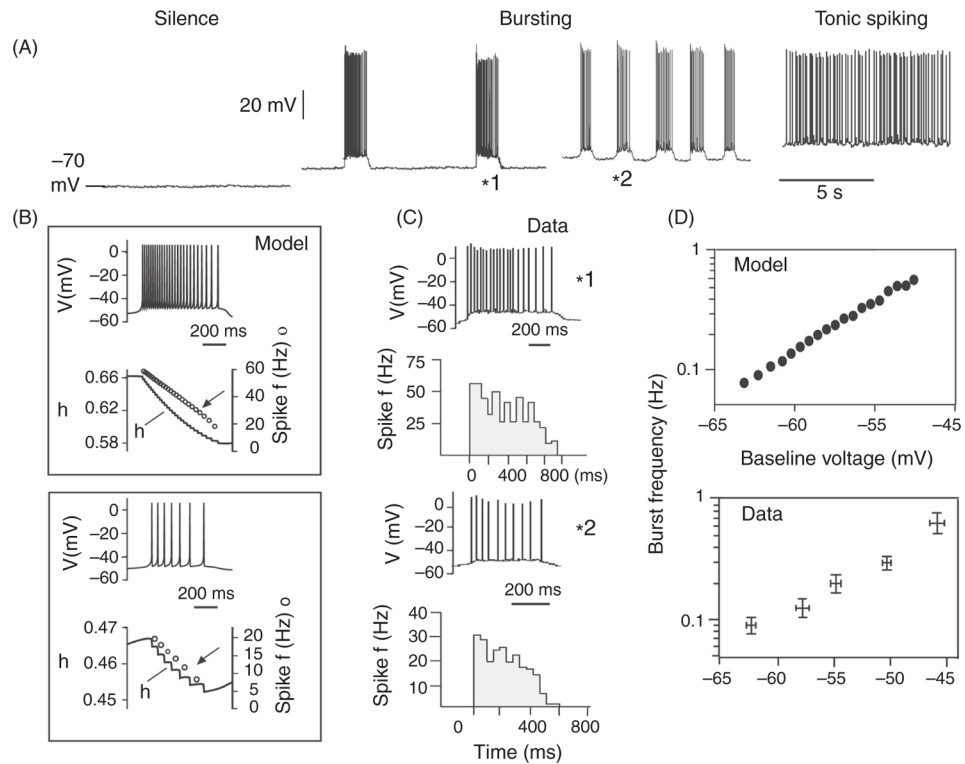
Figure 4.
Intrinsic electrophysiological behavior of inspiratory bursting "pacemaker" neurons that represent the cellular basis for pre-Bötzinger (pre-BötC) excitatory pacemaker-network models incorporating I_{NaP}-dependent bursting properties. (A, B) Example of voltage-dependent activity states (silence, oscillatory bursting, and tonic spiking) (A) and temporal features of bursting (B) of a pre-BötC inspiratory neuron recorded after blocking synaptic inputs *in vitro*, with corresponding bursting features (C) in the pacemaker neuron model (model 1) developed by Butera et al. (29). This H-H style conductance-based, biophysically minimal model incorporates I_{NaP} as the main subthreshold voltage-activating, burst generating inward current, with voltage-dependent slow inactivation, represented in the model by the kinetics of the inactivation parameter h. The pre-BötC neuron transitions from silence to oscillatory bursting and then tonic spiking as the baseline membrane voltage is depolarized by constant applied current—conditional bursting behavior also exhibited by the model (29). In the oscillatory bursting regime, in both the model and data, bursting frequency increases (see A and D) and burst durations decrease (see B and C) with steady depolarizing shifts of baseline potential. (B, C) Neuronal spiking profiles during individual bursts at two different voltage levels in the neuron model simulations (B) and from the example recordings (individual bursts from A indicated by *1 and *2 are shown in panel C with an expanded time scale), illustrating the declining spiking frequency (f) during the burst as shown in spike frequency histograms; histograms illustrated in C from recordings are averaged over multiple bursts. This spiking profile results from progressive inactivation of I_{NaP}, indicated by the time course of the inactivation parameter h during the burst phase (B), which causes burst termination followed by a slow recovery from inactivation that controls the period of the interburst interval and thus timing of the next burst (for full descriptions of the kinetics of the bursting cycle including dynamic interactions of I_{NaP} and the K+-dominated leak current in the model see references (29, 30). (D) The model reproduces the monotonic increase in bursting frequency over a wide dynamic range as baseline membrane voltage is depolarized. This voltage-dependent control of bursting

frequency is reflected in the control of neuronal population bursting frequency by tonic excitatory inputs in models of pre-BötC heterogeneous excitatory networks incorporating subpopulations of I_{NaP}-dependent bursters (see Fig. 5). Adapted, with permission, from reference (30) (Fig. 12.1, with permission, from World Scientific Press).
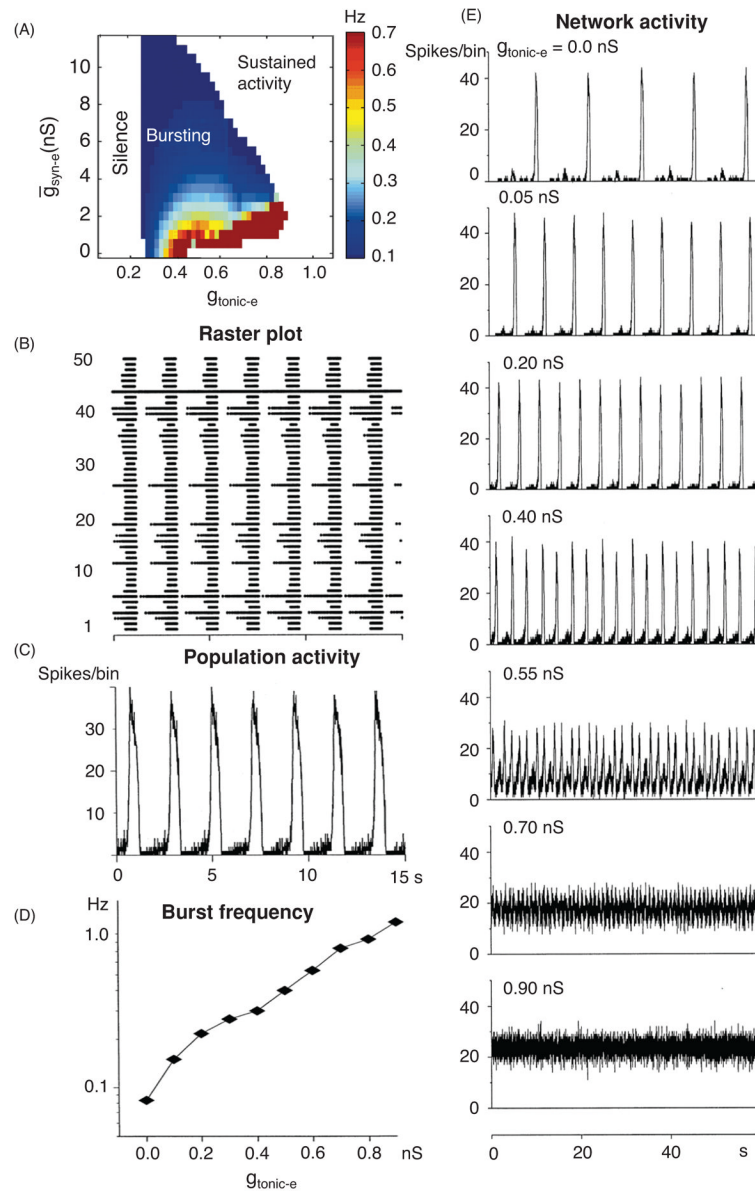
Figure 5.
Generation of oscillations in model excitatory networks incorporating neurons with intrinsic bursting properties. (A) Behavior of a small (two-cell) network illustrating effects of a mean level of tonic excitatory input, represented by the conductance $g_{tonic-e}$, and excitatory synaptic conductance g_{syn-e} on the dynamics of bursting and sustained spiking activity of pairs of identical coupled Butera et al. (29) model 1 neurons. Each neuron incorporates the persistent (slowly inactivating) Na$^+$ current (I_{NaP}), a K+-dominated leak current, and spike-generating transient Na$^+$, and delayed rectifier K$^+$ currents representing a biophysically minimal set of ionic conductances. The model neurons are mutually coupled in an excitatory network by modeled glutamatergic-like synapses (non-NMDA (N-Methyl-D-aspartate) receptor mediated) with synaptic dynamics generating fast postsynaptic responses with conductance g_{syn-e} as described in detail in reference (29). The plot represents burst frequency; colored areas indicate frequencies for the $g_{tonic-e}$– g_{syn-e} parameter sets producing oscillatory bursting. Range of burst frequencies is indicated by the color bar on

the right. Parameter sets to the left or right of the oscillatory bursting region result, respectively, in no activity (silence) or sustained spiking activity. (B, C) Synchronized activity of a heterogeneous population of 50 bursting model 1 neurons represented as a raster plot (B) of spike times across the population and histogram of population spiking activity (bin size = 10 ms) (C). Neurons are coupled (all-to-all) by the fast glutamatergic-like excitatory synapses with g_{syn-e}. Heterogeneity, due to a distribution of leak currents within the model population, results in a temporal dispersion of spiking onset times in the population including cells generating preinspiratory/inspiratory (pre-I/I) spiking activity as seen in the raster plot. As a result of heterogeneity of cellular properties in the network, only a fraction of the neurons in the population exhibit intrinsic pacemaker-like rhythmic bursting activity when synaptically uncoupled. Single neuron spiking behavior and population oscillations generated by the intact network have temporal patterns (C) similar to those recorded from the neonatal rodent pre-Bötzinger (pre-BötC) network isolated in medullary slices *in vitro.* (D) Network burst frequency for a model 50-cell network as a function of $g_{tonic-e}$. (E) Histograms of network spiking activity (10-ms bin size) as the mean level of $g_{tonic-e}$ is increased. Elevation of this input (from top to bottom) increases burst frequency and, finally, switches the population activity from rhythmic bursting to sustained asynchronous activity. Adapted, with permission, from reference (28) (Figures 3B1, 3B2, 2C, 7B, and 7A1–7A7).
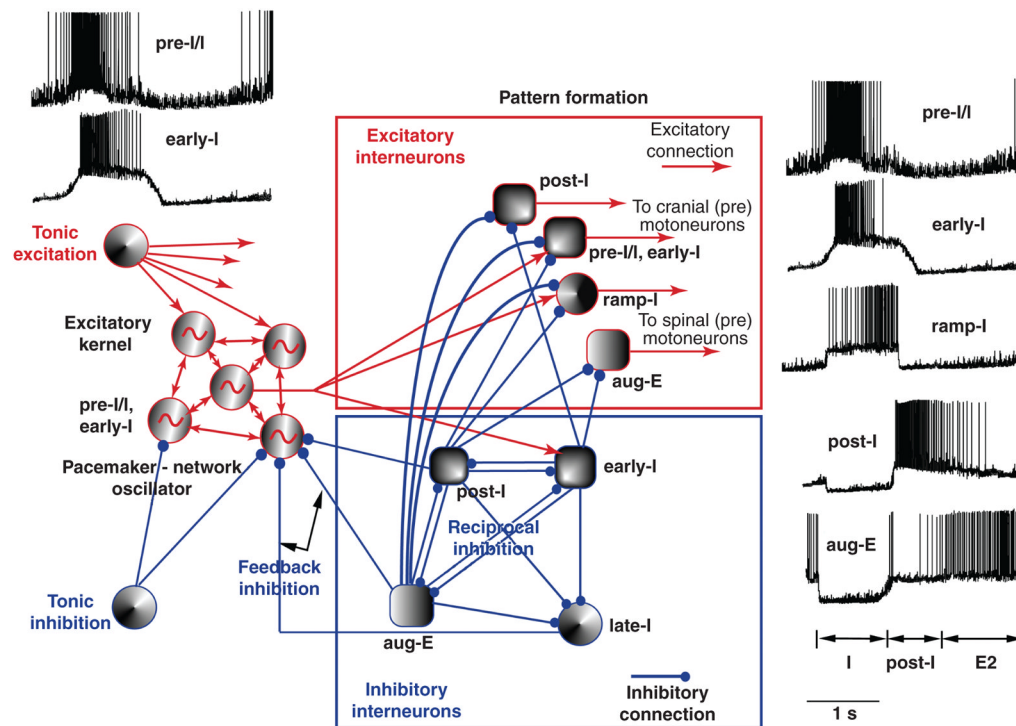
Figure 6.
The hybrid pacemaker-network model. Core circuits of the respiratory CPG network in this conductance-based neuronal model consist of interacting populations of different medullary excitatory and inhibitory interneurons and incorporate the excitatory pacemaker-network "kernel," representing the pre-Bötzinger (pre-BötC) network composed of a heterogeneous population of inspiratory neurons [excitatory preinspiratory/inspiratory (pre-I/I) and early-inspiratory (early-I types)] with I_{NaP} (their activity from model simulations is shown at the top left). Subsets of these excitatory neurons had Butera et al. model 1-type, conditional oscillatory bursting properties when synaptic interactions are eliminated. Excitatory interneurons (see examples of activity patterns at right) in premotor pattern formation circuits driven by the pre-BötC network generate excitatory synaptic drive in parallel transmission pathways to cranial and spinal (pre)motor neurons. Interconnected inhibitory interneurons [e.g., postinpiratory (post-I), second expiratory (E2), augmenting E neuron (aug-E), and early-I types with reciprocal connections, as well as late-inspiratory (late-I) spiking neurons, middle bottom] generate temporal patterns of synaptic inhibition that dynamically control activity of the pre-BötC network via feedback connections from the late-I, post-I, and E2 populations (only a few connections are shown for simplicity). Inhibitory interneurons also provide feed-forward inhibition projecting to the excitatory drive transmission populations (connections from post-I, E2, and early-I neurons are shown) to sculpt premotor output activity to form a three-phase activity pattern with preinspiratory/ inspiratory (pre-I/I), early-I, ramp-inspiratory (ramp-I), post-I, and E2 spiking patterns. This activity mirrors the three-phase activity pattern of the interacting excitatory kernel and inhibitory interneurons. This model incorporated the concept of the excitatory kernel network with state-dependent intrinsic oscillatory bursting properties in the pre-BötC and their dynamic regulation by inhibitory expiratory neuron populations giving rise to multiple possible modes of rhythm generation. The model also represents the various types of medullary respiratory interneurons as consisting in most cases of both inhibitory and excitatory neurons. Modified, with permission, from reference (312) (Fig. 3, with permission, from Elsevier).
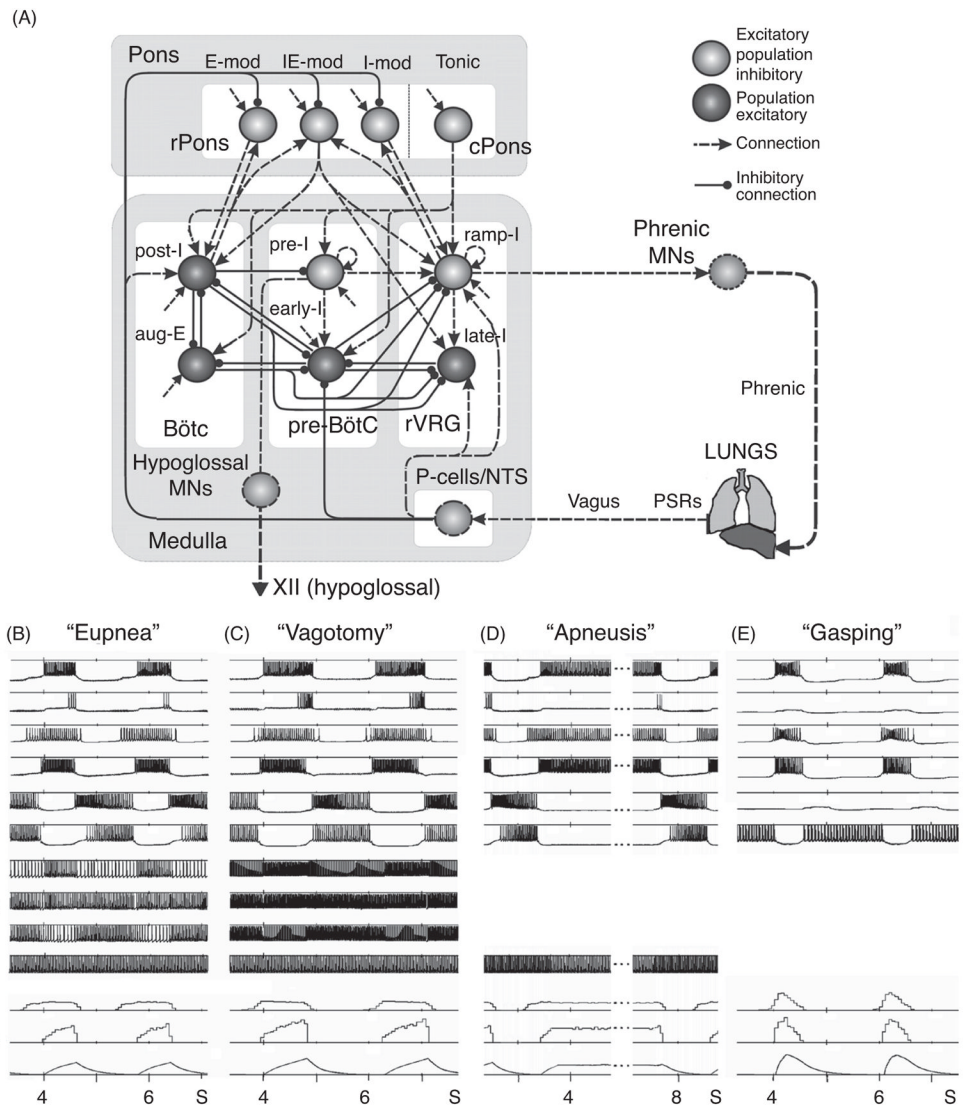
Figure 7.
A ponto-medullary model of the respiratory CPG developed by Rybak et al. (285) that incorporates compartmentalized network components and regulation of medullary network activity by pontine inputs as well as feedback signals via peripheral respiratory system, lung-related afferent inputs conveyed by the vagus nerve. (A) Model schematic. Each sphere represents a population of 50 neurons incorporating various membrane conductances. Dashed lines with arrows represent excitatory synaptic connections and solid lines ending with small circles show inhibitory connections. Additional arrows at the population circles indicate external excitatory tonic drive to each population. Simulations in B-E illustrate model performance under different conditions. The top six traces show membrane potential trajectories of a randomly selected neuron from each population, and the next four traces show respiratory modulated (mod) or tonic spiking patterns of pontine populations; the three bottom traces show simulated integrated hypoglossal (XII) and phrenic nerve activities and lung volume excursions (the bottom trace), which provide afferent mechanosensory input signals for control of respiratory phase durations and activity patterns. (B) Performance of the intact network (eupnea). (C) "Vagotomy": vagal feedback in the model is disconnected. (D) "Apneusis" produced by removal of inputs from rPons (E-mod, IE-mod, and I-mod). (E)

Complete removal of the pons switches the system to the state in which the rhythm in the network is completely driven by I_{NaP}-dependent bursting pacemaker activity originating in the pre-Bötzinger complex (pre-BötC). Adapted, with permission, from reference (285) (Figures 1, 2A, B, and 5, with permission, from Elsevier).
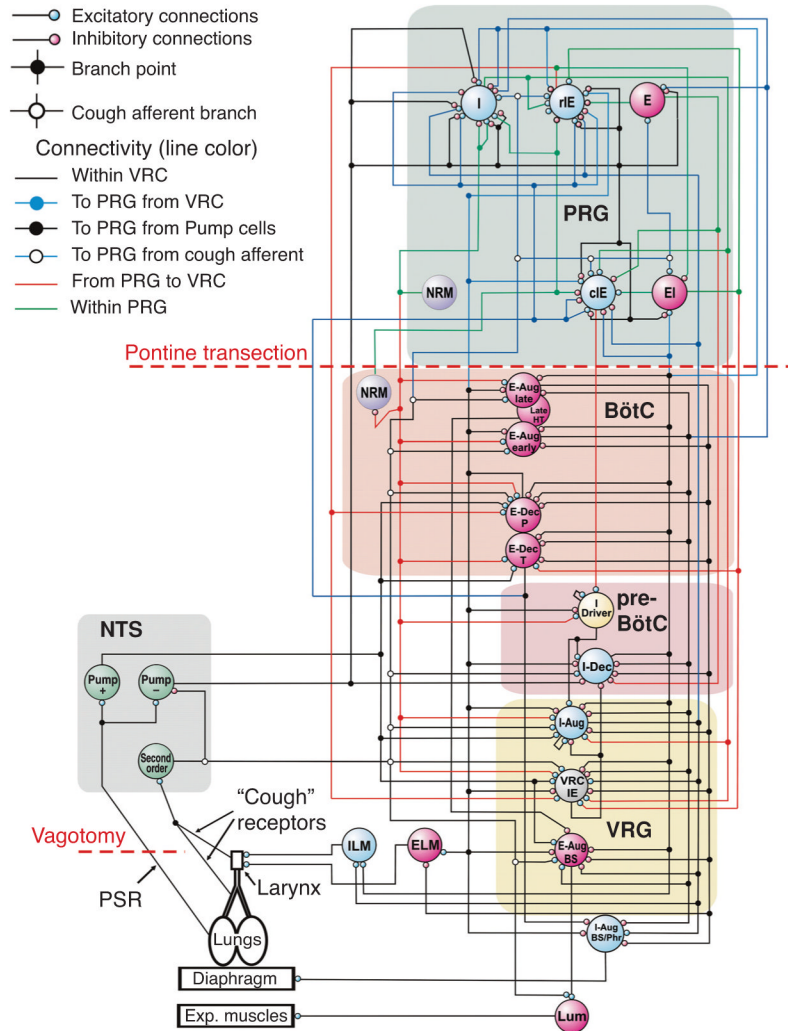
Figure 8.
Schematic of the brainstem respiratory network model incorporating connections inferred from *in vivo* multielectrode array recordings in decerebrate cats (297). Each large-labeled circle represents a distinct neuron population using nomenclature conventions summarized in Table 1. Intra- and interregional connections are indicated by color-coded lines; dots mark branch points of divergent projections. Model parameters for cell properties and the connections among the populations are detailed in Tables 6 and 7 of Appendix in reference (279). Red dashed lines label specific simulated perturbations. Adapted, with permission, from reference (279) (Fig. 4).
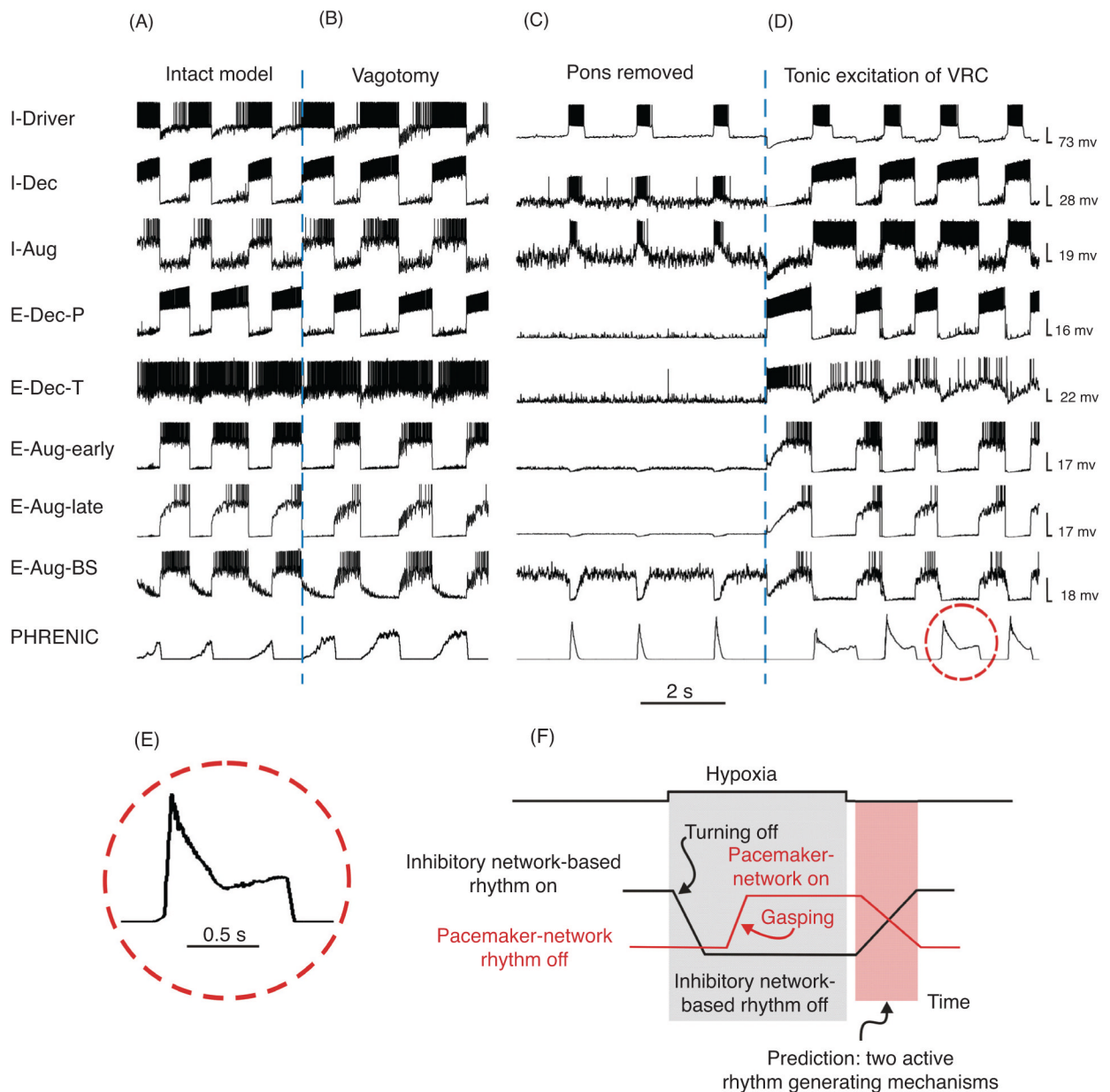
Figure 9.
Performance of the large-scale brainstem respiratory network model as shown schematically in Figure 8 under different conditions. The top traces (except the bottom trace for phrenic activity) show simulations, based on integrate-and-fire (IF) cellular models, of membrane potential trajectories of one, randomly selected neuron from the major neural populations represented in the model. Note that the labels for the inspiratory decrementing (I-DEC) and expiratory decrementing (E-DEC) neuron membrane potential traces refer to the decrementing rate of spike generation in each cycle due to an elevation of threshold in the IF style neurons not reflected in the membrane potential trace. (A) Performance of the intact network (eupnea). (B) "Vagotomy"—vagal feedback in the model is disconnected (indicated by a blue vertical dashed line). (C) Gasp-like pattern originating in the pre-Bötzinger (pre-BötC) population with I_{NaP}-dependent bursting behavior after pontine transection (pons removed). (D) Model prediction of coexpression of gasp-like burst and eupneic-like ramp

pattern of phrenic nerve activity with progressive increase of tonic excitation of ventral respiratory column (VRC) populations. A "burst-ramp" type phrenic motor pattern emerged with the onset of tonic reexcitation of the VRC network populations (red dashed line). (E) Expanded time scale trace from D shows a burst-ramp type pattern during an inspiratory phase. (F) Summary of a prediction from the model showing that two active rhythmic burst pattern generating processes (inhibitory network-based and I_{NaP}-dependent excitatory pacemaker-network-based mechanisms) can be simultaneously expressed during recovery from hypoxic gasping. See text for details. Adapted, with permission, from reference (279) (Figures 5 and 10).
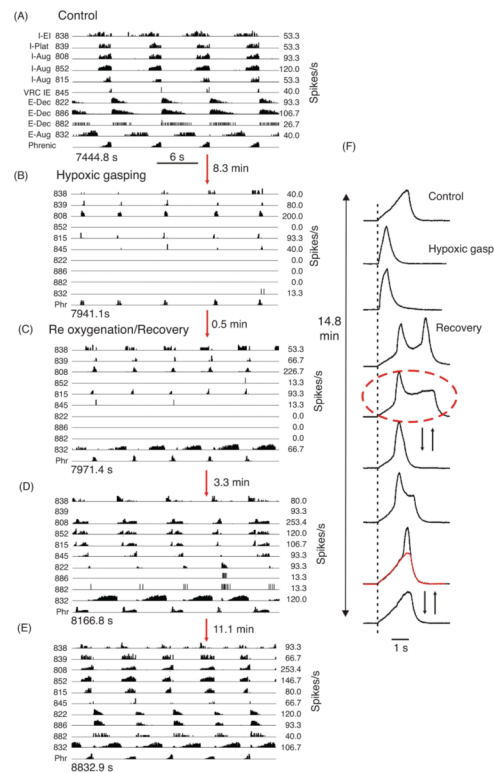
Figure 10.
In vivo ventral respiratory column (VRC) neuronal activity profiles during control conditions, hypoxic gasping, and recovery. (A–E) Firing rates of ten simultaneously recorded VRC inspiratory/expiratory neurons and phrenic nerve activity from decerebrate cat during the prehypoxia control period (A), hypoxia-induced gasp-like activity (B), and reoxygenation (C–E). (F) Integrated phrenic nerve activity profiles detail control, gasping, and a return to eupneic-like (ramping) phrenic activity patterns with superimposed augmented bursts. Pattern with dashed line ellipse is similar to the phrenic activity profile observed in model simulations as shown in Figure 9. This pattern occurs during successive cycles and occasionally alternates (bidirectional arrows) with the gasp-like phrenic burst pattern. See text for details. Adapted, with permission, from reference (279) (Fig. 11).
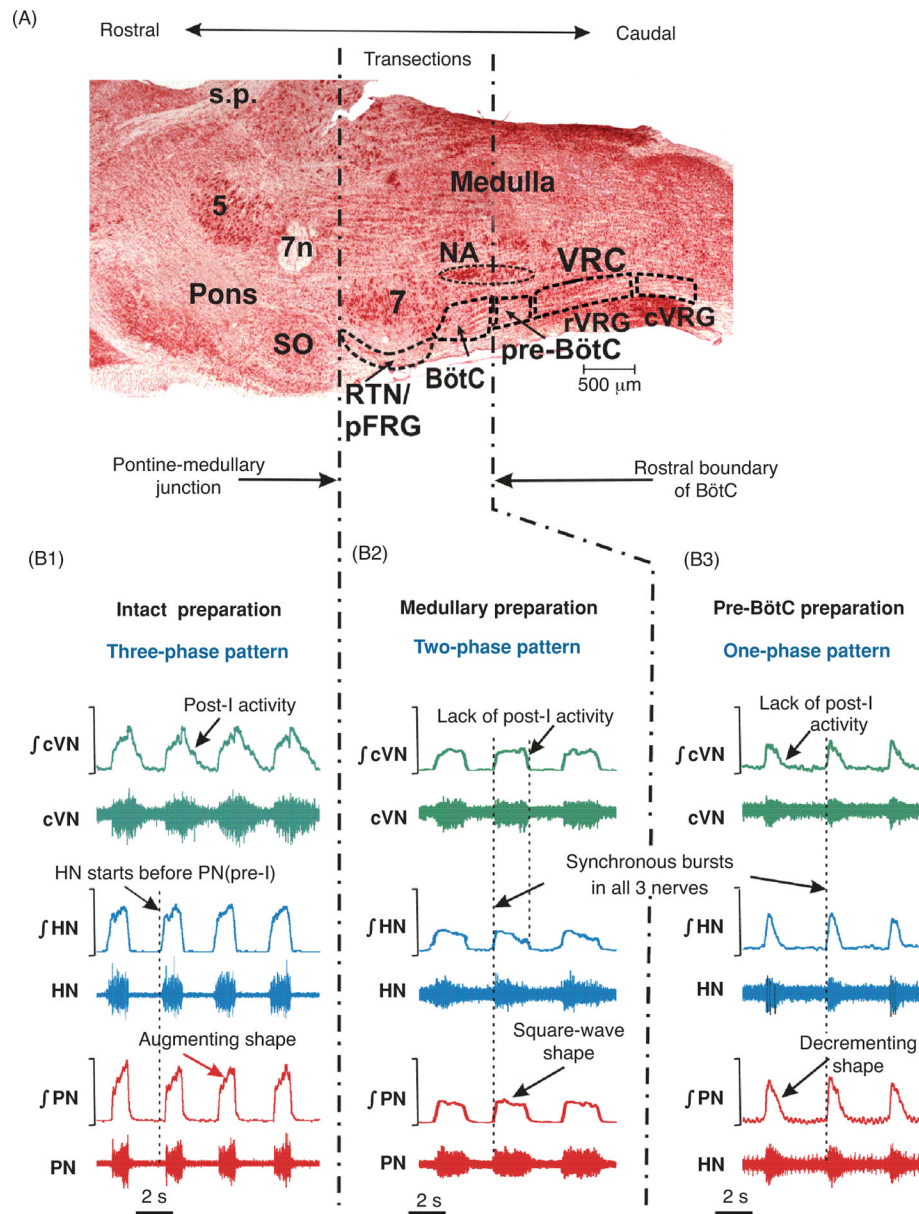
Figure 11.
Transformations of respiratory rhythm and motor pattern following sequential brainstem transection in the *in situ* arterially perfused brainstem-spinal cord preparation from juvenile rat, revealing three rhythmic states of the respiratory network as the circuitry is progressively reduced. (A) Parasagittal section (neutral red stain) of the brainstem at the level of the ventral respiratory column (VRC), and lateral pons (5, trigeminal nucleus; 7, retrotrapezoid nucleus (RTN); 7n, facial nerve; BötC, Bötzinger complex; cVRG, caudal ventral respiratory group (VRG); NA, nucleus ambiguous; pre-BötC, pre-Bötzinger complex; rVRG, rostral VRG; RTN/pFRG, retrotrapezoid nucleus/parafacial respiratory group; s.p., superior cerebellar peduncle; SO, superior olive; VRC, ventrolateral respiratory column). (B1–B3) Representative activity patterns of phrenic (PN), hypoglossal (HN), and central vagus (cVN) nerves recorded from the intact preparation (B1), "medullary preparation" obtained by transections at the pontine-medullary junction performed to

remove the pons (vertical dot-dashed line, middle panel) (B2), and "pre-BötC preparation" obtained by transections at the rostral boundary of the pre-BötC made to remove all compartments (RTN/pFRG, BötC) rostral to pre-BötC (vertical dot-dashed line, right panel). Each panel shows raw (bottom traces) and integrated (upper traces) recordings of motor nerve discharge. Vertical dashed lines in B1 indicate onsets of HN inspiratory burst. Dashed lines in B2 and B3 indicate synchronous onset of inspiratory bursts in all nerves characteristic of the two-phase and one-phase rhythmic patterns. Motor nerve discharges have square-wave and decrementing shapes in the two-phase and one-phase patterns, respectively, which characterize these two different rhythmic states. Adapted, with permission, from reference (311) (Fig. 2).
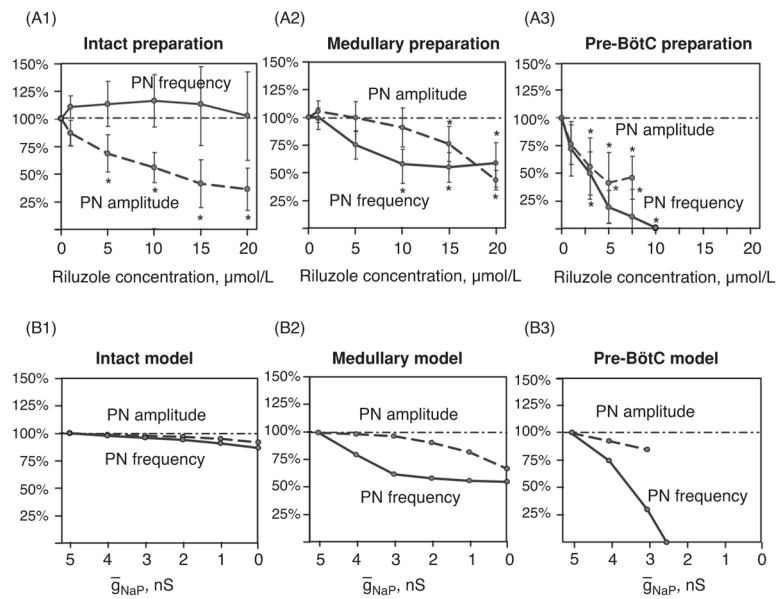
Figure 12.
Role of the persistent sodium current (I_{NaP}) in rhythm generation in different network states. (A1–A3) Steady-state dose-dependent effects of I_{NaP} blocker, riluzole, on burst frequency (solid lines) and amplitude (dashed lines) of integrated phrenic nerve (PN) activity recorded in the intact (A1), medullary (A2), and pre-BötC (A3) preparations with motor patterns shown in Figure 11. PN discharge amplitudes and frequency are normalized (% control). Burst frequency does not change significantly in the intact preparation (A1), but is reduced to a constant value in medullary preparations (A2). In pre-BötC preparations (A3), PN burst frequency is reduced monotonically with increasing riluzole concentration, and rhythmogenesis is abolished at drug concentrations 10 μmol/L or more. All values represent means ±SD (error bars). *Statistical significance ($P < 0.05$). (B1–B3) Effects of reducing I_{NaP} on frequency and amplitude of motor output (PN) in the intact (B1), medullary (B2), and pre-BötC (B3) network models (refer to Figure 11). Attenuation of I_{NaP} is modeled by uniformly reducing the maximum conductance for the persistent sodium channels ($\bar{g}_{NaP}$) in all neurons of the pre-I/I population in the pre-BötC network. Effects of reducing $\bar{g}_{NaP}$ on frequency (solid lines) and amplitude (dashed lines) of simulated PN bursts (% control) closely reproduce experimental data shown in A1–A3, including the initial decrease in burst frequency in the medullary preparation (B2, cf. with A2), and the decrease in burst frequency with decreasing $\bar{g}_{NaP}$ with termination of rhythm generation (at $\bar{g}_{NaP} = 2.5$ nS) in the case of the one-phase rhythmic state (B3, cf. with A3). Reduction of burst amplitudes (dashed lines) is also consistent with experimental data, although perturbations in model are smaller than those observed experimentally. Adapted, with permission, from reference (310) (Figures 6A and 9).
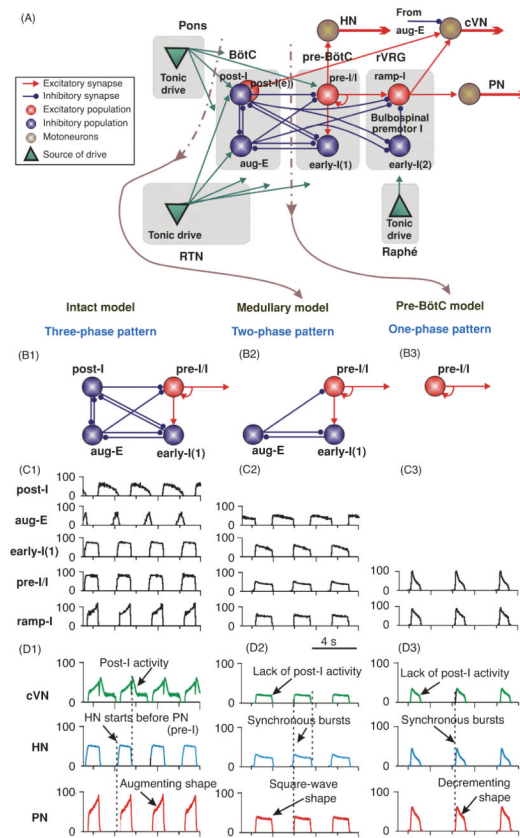
Figure 13.

Computational model of the brainstem respiratory network by Smith et al. (310). (A) Schematic of the model network showing interactions between different populations of respiratory neurons within major brainstem compartments involved in the control of breathing [Bötzinger (BötC), pre-Bötzinger (pre-BötC), and rostral (rVRG) and caudal (cVRG) ventral respiratory groups]. Each population consists of 50 single-compartment neurons incorporating H-H style conductances with heterogeneous distributions of parameters within the population. Green triangles represent sources of tonic excitatory drives (from pons, RTN/pFRG, and raphé nuclei) to different neural populations (only several drives are shown connected). Simulated "transections" (dot-dashed lines) mimic those performed *in situ* as shown in Figure 11. (B1–B3) Key elements and circuits within the intact (B1), medullary (B2), and pre-BötC (B3) models involved in rhythmogenesis (excitatory drives are not shown). The three-phase pattern is generated by a core circuit with a three-population mutual inhibitory ring-like architecture interacting with the preinspiratory (pre-I/I) pre-BötC excitatory kernel network. A reduced network configuration lacking the BötC postinspiratory (post-I) inhibitory population generates the two-phase inspiratory-expiratory rhythmic pattern, which is dependent on mutual inhibitory interactions of the active augmenting E neurons (aug-E) and early inspiratory (early-I) (type 1) populations in a "half-center"-like circuit that interacts with the pre-I/I population. The one-phase pattern is generated by I_{NaP}-dependent rhythmic bursting activity of the pre-I/I excitatory population in pre-BötC that synaptically drives the downstream HN and excitatory rVRG populations for inspiratory (pre)motor output generation. (C1–C3) Simulations of activity of selected neuronal populations in the model. Activity of each population is represented by a histogram of the average neuronal spiking frequency within the population (spikes/s/neuron, bin size =

30 ms). (D1–D3) Simulated motor outputs (cVN, HN, and PN) in each model. Adapted, with permission, from reference (310) (Figures 7 and 8).
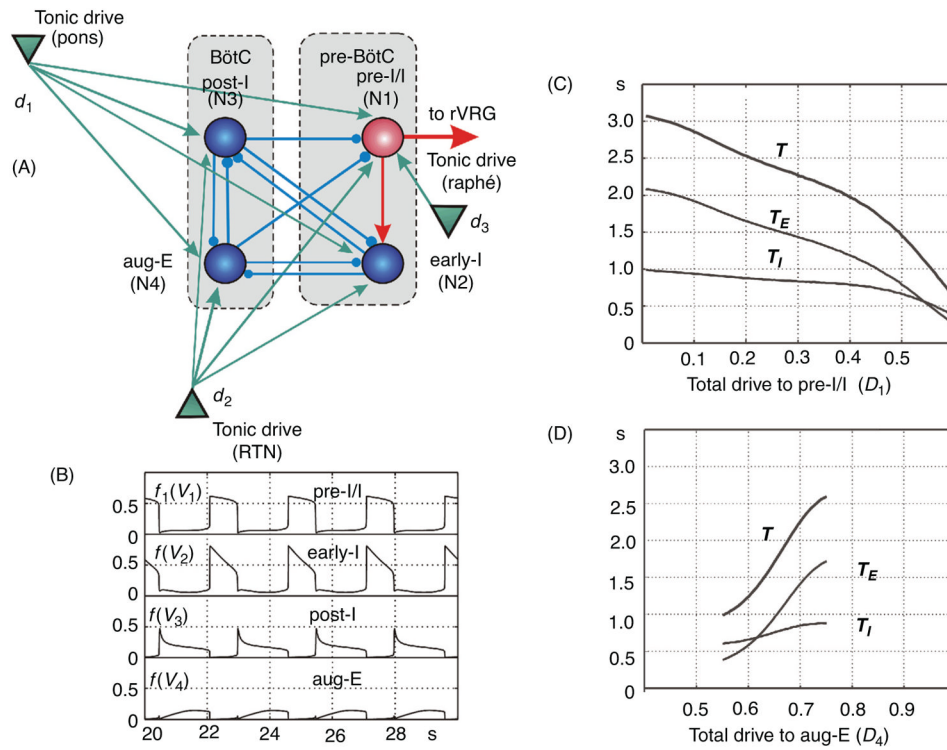
Figure 14.
An activity-based model of the four-population core of the brainstem respiratory network generating the three-phase respiratory pattern. (A) Model schematic of the BötC-pre-BötC network with preinspiratory (pre-I/I), early-inspiratory (early-I), postinspiratory (post-I), and augmenting-inspiratory (aug-E) neuron types. Spheres represent neurons (excitatory: red; inhibitory: blue); green triangles represent three sources of tonic excitatory drives [from pons, retrotrapezoid nucleus (RTN), and raphé] to different neural populations, each modeled as a single element described mathematically by activity functions $f(V)$. (B) Model performance. Traces of simulated model output activities for all four neurons ($f1(V_1)$, $f(V_2)$ – $f(V_4)$). (C, D) Control of oscillation period and phase durations by excitatory drive. Changes of the oscillation period (T) and durations of inspiration (T_I) and expiration (T_E) were produced by changes in the total (net) drive to the preinspiratory (pre-I/I) neuron ($D1$, C) and to the augmenting expiratory (aug-E) ($D4$, D) neuron. Adapted, with permission, from reference (276) (Figures 1B, 2A, 3A, and D).
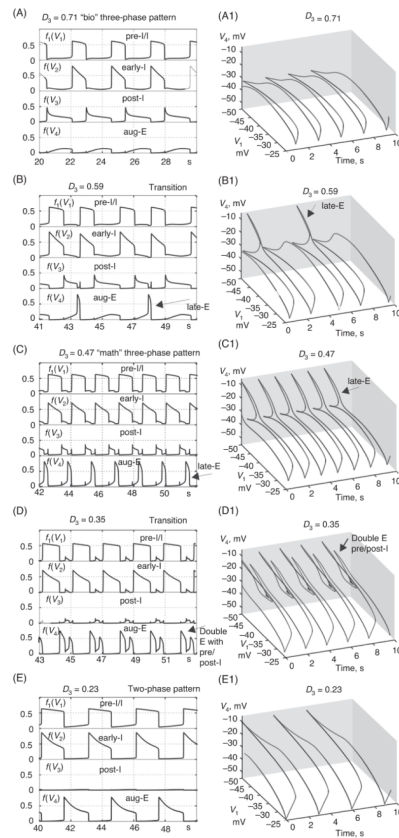
Figure 15.
Transition from the "bio" three-phase pattern to the two-phase pattern with progressive reduction of drive to the postinspiratory (post-I) neuron ($D3$) in the activity-based model of Rubin et al. (273). Traces in A–E (left) show output activities of all four neurons ($f1(V_1)$, $f(V_2) – f(V_4)$). (A1–A4) show corresponding dynamic trajectories of preinspiratory (pre-I/I) versus augmenting E (aug-E) neuron voltages (V_1 vs. V_4) over successive cycles illustrating the emergence of additional aug-E activity patterns in transitional regimes between the three-phase and two-phase patterns when $D3$ is reduced from top to bottom (from A, A1 to E, E1), as indicated in the diagram labels. Panels A and A1 correspond to the initial "bio" three-phase pattern. Note the emergence of late-E bursts in aug-E neuron in panels B, B1 and C, C1. Diagrams C, C1 represent the "math" three-phase oscillations. Diagrams D, D1 show an example of the double burst, biphasic-E activity pattern in the aug-E neuron. Finally, diagrams E, E1 illustrate two-phase oscillations. Adapted, with permission, from reference (276) (Fig. 11 A–E).
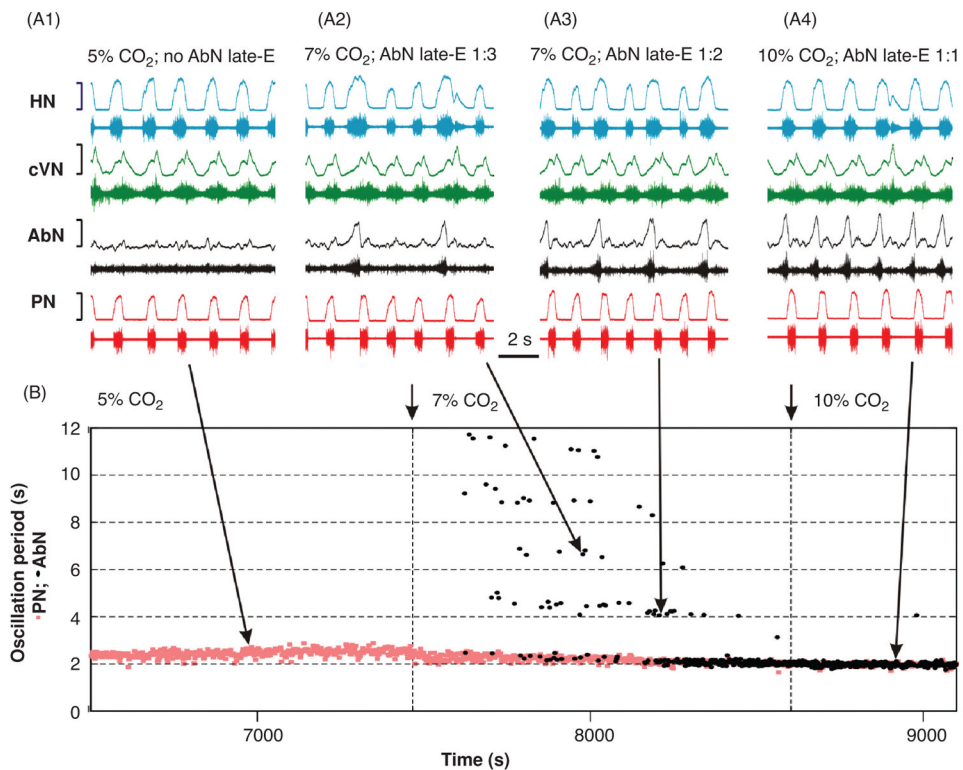
Figure 16.
Experimental data illustrating quantal acceleration of late-expiratory (late-E) abdominal activity with the development of hypercapnia (increase in the CO_2 concentration in the perfusate of an arterially perfused *in situ* juvenile rat brainstem-spinal cord preparation). (A1–A4) Simultaneously recorded activity of (bottom-up) phrenic (PN, red), abdominal (AbN, black), cervical vagus (cVN, green), and hypoglossal (HN, blue) nerves. Activity of each nerve is represented by two traces: raw recording (lower trace) and integrated activity (upper trace). (A1) Normocapnia (5% CO_2): late-E activity is absent in the AbN. (A2–A4) Quantal acceleration of AbN activity: with the development of hypercapnia, the ratio between the AbN and PN frequencies goes through step-wise changes from 1:3 and 1:2 (A2 and A3, 7% CO_2) to 1:1 (A4, 10% CO_2). (B) Time-series representation of the entire experimental epoch with the oscillation periods in the PN (red squares) and AbN (black circles) plotted continuously. The AbN late-E bursts were synchronized with the PN bursts with a ratio increasing quantally from 1:5 to 1:1. The content of CO_2 in the perfusate of this preparation was changed at times indicated by short arrows and vertical dashed lines. Large arrows indicate times corresponding to the episodes shown in A1–A4. Adapted, with permission, from reference (200) (Fig. 1).
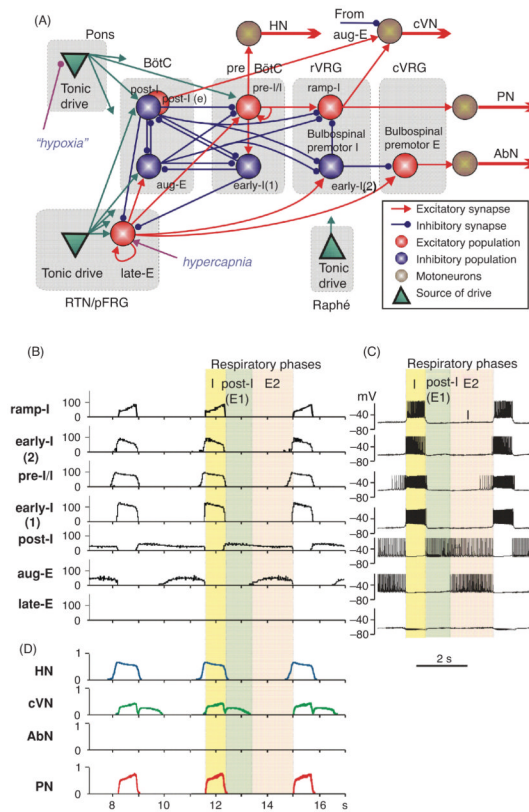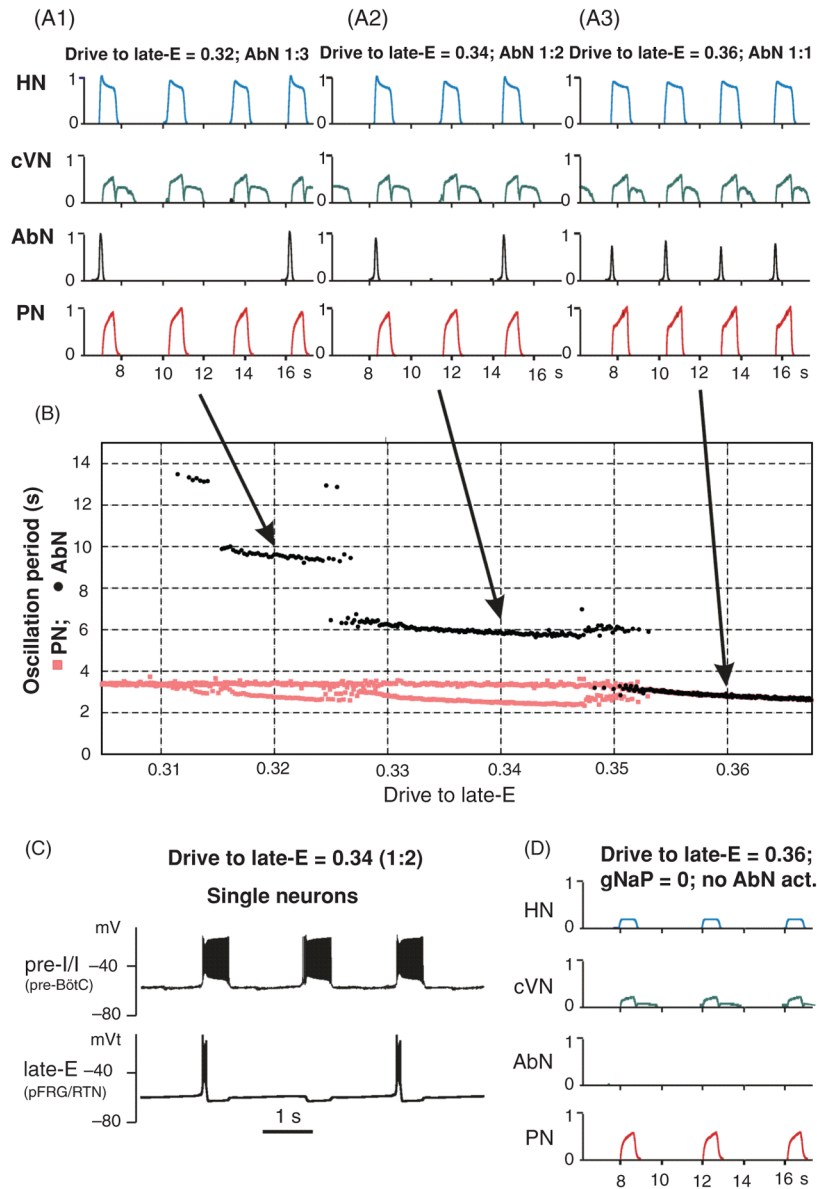
Figure 17.
The extended model of the brainstem respiratory network by Molkov et al. (200). (A) Schematic of the model showing interactions between different populations of respiratory neurons within major brainstem compartments [pons, retrotrapezoid nucleus (RTN)/ parafacial respiratory group (pFRG), Bötzinger (BötC), pre-Bötzinger (pre-BötC), and rostral (rVRG) and caudal (cVRG) ventral respiratory groups). Each population (shown as a sphere) consists of 50 single-compartment neurons described in the H-H style. In comparison with the previous model (310), see Figure 13A, this model additionally incorporates the population of bulbospinal premotor expiratory (E) neurons in cVRG, representing the source of AbN activity, and the late-E population in the RTN/pFRG compartment, serving as a source of I_{NaP}-dependent oscillations in RTN/pFRG. The model includes three sources of tonic excitatory drive: pons, RTN and raphé shown as green triangles. These drives, especially those from the pontine and RTN sources project to multiple neural populations in the model (green arrows, only the most important connections are shown to particular populations). The late-E population receives an additional external drive simulating the effect of hypercapnia; the pontine drive is considered to be hypoxia/ anoxia dependent and was reduced in simulations of hypoxic conditions [see examples in Molkov et al. (200)]. (B) Model performance under normal conditions. The activities of major neural populations in the model are represented by average histograms of activity of all neurons in each population (spikes/s/neuron, bin size = 30 ms). The populations shown include (top-down): ramp-inspiratory (ramp-I located in rVRG), early-inspiratory [early-I(2) in rVRG], preinspiratory/inspiratory (pre-I/I in pre-BötC), early-inspiratory [early-I(1) in pre-BötC], postinspiratory (post-I in BötC), augmenting expiratory (aug-E in BötC), and late-expiratory (late-E in RTN/pFRG). The latter population is silent under normal conditions. (C) Traces of membrane potentials of the corresponding single neurons (randomly selected from each population). (D) The model's motor outputs: hypoglossal

(HN, blue); cervical vagus (cVN, green); abdominal (AbN, black, silent under normal conditions); phrenic (PN; red). In B–D, the three phases of respiratory cycle are highlighted: I (yellow), post-I (light green), second expiratory (E2, pink). It is seen that pre-I/I neurons and HN start firing in advance of the beginning of inspiration defined by the onset of PN (and the ramp-I population) activity. Adapted, with permission, from reference (200) (Fig. 7).

Figure 18.
Modeling the effects of progressive hypercapnia and I_{NaP} blockade in the extended model of Molkov et al. (200). (A1–A3) The activity of motor outputs in the model during simulated hypercapnia. The late-E bursts in the abdominal nerve motor output (AbN) were always phase-locked with phrenic (PN) bursts and the ratio between AbN and PN burst frequencies quantally increased through 1:3 (A1) to 1:2 (A2) and to 1:1 (A3) regimes as "hypercapnic" drive to the late-E population of RTN/pFRG was gradually increased to simulate progressive hypercapnia. (B) The dependence of oscillation periods in AbN (black circles) and PN (red squares) activities on the hypercapnic drive (horizontal axis). This simulation shows a quantal acceleration of AbN activity during a gradual increase in the simulated hypercapnic drive. The ratio between AbN and PN burst frequencies sequentially jumped from 1:4 to 1:3 (as in A1), then to 1:2 (as in A2), and finally to 1:1 (as in A3). See Figure 15 for comparison to experimental data. With quantal acceleration of AbN activity (after it emerges at a simulated drive level of 0.31 and before it reaches the 1:1 ratio at 0.35). Branches of red

lines (bottom) represent alternating values of PN burst period depending on the presence or absence of an AbN burst during the corresponding cycle. (C) Membrane potential traces of single neurons from the preinspiratory/inspiratory (pre-I/I) population of pre-Bötzinger (pre-BötC) (upper trace) and the late expiratory (late-E) population of retrotrapezoid nucleus (RTN)/parafacial respiratory group (pFRG) (bottom trace) corresponding to the regime of 1:2 coupling between AbN and PN bursts (A2). (D) Simulation of the effect of I_{NaP} blockade. Model output motor activities illustrated correspond to the 1:1 coupling regime shown in A3. The blockade of I_{NaP} was simulated by setting its maximal conductance to zero in all pre-I/I and late-E neurons of the model, which eliminated AbN activity and reduced the amplitude and frequency of other simulated motor outputs (compare with A3). Adapted, with permission, from reference (200) (Fig. 8).
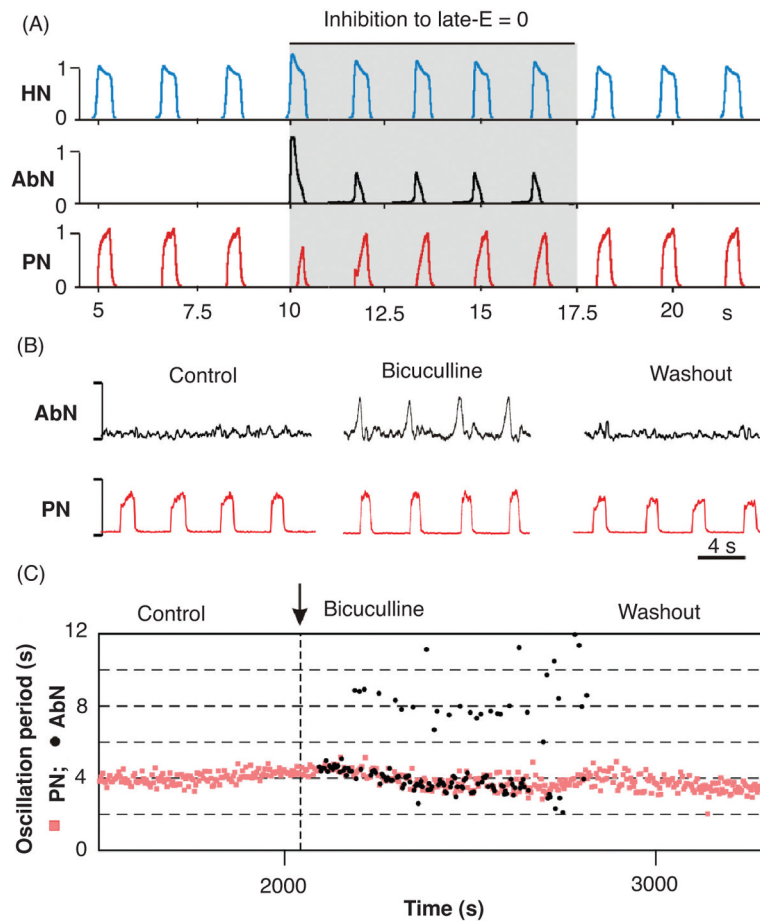
Figure 19.
Release of the abdominal nerve motor output (AbN) late-expiratory (late-E) bursting under normal conditions by suppressing inhibition in retrotrapezoid nucleus (RTN)/parafacial respiratory group (pFRG). (A) Simulation results from the Molkov et al. (200) model. The traces of motor outputs [PN, AbN, and hypoglossal motor output (HN)] generated by the model are shown. Drive to the late-E population was set to 0.3, below the threshold for late-E population activation (see Fig. 18B). To simulate the blockade of inhibition within RTN/ pFRG, the weights of inhibitory synapses in late-E neurons were set to zero during the time interval between 10 and 17.5 s (indicated by gray area). Removing inhibition evoked late-E oscillations in both the late-E population in the RTN/pFRG (not shown) and in the model's AbN output. The bursts generated were phase-locked to PN oscillations. After inhibition returned to the previous level (at 17.5 s) AbN activity disappears. (B, C) Experimental testing of the earlier described modeling prediction. The experiment shown was performed at normal metabolic conditions with 5% CO_2 in the perfusate of an arterially perfused juvenile rat brainstem-spinal cord preparation. Under control conditions there was no late-E bursting activity in AbN (see AbN activity in B, left column, and a lack of black circles in C under "control"). Bicuculline (10 μmol/L), a blocker of $GABA_A$ receptor-mediated synaptic inhibition, was bilaterally microinjected in the ventrolateral (vl) RTN/pFRG at the time point shown in C by the vertical dashed line. As seen in B (middle column) and C (black circles), the application of bicuculline evoked rhythmic late-E activity in AbN phase-locked with PN bursts. The AbN activity evoked by disinhibition then disappeared with drug washout (see right column in B and lack of black circles in C, right part). Adapted, with permission, from reference (200) (Fig. 12).
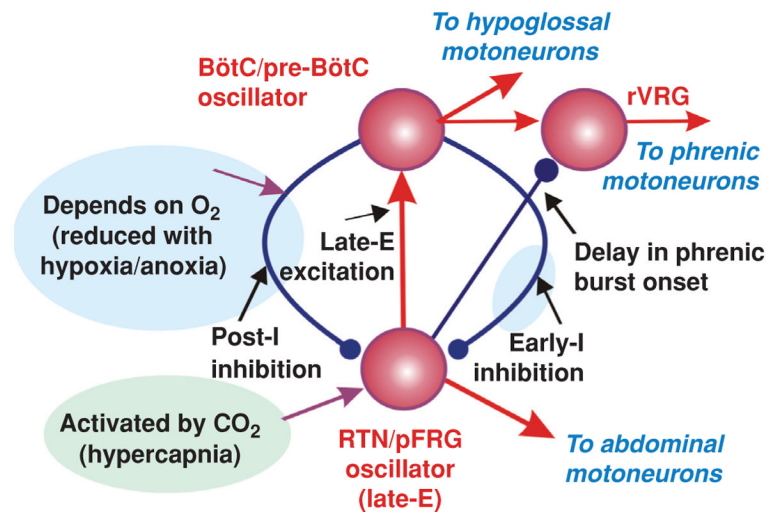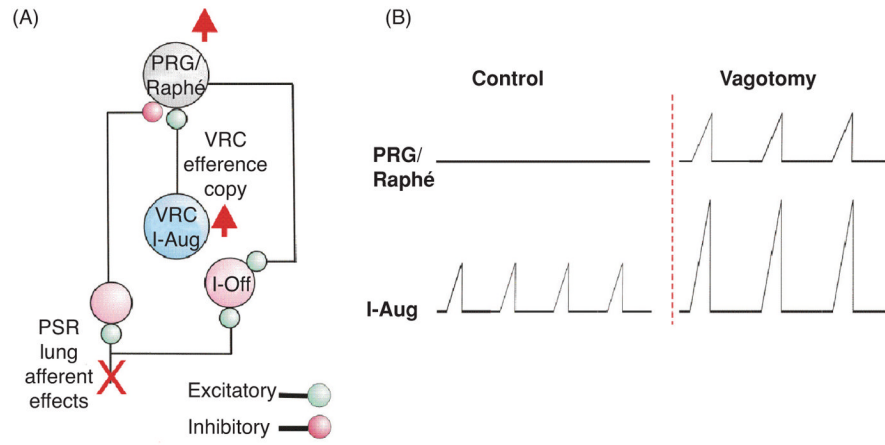
Figure 20.
Proposed interactions between Bötzinger-pre-Bötzinger (BötC-pre-BötC) and retrotrapezoid nucleus (RTN)/parafacial respiratory group (pFRG) oscillators in juvenile/adult mammals *in vivo* based on experimental observations and model simulations. Red arrows represent excitatory influence; blue lines terminated with circles indicate inhibitory influence; violet arrows indicate metabolic dependence. Under normal metabolic conditions, the RTN/pFRG oscillator is inhibited by the BötC-pre-BötC core circuit oscillator during both inspiration [by the inhibitory early-inspiratory (early-I) neurons of pre-BötC] and expiration [by the post-inspiratory (post-I) neurons of BötC] and remains quiescent. The normal expression of post-I inhibition requires excitatory drive from the pons (not shown). The RTN/pFRG oscillator can be activated either by hypercapnia, which directly excites RTN/pFRG neurons, or by hypoxia/anoxia (or suppression of pontine activity), which reduces RTN/pFRG inhibition by the BötC-pre-BötC oscillator, or by both of the above metabolic conditions. When activated, the RTN/pFRG oscillator provides excitation of the BötC-pre-BötC oscillator and transient inhibition of rVRG premotor neurons, hence increasing the delay between hypoglossal and phrenic motor discharges. Adapted, with permission, from reference (200) (Fig. 13).
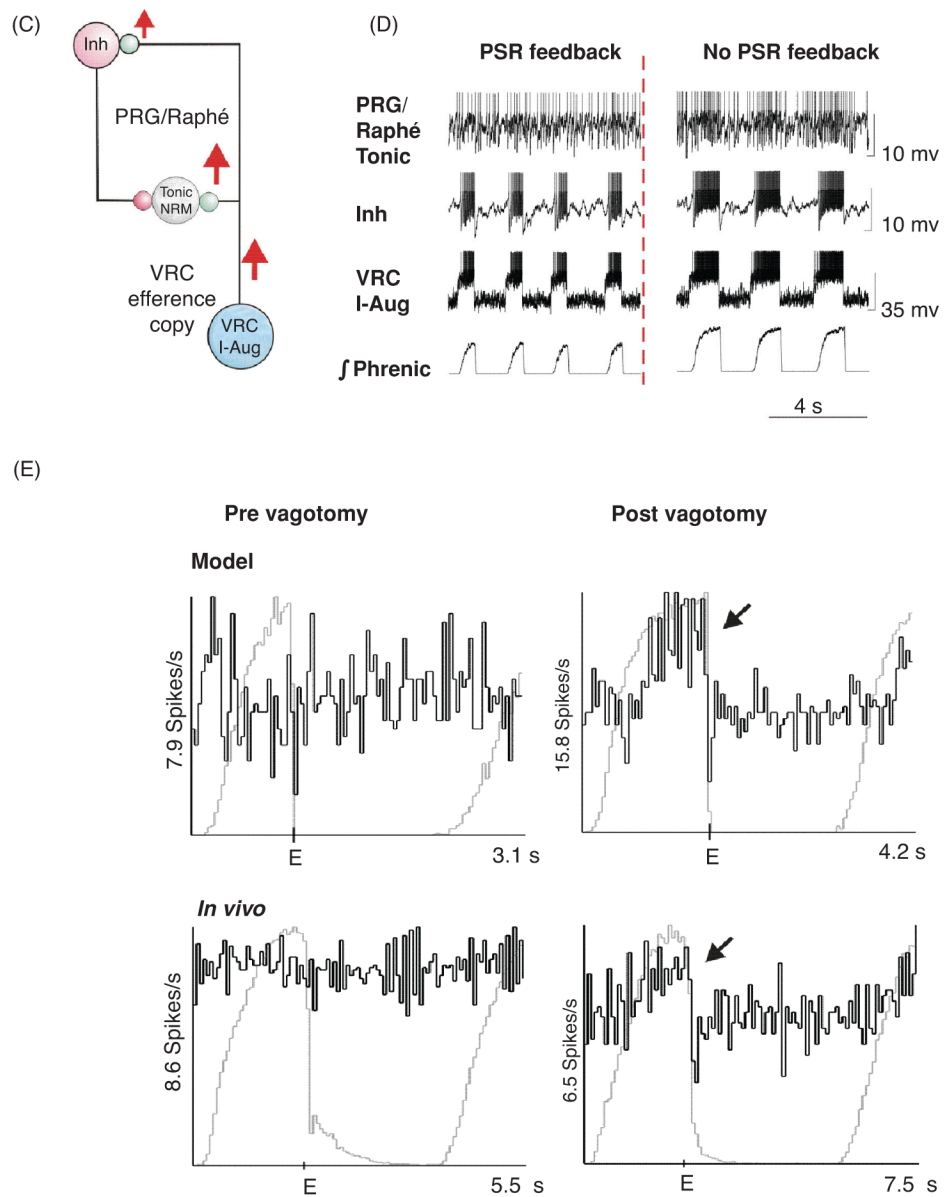
(A)

(B)

Figure 21.
Conceptual and computational model circuits for producing respiratory modulated firing in nonrespiratory modulated (NRM) tonic neurons due to increased I-Aug neuron activity following simulated loss of pulmonary stretch receptor (PSR) feedback as would occur during withholding of lung inflation or after vagotomy. (A) Schematic of the conceptual model for increased inspiratory modulation of pontine respiratory group (PRG) neurons with vagotomy via loss of inhibitory "gating" of ventral respiratory column (VRC) inspiratory-augmenting (I-Aug) neuron excitation. (B) Schematic representation of the change in modulation of some PRG and raphé neurons observed after vagotomy.
(C) Schematic of an alternative feed-forward inhibitory circuit module embedded in a larger respiratory network model with PSR inputs similar to the network model shown in Figure 8. The VRC I-Aug neurons drive, via an efferent copy mechanism (e.g., collateral axons), a population of tonic neurons and a less excitable phasically active population (Inh) that inhibits the tonic neurons. Under control conditions, the tonic population includes neurons

without respiratory modulated activity because of the balanced effects of synaptic inputs from the I-Aug and Inh populations. (D) Nonrespiratory modulated tonic neurons are "converted" to a respiratory modulated pattern following simulated vagotomy because of increased I-Aug population activity and the excitability properties of the Inh population. Representative traces of firing behavior of individual cells from the three integrate-and-fire neuron populations represented in C, before (*left*) and after (*right*) elimination of pulmonary stretch receptor feedback. Note the lack of respiratory modulation of the tonic neuron (NRM) before vagotomy. (E) Spike frequency histograms of model and electrophysiologically recorded tonic neuron comparing spiking patterns before and after vagotomy. Gray traces show corresponding phrenic activity to define the inspiratory phase. Circuit module simulation parameters were as described in Dick et al. (60). Adapted, with permission, from Dick et al. (60) [Fig 10 and (208), Fig 7].
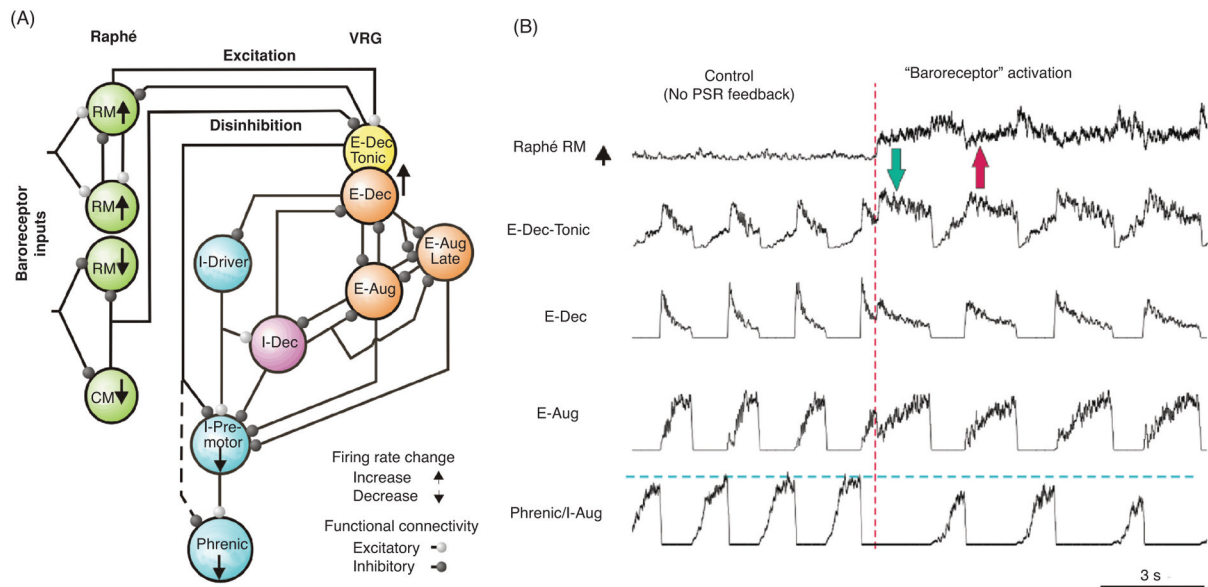
Figure 22.
Schematic of a raphé-ventral respiratory column (VRC) circuit model proposed to contribute to baroreceptor modulation of breathing, and changes in the integrated neuronal discharge patterns from the model with simulated baroreceptor stimulation. (A) Each neuron population is represented by a large circle labeled to indicate the corresponding respiratory modulation (see Table 1 for VRC nomenclature; other abbreviations for raphé neurons: RM, rostral midline; CM, caudal midline). Arrows indicate firing rate response to elevated arterial blood pressure in raphé, expiratory-decrementing (E-Dec) and inspiratory premotor and phrenic motor neuron (I-Aug) populations. Circuit connections were inferred from cross-correlation analysis of simultaneous multineuronal recordings in the anesthetized cat. Adapted, with permission, from reference (162) (Fig. 12). (B) The raphé circuits and connections with the VRC were incorporated into the enhanced ponto-medullary network model consisting of integrate-and-fire neurons as defined in reference (279) to perform simulations. Integrated population activity traces (simulated excitatory raphé population and four VRC populations, including I-Aug neurons as a surrogate for phrenic motor neurons represented in Panel A) from before and after (red vertical dashed line) baroreceptor afferent fiber population-mediated perturbation of the raphé populations ($n = 100$ neurons each). Note the reduced integrated phrenic discharge amplitude (blue dashed line) and prolonged expiratory duration. The short green and red arrows highlight the effects of the reciprocal connectivity between the excitatory RM raphé population and the inhibitory E-Dec-Tonic population following stimulus onset. Raphé-to-E-Dec and raphé-to-E-Dec-Tonic population connections were mediated by 100 synaptic terminals; both excitatory [0.2 synaptic strength (ss)] and inhibitory (0.01 ss) synapses had a 5-ms time constant (tau). The E-Dec-Tonic-to-raphé connections were also via 100 synaptic terminals (0.001 ss, 1.5 ms tau), as were the E-Dec-Tonic-to-I-Aug interactions (0.05 ss, 1.5 ms tau). Adapted, with permission, from reference (166) and unpublished results.
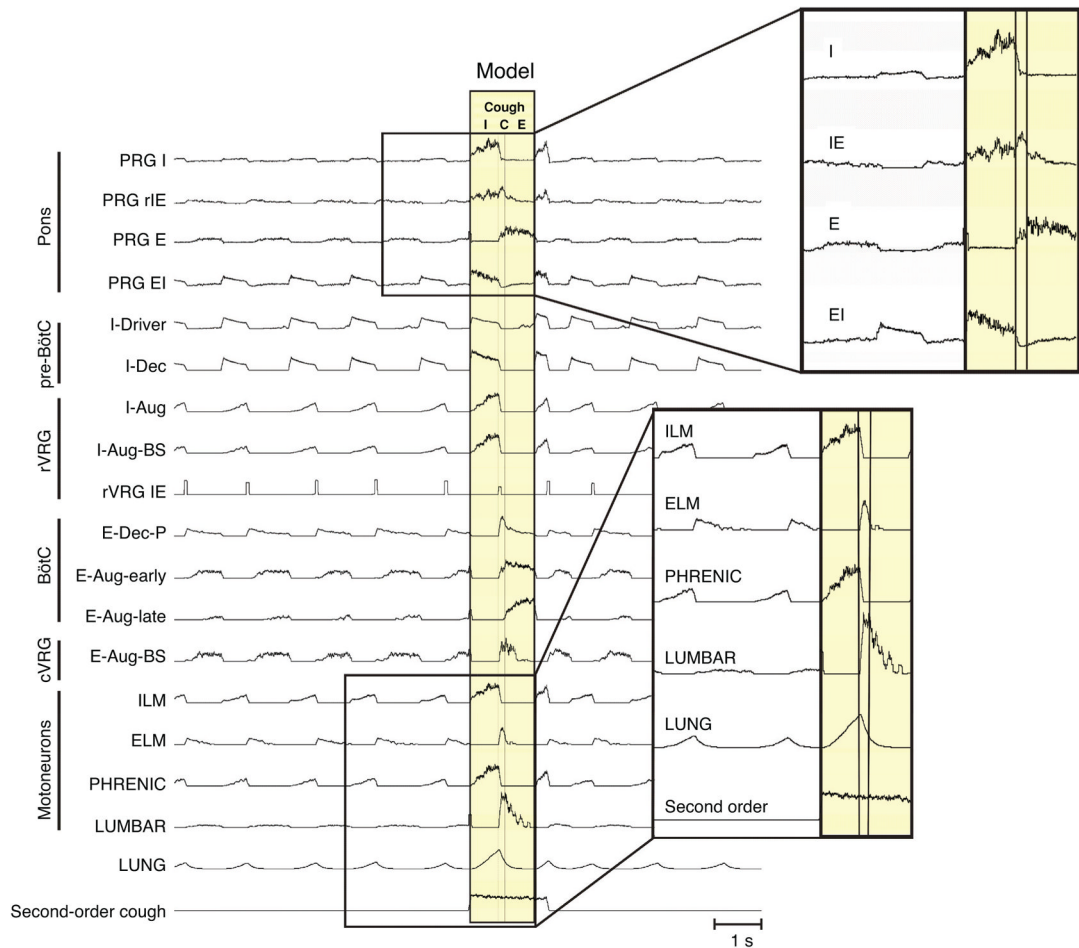
Figure 23.
Model simulations of cough. Activity profiles of ponto-medullary and motor neuron populations during eupnea-like and cough motor patterns from the ponto-medullary network model detailed in Rybak et al. (279). Transformations during simulated cough of the model's eupneic activity patterns of pontine neurons, ventral respiratory column (VRC) inspiratory/expiratory neurons, and respiratory motor outputs (laryngeal, phrenic, and lumbar) are highlighted with expanded time scale traces at right. Adapted, with permission, from reference (279) (Fig. 7).
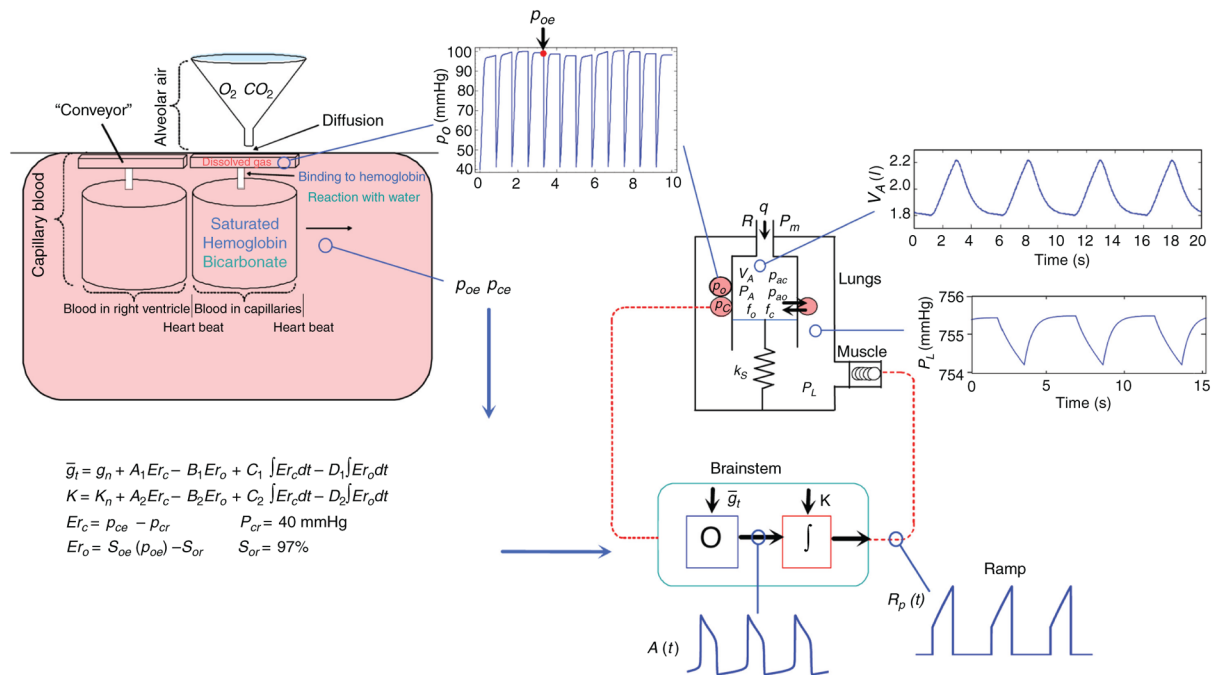
Figure 24.

Integrated model of brainstem respiratory controller and peripheral gas exchange and transport. This model incorporates simplified mathematical models of the lungs with O_2 and CO_2 exchange and transport processes coupled to a simplified model of the brainstem respiratory neural control network. The latter is represented by a pre-BötC oscillator (O) generating the inspiratory rhythm coupled to an inspiratory pattern generator in the rVRG that transforms the oscillatory drive signal into a ramping activity pattern [$R_p(t)$] via a neural integration (leaky integrator) process. The oscillator is modeled by activity-based [$A(t)$] descriptions that explicitly incorporate the kinetics of persistent sodium current inactivation to include a known biophysical mechanism allowing for frequency control by input drives ($\tilde{g}_t$ in the model) over a wide dynamic range, as well as multistate behavior (no activity, oscillations, and tonic activity). The ramp waveform drives the force generator at the level of respiratory muscles (diaphragm), modeled as a spring excited by an external force that is proportional to the ramp signal. The lungs are modeled by a single container that has a moving plate attached to the spring causing changes in the pleural pressure (P_L) surrounding the lungs, which causes the alveolar pressure (P_A) to change resulting in air flow in and out of the lung (the P_L and lung volume V_A as a function of time are shown at the upper right). Gas exchange and transport are modeled by a "conveyor" model (top left). The moving "conveyor" is simulated by reinitializing the values of p_c and p_o [the blood partial pressures of carbon dioxide and oxygen, respectively (middle top)), every heart beat (for more details see (12). The values of p_c and p_o at the end of each interbeat interval represent the blood partial pressures at the end of the capillaries and are denoted by p_{ce} and p_{oe}, respectively. These values are updated every heart beat and are used to calculate input drives to the oscillator and ramp generator ($\tilde{g}_t$ and K, respectively), which are the two control parameters in the model described by the feedback functions shown at the bottom left. These functions are formulated mathematically to represent two different types of feedback controllers (proportional and proportional plus integral controllers) from standard control theory that incorporate "error" terms (Er$_c$, Er$_o$, bottom left) and also the model accounts for delays associated with blood transport and dynamics of chemosensory-related afferent feedback

signals. Full details of the model system components are provided in Ben-Tal and Smith (13) (Fig. 1, with permission from Elsevier).

Table 1

Respiratory Neuron Types and Their Corresponding Terms and Abbreviations Used in Different Models of the brainstem respiratory network

Category	Alternative terms Modifiers	Description and properties
I-E/I	I-driver; pre-I/I; pre-I (type I)	Neurons that start activity at the end of expiration (i.e., prior to the onset of phrenic nerve discharge), and fire throughout the inspiratory phase. Many of these neurons are (presumptively) excitatory and are located in the pre-BötC. Some of these neurons have intrinsic bursting properties *in vitro* and *in situ*. These neurons principally differ from the pre-I (or late-E or biphasic-E—see later) neurons that are inhibited during inspiration and presumably are located in RTN/pFRG.
I-DEC	Early-I	Inhibitory/excitatory inspiratory neurons with decrementing firing rate pattern (i.e., with spike frequency progressively decreasing during the inspiratory phase)
I-CON	I-constant; Const-I	Neurons with relatively constant level of firing activity throughout the inspiratory phase
I-AUG	Ramp-I	Excitatory inspiratory neurons with an augmenting firing pattern (with spike frequency progressively increasing during the inspiratory phase)
	PB	Propriobulbar: axons confined to brainstem
	BS	Bulbospinal: axons project to spinal cord; may have collateral axons in the brainstem
IE	Late-I	Neurons whose activity starts in and increases to the end of inspiration, reaches a peak at the inspiratory-expiratory (-E) transition and then decrements during expiration
E-DEC	Post-I; Dec-E	Expiratory neurons (many inhibitory) with decrementing firing rate most active during the early-expiratory (postinspiratory) interval
	-T	Decrementing expiratory neurons with a reduced but tonic firing rate during inspiration
E-AUG	Aug-E; E2	Expiratory neurons with augmenting discharge pattern (with spike frequency progressively increasing during expiration. This category includes both neurons starting activity from the beginning of expiration and neurons with onset of activity in the second part of expiration (so-called E2 phase).
	Early	E-AUG neurons with activity starting with the onset of expiration; also include E-"constant" firing rate pattern.
	Late	E-AUG neurons with activity onset delayed and limited primarily to the second half of the expiratory phase (same as E2).
	BS–	"Bötzinger" inhibitory neurons; some bulbospinal and may have axon collaterals.
	BS+	Excitatory bulbospinal
	HT	High threshold; e.g., subset of late E-Aug evoked during cough
LATE-E	Late-E; Pre-I (type 2); Pre-I*	Excitatory neurons that exhibit short activation at the very end of expiration just prior to the onset of the inspiratory phase (phrenic burst). These neurons are inhibited during inspiration, but can have a second rebound post-I burst (in this case they are also called Biphasic-E, see later). These neurons are presumably located in RTN/pFRG and have been called "pre-I" by Onimaru and Homma (230); (see later). These neurons also differ from aug-E (E-AUG) neurons many of which are inhibitory neurons and uniformly have an earlier onset during expiration.
Biphasic E	Late-E (biphasic type)	Late-E neurons that typically have a second burst at the beginning of expiration (in the postinspiratory phase, see earlier text).
	Pre/post-I Pre-I*	*Also called pre-I by Onimaru and Homma (230), some of which exhibit intrinsic rhythmic bursting properties *in vitro* [for review see reference (233)].
EI		Neurons with peak firing rates at the expiratory-to-inspiratory (E-to-I) phase transition
NRM (+, −)		*Nonrespiratory modulated:* Neurons without respiratory-modulated activity as judged by statistical methods; (excitatory or inhibitory, respectively)
PRG I		*Pontine Respiratory Group, including* Dorsolateral pons (dlP) (parabrachial—Kölliker Fuse regions) with peak firing rates during the second half of the inspiratory phase and with a generally augmenting activity profile during the phase.

Category	Alternative terms Modifiers	Description and properties
PRG E		PRG neurons with peak firing rates during the second half of the expiratory phase and with an augmenting activity profile during the phase.
PRG IE		PRG neurons with peak firing rates during the I-to-E phase transition and with a decrementing activity profile in the latter phase.
PRG EI		PRG neurons with peak firing rates during the E-to-I phase transition and with a decrementing activity profile in the latter phase.
ILM	(PCA)	Inspiratory laryngeal motoneurons (e.g., posterior cricoarytenoid, PCA)
ELM	(TA)	Expiratory laryngeal motoneurons, (e.g., thyroarytenoid, TA)
PHR		Phrenic motor neuron
EXP MN	Lum	Spinal (lumbar) motoneurons innervating (abdominal) expiratory muscles
PSR	SAR	Slowly adapting pulmonary stretch receptors
Pump+/−		Neuron in region of nucleus of solitary tract (NTS) excited by pulmonary stretch receptors during lung inflation, but do not have direct central respiratory drive. Pump + neurons are excitatory; Pump− neurons are inhibitory.
RAR		Rapidly adapting pulmonary stretch receptors
"Cough" receptors		Recently described sensory receptors located in the trachea and larger airways that have response patterns uniquely suited for the production of cough.
Second-order (cough)		Second-order NTS neurons that affect respiratory neurons in both VRC and PRG, causing reconfiguration of the respiratory network to produce the cough motor pattern

Note that different authors use different nomenclatures for the same neuron types; see Alternative terms.